

Dissertation  
der Fakultät für Biologie  
der Ludwig-Maximilians-Universität München

Organisation of central amygdala  
circuits regulating appetitive and  
aversive behaviours

**Marion Ponserre**

München, den  
29.01.2018





Erstgutachter: Prof. Dr. Rüdiger Klein

Zweitgutachter: Prof. Dr. Laura Busse

Tag der Einreichung: 29.01.2018

Tag der mündlichen Prüfung: 9.10.2018

The work presented in this dissertation was performed in the laboratory of Prof. Dr. Rüdiger Klein, Department of Molecules – Signaling – Development, Max-Planck Institute of Neurobiology, Martinsried, Germany.



## EIDESSTATTLICHE ERKLÄRUNG

Ich versichere hiermit an Eides Statt, dass die vorgelegte Dissertation von mir selbständig und ohne unerlaubte Hilfe angefertigt ist.

München, den 27.08.2019

Marion Ponserre

## ERKLÄRUNG

Hiermit erkläre ich, dass die Dissertation nicht ganz oder in wesentlichen Teilen einer anderen Prüfungskommission vorgelegt worden ist und ich mich anderweitig einer Doktorprüfung ohne Erfolg nicht unterzogen habe.

München, den 27.08.2019

Marion Ponserre



## ACKNOWLEDGMENTS

First and foremost, I would like to express my gratitude towards my supervisor Rüdiger Klein for supporting and guiding my scientific development in his lab and giving me the opportunity to work in such a stimulating environment. He made my PhD to a valuable and formative experience that I would not want to have missed.

I would also like to acknowledge Nadine Gogolla, and Klaus Conzelmann who gave important critical feedback on the progress of my project.

I am fortunate to have profited from the help and support of the great Klein-lab technicians Louise, Jana, Gönül and especially Pilar who has engineered and generated essential transgenic mouse lines and performed such brilliant *in-situs* for this project.

Many thanks to all present and former members of the Klein-lab with whom it was a pleasure to interact both scientifically and personally. I especially want to thank my amazing friends Louise, Tom and Sonia for things way too numerous that I could write them down. You have become so much more than just colleagues. Aarathi and Johanna, my bench-mates and very good friends to whom I could always turn to when in doubt; Annelies for her cheerful and enthusiastic attitude; Federica and Cornelia to see through the ups and downs of the amygdala project; Irene my climbing holiday buddy; Dani and Tobias, my bitcoin consultants; Daniel, Jorg, Pontus and Graziana who made the atmosphere in the lab thoroughly enjoyable.

Furthermore I am deeply thankful to all the people I have met at the MPI, especially Etienne, Aljoscha, Florian, Georg, Sandra, Michi D, Olivia and Laurence who have made the past five and a half years such an unforgettable time.

My deepest gratitude goes to my family, Elodie and Matthias for their love, emotional support and understanding. Without you I would have not overcome the challenging episodes of this experience.

Last, but certainly not least, a very big thank you to Louise for kindly reading and greatly improving this thesis.



# CONTENTS

<b>Erklärung</b>	<b>v</b>
<b>ACKNOWLEDGMENTS</b>	<b>VII</b>
<b>ABSTRACT</b>	<b>XIII</b>
<b>1. INTRODUCTION</b>	<b>1</b>
<b>1.1. The amygdaloid complex</b>	<b>4</b>
1.1.1. Nuclei of the amygdaloid complex	4
1.1.2. Cyto- and chemoarchitecture of the CeA	5
<b>1.2. A functional overview of CeA afferents and efferents</b>	<b>6</b>
1.2.1. Long-range afferents to the CeA	6
1.2.2. Long range efferents of the CeA	8
1.2.3. Intrinsic connections	9
<b>1.3. Circuits for defensive behaviours</b>	<b>9</b>
1.3.1. Acquisition of conditioned fear	10
1.3.2. Expression of conditioned fear	11
1.3.3. Beyond conditioned fear in the CeA	15
<b>1.4. Representation of reward in the amygdala</b>	<b>17</b>
1.4.1. Encoding of reward stimuli in the CeA	18
1.4.2. Populations of valence-selective neurons in the CeA	20
<b>1.5. Monosynaptic circuit tracing using recombinant rabies virus technology</b>	<b>21</b>
<b>1.6. Aim of the study</b>	<b>23</b>
<b>2. RESULTS</b>	<b>25</b>
<b>3.1. Phenotypic characterization of CeA<sup>Htr2a</sup> neurons</b>	<b>27</b>
3.1.1. Molecular profile of CeA <sup>Htr2a</sup> neurons	27
3.1.2. Spatial segregation of CeA <sup>Htr2a</sup> and CeA <sup>PKCδ</sup> neurons	28
<b>3.2. Organisation of CeA inhibitory microcircuits</b>	<b>30</b>
3.2.1. Strategy to identify monosynaptic inputs to CeA <sup>Htr2a</sup> , CeA <sup>PKCδ</sup> and CeA <sup>Sst</sup> neuronal populations	30
3.2.2. Interaction between CeA <sup>Htr2a</sup> , CeA <sup>PKCδ</sup> and CeA <sup>Sst</sup> neuronal populations	32
3.2.3. Identification of local inputs to PBN-projecting CeA neurons	34

<b>3.3. Identification of whole-brain inputs to CeA<sup>Htr2a</sup>, CeA<sup>PKCδ</sup> and CeA<sup>Sst</sup> neurons</b>	<b>36</b>
3.3.1. Contribution of LA and BLA inputs to CeA <sup>Htr2a</sup> and CeA <sup>PKCδ</sup> neurons	38
3.3.2. Quantitative analysis of CeA <sup>Htr2a</sup> , CeA <sup>Sst</sup> and CeA <sup>PKCδ</sup> input distribution	38
3.3.3. Characterization of transsynaptically labelled neurons in the IPBN	42
3.3.4. Covariance analysis between input regions to CeA <sup>Htr2a</sup> neurons	43
<b>3.4. Organisation of monosynaptic inputs to PBN-projecting CeA<sup>Htr2a</sup> and PBN-projecting CeA neurons</b>	<b>45</b>
<b>3.5. Identification of CeA<sup>Htr2a</sup> output pathways</b>	<b>48</b>
<b>3.6. Differential distribution of CeA projection neurons</b>	<b>50</b>
<b>3.7. Input-output relationship of CeA projection neurons</b>	<b>52</b>
<b>4. DISCUSSION</b>	<b>57</b>
<b>4.1. Summary of findings</b>	<b>59</b>
<b>4.2. CeA<sup>Htr2a</sup> neurons may function in parallel to the LA and BLA nuclei</b>	<b>59</b>
<b>4.3. CeA<sup>Htr2a</sup> neurons represent a heterogeneous population</b>	<b>60</b>
<b>4.4. CeA<sup>Htr2a</sup> neurons have the necessary connections to influence appetitive behaviours</b>	<b>61</b>
<b>4.5. CeA neurons may form stimulus-valence associations necessary for both aversive and appetitive learning.</b>	<b>62</b>
<b>4.6. Parallel collaborative circuits in the CeA may control behaviour</b>	<b>64</b>
<b>4.7. Limitations of the rabies virus-based monosynaptic tracing technology</b>	<b>65</b>
<b>4.8. Conclusions and outlook</b>	<b>66</b>
<b>5. METHODS</b>	<b>69</b>
<b>5.1. Animals</b>	<b>71</b>
<b>5.2. Viral constructs</b>	<b>71</b>
<b>5.3. Stereotaxic surgeries</b>	<b>71</b>
5.3.1. Negative control experiments for monosynaptic tracing	72
5.3.2. Identification of monosynaptic inputs to CeA <sup>Htr2a</sup> , CeA <sup>PKCδ</sup> and CeA <sup>Sst</sup> neurons	72

5.3.3.	Identification of monosynaptic inputs to BNST, LH, PAG and PBN-projecting CeA neurons (TRIO experiments)	72
5.3.4.	Identification of monosynaptic inputs to PBN-projecting CeA <sup>Htr2a</sup> neurons (cTRIO experiments)	72
5.3.5.	Analysis of spatial segregation of CeA projection neurons	73
5.3.6.	Axonal projections of CeA <sup>Htr2a</sup> and CeA <sup>PKCδ</sup> neurons	73
<b>5.4.</b>	<b>Histology</b>	<b>74</b>
<b>5.5.</b>	<b>Brain tissue clearing</b>	<b>75</b>
<b>5.6.</b>	<b>Fluorescence in situ hybridization (FISH)</b>	<b>75</b>
<b>5.7.</b>	<b>Immunohistochemistry (IHC)</b>	<b>76</b>
<b>5.8.</b>	<b>Microscopy and image processing</b>	<b>77</b>
<b>5.9.</b>	<b>Data analysis</b>	<b>77</b>
5.9.1.	Molecular characterization of CeA <sup>Htr2a</sup> neurons	77
5.9.2.	Identification of local inputs to CeA <sup>Htr2a</sup> , CeA <sup>PKCδ</sup> , CeA <sup>Sst</sup> and PBN-projecting CeA neurons	77
5.9.3.	Whole brain monosynaptic inputs to CeA <sup>Htr2a</sup> , CeA <sup>PKCδ</sup> , CeA <sup>Sst</sup> , PBN-projecting CeA and PBN-projecting CeA <sup>Htr2a</sup> neurons	78
5.9.4.	Identification of IPBN inputs onto CeA <sup>Htr2a</sup> and CeA <sup>PKCδ</sup> neurons	79
5.9.5.	Identification of axonal projections of CeA <sup>Htr2a</sup> and CeA <sup>PKCδ</sup> neurons	79
5.9.6.	Digital three-dimensional (3D) CeA and mouse brain reconstructions	80
<b>5.10.</b>	<b>Statistical analysis</b>	<b>81</b>
<b>LIST OF FIGURES AND TABLE</b>		<b>83</b>
<b>ABBREVIATIONS</b>		<b>85</b>
<b>REFERENCES</b>		<b>89</b>
<b>Publication from the work presented in this dissertation</b>		<b>103</b>
<b>Curriculum Vitae</b>		<b>105</b>



## ABSTRACT

An organism's survival is contingent on its ability to evaluate whether environmental cues predict a threat or an opportunity. The amygdala has long been studied for its pivotal role in providing an emotional tag to environmental stimuli so that individuals can engage in the appropriate behavioural response. The amygdala is composed of a collection of nuclei including the basolateral (BLA) and central amygdala nuclei (CeA), which have been proposed to participate in the formation of memories that link sensory information to aversive or rewarding representations, and to provide the output pathway through which these memories are translated into behavioural actions, respectively. Although previous work has provided a wealth of information on the amygdala circuits that govern aversive behaviours, such as avoidance of threats or potentially poisonous substances, information on CeA circuits that process appetitive signals is incomplete. In this context, this study aimed to decipher the organisation of CeA circuits that control feeding and rewarding behaviours. By using a combination of behavioural and optogenetic approaches, it was revealed that increase in the activity of CeA neurons expressing the serotonin receptor 2a (Htr2a) can counteract the anorexigenic effect induced by the activation of protein kinase C delta- (PKC $\delta$ ) expressing neurons. The mechanisms underlying this behaviour were untangled by showing that CeA<sup>Htr2a</sup> neurons promote food consumption and positive reinforcement via inhibition of the parabrachial nucleus (PBN) (experiments conducted by Amelia M. Douglas). Yet, the question of how the appetitive information is relayed onto PBN-projecting CeA<sup>Htr2a</sup> neurons remained. Using recombinant rabies virus technology, I found a reciprocal inhibitory interaction between PBN-projecting CeA<sup>Htr2a</sup> and CeA<sup>PKC $\delta$</sup>  neurons - a motif circuit by which they might exert opposing influences on food intake. I further examined putative sources of excitatory inputs and demonstrated that CeA<sup>Htr2a</sup> neurons are composed of several subpopulations by virtue of their specific presynaptic partners. Those CeA<sup>Htr2a</sup> neurons projecting to the PBN constitute one distinct unit that receives monosynaptic inputs from a specific combination of brain nuclei with known roles in reward processing and food intake. Interestingly, these regions were found to preferentially innervate CeA<sup>Htr2a</sup> cells compared to CeA<sup>PKC $\delta$</sup>  neurons. In an attempt to further characterize all the CeA<sup>Htr2a</sup> subunits, I obtained preliminary results indicating that sensory information from the cortex and thalamus might not directly target CeA projection neurons, suggesting that the encoding of the value of a stimulus and the instruction of the underlying behaviour to downstream effectors might be mediated by two distinct populations of CeA neurons. In summary, this work substantially extends our knowledge of the organisation of CeA circuits that govern appetitive and aversive behaviours, and provides insights into how they can select output pathways targeting distinct downstream structures depending on the pattern of their monosynaptic inputs.



# 1. INTRODUCTION



From an evolutionary stand point, the ultimate goal of an organism is to survive long enough to pass on one's own genetic material to its offsprings. To assist in this task, brain programs have evolved to ensure adaptive behavioural responses. These behavioural actions can be as elementary as avoiding an imminent danger, or as complex as adopting and maintaining appropriate social interactions that would increase one's reproductive chances. To do so, individuals must be able to constantly weigh environmental stimuli and decide whether they signal a threat or an opportunity.

Previous work has provided a wealth of information on the neural substrates that facilitate these processes. Research has particularly focused on the amygdala, a region that is critical to appraise a continuum of positively- (rewarding) and negatively- (aversive) valence stimuli and for the formation and storage of memories associated with emotional events<sup>1,2</sup>.

Initial evidence of the role of the amygdala was reported in 1888 by Brown and Schäfer<sup>3</sup> and later in 1937 by Klüver and Bucy<sup>4</sup> who observed that Rhesus Monkeys with an ablation of the temporal lobe that included the amygdala, showed a profound alteration in aggression, fear and defensive behaviours. The animals were emotionally dulled.

Later studies took advantage of Pavlovian auditory fear conditioning paradigms in rodents<sup>5,6</sup> to delve into details of the brain mechanisms underlying these behaviours. During auditory fear conditioning, animals are presented with an initial neutral conditioned stimulus (CS), typically a tone, paired with an aversive unconditioned stimulus (US), usually a mild electrical shock. After a relatively small number of tone-shock pairings, the animals will eventually learn that the tone precedes the shock, and a fear response will be elicited in the presence of the CS only. The amygdala's function in this paradigm was studied using a range of traditional methods to ablate or partially lesion this region and these studies robustly demonstrated that animals were no longer able to recognize the CS as a fearful stimulus<sup>5,6</sup>.

This led to the concept that the amygdala is necessary to provide a value – either positive or negative – to sensory information through associative learning so that the animal can engage in the appropriate behaviour<sup>2</sup>.

Although the amygdala has been extensively studied for its function in mediating aversive behaviours, strong evidence supports a role for this region in processing positive emotions in addition to negative ones<sup>2,7,8</sup>.

## 1.1. THE AMYGDALOID COMPLEX

### 1.1.1. Nuclei of the amygdaloid complex

The rodent amygdaloid complex, located in the temporal lobe, is composed of a heterogeneous assortment of around a dozen of nuclei depending on the nomenclature. Each of these nuclei can be further separated into subdivisions, all of which are extensively interconnected. According to the classification of Price *et al.*,<sup>9</sup> which was further developed by Swanson and Petrovich<sup>10</sup> and McDonald<sup>11</sup>, the amygdaloid complex is classically clustered in three groups (**Figure 1**). The first group constitutes the deep or basolateral complex. Its main nuclei, the lateral (LA), basolateral (BLA) and basomedial amygdala (BMA), harbour a cortical-like structure but lack the layered anatomical organisation of the cortex. They contain projection neurons of a pyramidal type that synthesize glutamate, intermingled with GABAergic interneurons. The second set represents the superficial group that comprises the cortical (COA) and piriform (PAA) amygdala areas to cite a few, and is related to the main and accessory olfactory systems. Finally, the centromedial group is composed of the central (CeA), medial amygdala (MeA) and the amygdaloid part of the bed nucleus of stria terminalis (BNST) and displays striatopallidal-like structure. The CeA classically encompasses three parts: the capsular (CeC), lateral (CeL) and medial (CeM) (**Figure 1**). A few additional nuclei do not belong to any of these three categories. Among them, the intercalated cell masses (IA), which are small clusters of densely packed GABAergic neurons (**Figure 1**).

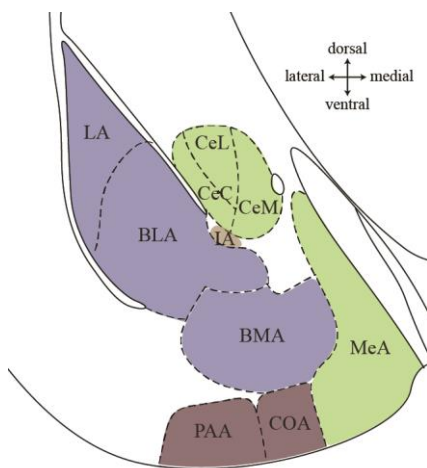


**Figure 1: Nuclear divisions of the amygdaloid complex.** Drawing based on Paxinos and Franklin's atlas of a coronal section depicting the three groups of the amygdaloid complex: deep or basolateral (blue), superficial (burgundy) and centromedial (green). The intercalated cell masses are represented in brown. LA, lateral amygdala; BLA, basolateral amygdala; BMA, basomedial amygdala; CeL, central lateral amygdala; CeC, central capsular amygdala; CeM, central medial amygdala; MeA, medial amygdala; COA, cortical amygdala area; PAA, piriform amygdala area; IA, intercalated amygdala nucleus. To simplify the scheme, more rostrally located divisions such as the amygdaloid part of the BNST, the anterior amygdala area, the bed nucleus of the accessory olfactory tract, the nucleus of the lateral olfactory tract as well as caudally located postpiriform transition area are not depicted here.

### 1.1.2. Cyto- and chemoarchitecture of the CeA

Here, I will focus on the CeA nucleus which is of most relevance to this study. The three divisions of the CeA, namely the CeC, CeL and CeM are defined based on cytoarchitecture, neurochemistry and connectivity<sup>9-11</sup>. As the CeL and CeC are not easily distinguishable, I further grouped these two subdivisions into one that I named CeL/C.

The CeA is a striatally derived structure originating from the caudal ganglionic eminence<sup>12</sup> in which the vast majority of CeA neurons exhibit a medium spiny-like morphology in reference to the striatal neurons<sup>13</sup>.

In terms of physiology, three different cell types can be identified based on their firing properties: the late firing, regular spiking, and low-threshold bursting neurons<sup>14</sup>.

Cells from all subdivisions synthesize GABA<sup>15</sup> and neuropeptides: such as opioid peptides (enkephalins<sup>16</sup>, dynorphin<sup>17</sup>), somatostatin (Sst)<sup>18</sup>, tachykinin 2 (Tac2)<sup>19</sup>, corticotropin-releasing hormone (Crh)<sup>20</sup>, neurotensin (Nts)<sup>18</sup>, substance P<sup>18</sup>, orexin/hypocretin<sup>21</sup> and cholecystokinin<sup>18</sup>. Some of these peptides and others, such as calcitonin gene-related peptide (CGRP)<sup>22</sup>, are also present in the incoming axonal terminals of CeA neurons. Like those of the striatum, GABAergic neurons of the CeA containing one or more neuropeptides are projection neurons<sup>23</sup>.

Additionally, CeA neurons express serotonin receptor 2a<sup>24</sup> (Htr2a), dopamine receptors 1 and 2 (ref: 25), kappa- opioid receptors, mu- opioid receptors and delta- opioid receptors<sup>26</sup>, glucocorticoid receptors<sup>27</sup>, melanocortin receptor 4 (ref: 28), oxytocin (OXR), vasopressin receptors<sup>29</sup>, galanin receptors<sup>30</sup>, Crh receptors<sup>31</sup> and calcitonin- gene related peptide receptors (CGRPR)<sup>25</sup>. More recently, a population of protein kinase C delta- (PKC $\delta$ ) expressing neurons has also been described<sup>32</sup>.

The coexistence of these markers in CeA neurons has been investigated by many groups<sup>20,32-38</sup>. A recent work from Kim *et al.*,<sup>25</sup> proposes that CeL/C comprises four major cell populations: the first is composed of CGRPR+ neurons; the second consists of PKC $\delta$ + neurons that are CGRPR negative; the third is constituted of Sst+ cells; and the fourth contains Crh+, Tac2+ and Nts+ neurons. The situation in the CeM is less clear. Here, Sst-, Crh-, Tac2- and Nts- expressing cells appear to show very little overlap<sup>25</sup>.

## 1.2. A FUNCTIONAL OVERVIEW OF CEA AFFERENTS AND EFFERENTS

### 1.2.1. Long-range afferents to the CeA

Afferents to the CeA can be classified into six different kinds depending of the type of information they convey: 1) gustatory, visceral and nociceptive, 2) chemosensory, 3) multimodal, 4) contextual, 5) modulatory and 6) feedback afferents (**Figure 2**).

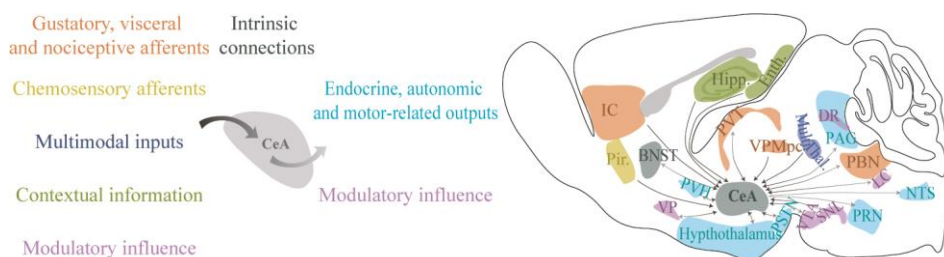


**Figure 2: Summary of CeA connectivity.** Diagrams illustrating the most substantial inputs and outputs of the CeA outside of the amygdaloid complex and with regards to the type of information conveyed. PBN, parabrachial nucleus; IC, insula cortex; VPMpc, ventral posteromedial nucleus of the thalamus, parvicellular part; PVT, paraventricular thalamus; Pir, piriform cortex; Multi. Thal., multimodal thalamus; Hipp, hippocampus; Enth, enthorinal cortex; VP, ventral pallidum; SN, substantia nigra; VTA, ventral tegmental area; DR, dorsal raphe; LC, locus coeruleus; PAG, periaqueductal gray; Hypothalamus, see text for detail on the hypothalamic nuclei connected with CeA; PVH, paraventricular hypothalamus; PSTN, parasubthalamic nucleus; NTS, nucleus of the solitary tract; PRN, pontine reticular nucleus; BNST, bed nucleus of the stria terminalis.

#### *Gustatory, visceral and nociceptive afferents*

The CeA is innervated by ascending sensory afferents relaying gustatory, viscerosensitive and nociceptive information. This information reaches the CeA via two different routes: a direct one originating in the parabrachial nucleus (PBN), and an indirect one from the gustatory and visceral thalamus and the insula cortices (IC)<sup>39</sup> (**Figure 2**). These pathways have been proposed to be engaged in various learning tasks in which a particular taste is linked to past consequences of its ingestion or in the formation of associations between tastants, gustatory and visceral sensations together with auditory, visual and somatosensory stimuli<sup>39,40</sup>. These processes are extremely important as they allow organisms to use environmental cues to predict food availability or in other circumstances, to promote avoidance behaviour toward potentially poisonous nutrients.

In the PBN, subpopulations of neurons encode taste<sup>41,42</sup>, pain<sup>43,44</sup>, sodium intake<sup>45,46</sup>, appetite suppression<sup>47,48</sup>, respiration<sup>49</sup> and thermosensation<sup>50</sup>. Notably, PBN neurons are activated during aversive visceral states such as nausea<sup>51</sup> and

by hormones that promote satiety<sup>52,53</sup> and stomach distention<sup>54,55</sup>. In the lateral division of the PBN (lPBN), a substantial proportion of these neurons express CGRP<sup>56,57</sup>. Additionally, CGRP cells strongly project to the CeA<sup>58</sup> and this connection has been shown to promote anorexia induced by stressful stimuli<sup>57</sup> and to convey pain-related information that is sufficient to create aversive memories<sup>37</sup>. While in the lPBN, CGRP+ neurons send axonal projections to the CeC and to a lesser extent the CeL; the medial division (mPBN) appears to preferentially contact the CeM<sup>59</sup>, although the relevance of this connection has not yet been revealed.

From the PBN, gustatory and visceral information are relayed to the gustatory thalamus (ventral posteromedial nucleus of the thalamus, parvocellular part: VPMpc), viscerosensitive thalamus (paraventricular (PVT), interanteromedial and central medial nuclei) and the IC, including the gustatory cortex<sup>39</sup>, which all project to the CeA<sup>60-63</sup> (**Figure 2**). Although connections between the gustatory thalamus and the CeA have not been studied in detail, projections from the IC to the CeA have been recently demonstrated to mediate associative learning that a non-gustatory stimulus (in this case an auditory cue) predicts an aversive taste so that animals can exhibit avoidance responses to unpleasant substances<sup>64</sup>.

#### *Chemosensory afferents*

The CeA receives chemosensory afferents mostly from the piriform cortex (Pir.)<sup>65</sup> which mediates sensory processing of odours and pheromones<sup>66</sup> (**Figure 2**).

#### *Multimodal inputs*

The CeA is also the target of the multimodal thalamic nuclei (Multi. Thal.) (**Figure 2**) including the medial geniculate nucleus (medial and dorsal part), subparafascicular thalamic nucleus (parvocellular part), supragenulate thalamic nucleus, and peripeduncular nucleus which gathers auditory, visual and somatosensory information from different parts of the brain<sup>62,67</sup>.

#### *Contextual information*

The hippocampal formation including the hippocampal region<sup>60,68</sup>, the subiculum<sup>60,69</sup> (Hipp.) and entorhinal cortex<sup>60,70</sup> (Ent.) also innervate the CeA (**Figure 2**). As memories of aversive events are linked to the context in which they are formed, the hippocampal formation has been shown to convey spatial and contextual information. Indeed, using *in vivo* Ca<sup>2+</sup> imaging in freely behaving animals, Xu *et al.*,<sup>71</sup> showed that the activity of ventral hippocampal neurons was upregulated after animals entered the context in which the fear memory was learned. Moreover, they demonstrated that a subset of these ventral hippocampal neurons project onto CeA cells and that this connection is necessary during context-dependent retrieval of fear memories.

#### *Modulatory influence*

Modulatory inputs onto CeA emanate from neurochemically defined centres such as: the ventral pallidum (VP)<sup>72</sup>, parabigeminal, laterodorsal tegmental and

pedunculopontine cell groups<sup>73</sup> that harbour populations of cholinergic neurons; the substantia nigra (SN) and ventral tegmental area (VTA)<sup>74</sup> that contain dopaminergic cells; the dorsal raphe (DR)<sup>75</sup> that produces serotonin and the locus coeruleus (LC)<sup>76</sup> that synthesizes noradrenaline (**Figure 2**). These afferents may play a role in attentional processing<sup>77,78</sup>.

As seen in the previous section (1.1.2. Cyto- and chemoarchitecture of the CeA), CeA neurons also express corticosteroid receptors, such as glucocorticoid receptors<sup>27</sup>, raising the possibility that the behavioural responses executed by CeA efferents may be influenced by stress-induced levels of corticosteroids.

Additionally, neuromodulators including those regulating the melanocortin system or opioid signalling, have been shown to affect food intake when injected into the CeA<sup>79-83</sup>.

#### *Feedback afferents from effector centres*

Finally, the CeA receives feedback inputs from the effector regions that it sends efferents to, namely, the hypothalamus<sup>84</sup> and ventro-lateral periaqueductal gray (vIPAG)<sup>84</sup> (**Figure 2**). In the hypothalamus, input cells originate from the supraoptic nucleus, ventromedial hypothalamus, lateral hypothalamus (LH), dorsomedial hypothalamus, paraventricular nucleus of the hypothalamus (PVH), parasubthalamic nucleus (PSTN), preoptic nucleus and posterior hypothalamus<sup>84</sup>. Of note, afferents from the PBN<sup>59</sup> can also be interpreted as feedback projections.

### 1.2.2. Long range efferents of the CeA

The CeA gathers sensory information from a diverse set of afferents and after complex local computations, broadcasts this information to three principal output pathways: 1) feedback projections to the sources of its sensory inputs, 2) endocrine, autonomic and motor-related outputs and 3) modulatory influence (**Figure 2**).

#### *Feedback projections*

The CeA maintains reciprocal connections with those thalamic nuclei that it receives afferents from (mostly the PVT)<sup>85</sup> (**Figure 2**). These feedback efferents suggest a function of the CeA in controlling the activity of the cortex by modulating its inputs. In addition, the CeA strongly innervates the lateral and medial part of the PBN<sup>23,86</sup> which has been proposed to modulate gustatory-evoked activity by shaping the response profiles of PBN cells<sup>87,88</sup> (**Figure 2**).

#### *Endocrine, autonomic and motor-related outputs*

The CeA sends efferents to the hypothalamus mostly in the dorsolateral part, PVH, LH and PSTN<sup>89</sup> (**Figure 2**). In the context of fear conditioning, as lesions of the LH disrupt arterial pressure<sup>90</sup>, projections from the CeA to LH have been proposed to activate the sympathetic autonomic nervous system.

Additionally, descending projections from the CeA reach the vIPAG<sup>91</sup> in the midbrain and this connection triggers conditioned-fear-induced freezing responses<sup>90,92</sup>. The CeA also projects to the rostralateral PAG which is necessary for prey-hunting behaviour<sup>93,94</sup> (**Figure 2**).

More caudally, it extends projections to the reticular formation (pontine reticular nucleus: PRN)<sup>95</sup>, a connection that has been recently shown to mediate biting attack during hunting behaviour<sup>94</sup> (**Figure 2**). Finally, projections to the nucleus of the solitary tract (NTS) (**Figure 2**) which is connected with the vagal complex (DVC)<sup>23,96</sup>, influence cardiovascular activity during emotional states<sup>97,98</sup>.

#### *Modulatory influence*

The CeA provides inputs to monoaminergic groups such as the SN<sup>99</sup> and the VTA<sup>100</sup> (dopamine), the LC<sup>99</sup> (noradrenaline) and the DR<sup>101</sup> (serotonin) (**Figure 2**). Additionally, it has outputs toward the cholinergic neurons of the VP<sup>102,103</sup> which in turn innervates large regions of the forebrain (**Figure 2**). Rather than providing a fast excitation similar to glutamatergic transmission, afferents to modulatory centres may affect information processing over large neuronal networks.

#### 1.2.3. Intrinsic connections

All nuclei of the amygdala are extensively interconnected. The most prominent amygdala's inputs to the CeA emanate from the BMA, BLA posterior (BLAp) and to a lesser extent anterior (BLAa) division<sup>104,105</sup>, the IA<sup>106,107</sup> and the postpiriform transition areas<sup>60</sup>.

Additionally, the BNST that belongs at least partially to the central extended amygdala exhibit high reciprocal connections with the CeA<sup>108</sup> (**Figure 2**).

### 1.3. CIRCUITS FOR DEFENSIVE BEHAVIOURS

Pavlovian fear conditioning is a highly replicable behavioural paradigm which has proven itself extremely powerful to study the amygdala circuits governing defensive behaviours. Conditioned animals typically exhibit a freezing behaviour (period of immobility) in response to the CS, which is the most common measured index of fear memory formation. The amygdala nuclei important in this task, the LA, BLA and CeA are a combination of cortex-like and striatum-like structures<sup>109</sup>, which raises the questions of where the memory is stored and which structures participate in the expression of the behaviour.

A widely accepted model of LA-BLA-CeA function<sup>1,109</sup> describes a serial organisation of the information flow within these nuclei. LA is considered the primary sensory input station to the amygdala, as auditory, somatosensory and nociceptive information converges in this region<sup>110,111</sup>. LA neurons project to the

BLA division and it is thought that sensory information is relayed from LA to BLA<sup>105</sup>. Both LA and BLA contact directly and indirectly via the intercalated masses CeL/C neurons, but projections from CeL/C to LA and BLA are weak or do not exist<sup>112,113</sup>. Finally, CeL/C neurons modulate the activity of CeM effector cells via monosynaptic inputs but this connection is not reciprocated<sup>102,114,115</sup>.

In this traditional yet simplified model, LA and BLA are the sites where associations between CS and US are formed to produce fear memory and the CeA is the main output centre where these associations will be turned into an appropriate behavioural response<sup>1,109</sup>. However, this network arrangement has been heavily challenged as several lines of research have now proposed that the CeA does not merely serve as an output pathway, but is also important for fear learning<sup>115,36</sup> (see below).

### 1.3.1. Acquisition of conditioned fear

#### *Synaptic plasticity and formation of CS-US associations in the LA and BLA*

There is a general agreement that LA is the primary site of synaptic plasticity for the acquisition of Pavlovian fear. According to the cellular hypothesis of auditory fear conditioning<sup>116-118</sup>, afferents carrying information about the auditory cue (CS) in the LA are weak before conditioning so the CS alone would not induce a fear response. However, after repeated exposure to tone-shock (CS-US) pairings, convergent information about the CS and US onto LA neurons would lead to enhanced strength of their excitatory synapses carrying CS information. After this Hebbian plasticity process has occurred, potentiated LA cells would be able to recruit downstream effectors of the fear response in the presence of the CS alone. As a result, the auditory cue could drive fear behaviour in the absence of the electric shock. These synaptic changes have been proposed to underlie the acquisition and storage of fear memory.

In support of this model, selective lesions of the LA disrupt the acquisition of conditioned fear<sup>5,6,119</sup>. Additionally, the use of *in vivo* recordings of single units in the LA revealed that LA neurons increase their firing rates in response to both tone and shock stimulations<sup>110</sup> providing compelling evidence that auditory (CS) and somatosensory (US) information converge onto these neurons. Finally, extracellular and intracellular recordings both *in vivo* and in slice preparations demonstrated that CS-evoked responses increase in LA after conditioning<sup>120</sup> and that LA neurons integrating inputs from auditory thalamus and somatosensory cortex present potentiation of their excitatory synapses<sup>121,122</sup>. LA neurons project to the BLA and as it was initially shown for the LA, BLA cells<sup>123</sup>, as well as CeM-projecting BLA cells<sup>124</sup>, exhibit enhancement of CS-evoked responses during fear learning.

### *Synaptic plasticity in CeA during fear learning*

Although the LA and BLA are conceptualized as the main sites of synaptic plasticity for the acquisition of Pavlovian fear, new findings support a role for the CeL/C in this process.

In their seminal work, Ciochi *et al.*,<sup>115</sup> revealed that acute inactivation of the CeL/C but not the CeM resulted in an impairment of the acquisition of conditioned freezing. This indicated that activity-dependent plasticity in the CeL/C instructs the formation of conditioned fear memory<sup>115</sup>. Following up on these findings, Li *et al.*,<sup>36</sup> showed that as a result of fear conditioning, Sst-expressing CeA neurons exhibit potentiation of their LA excitatory synapses. Notably, this synaptic plasticity can be blocked by inhibition of the posterior PVT (pPVT) which plays a role in acquisition and maintenance of fear memory<sup>125,126</sup>.

### *Formation of CS-US associations in the CeA*

Although there is no evidence of coincident occurrences of CS and US information onto single CeL/C cells, it appears that neurons in this nucleus have the necessary connections to contribute to the formation of CS-US associations. For instance, CeA neurons receive strong afferents from the IC<sup>63</sup> and PBN<sup>59</sup> that bypass the LA and may respectively carry CS and US information.

Supporting this view, inputs from the IC to CeL/C are essential to adopt an avoidance response to a cue that predicts an unpleasant taste, and optogenetic activation of this connection is sufficient to drive learning of such avoidance behaviour<sup>64</sup>.

The relevance of PBN inputs for learning about aversive events has also been recently examined. A distinct subset of IPBN neurons that express CGRP was shown to encode a pain-like signal during threat learning<sup>37</sup>. IPBN<sup>CGRP</sup> neurons strongly project to neurons in the CeL/C that express the CGRP receptor (CGRPR) and this connection was proposed to carry a US teaching signal which is sufficient to generate both context and CS dependent memories<sup>37</sup>.

In essence, these findings support the view that fear conditioning produces synaptic plasticity mechanisms that are necessary to establish a fear memory. Clearly, the necessity of a serial model of LA-BLA-CeA function is questioned as CeA plays a role in the task of fear memory acquisition and may do so in association or independently of the BLA complex.

### 1.3.2. Expression of conditioned fear

The CeA and in particular, the CeM, supply most amygdala projections to the brainstem nuclei that generate the behavioural and visceral correlates of conditioned fear<sup>23,90,118</sup>. This implies that information about the CS should be transmitted from the LA onto CeM effector cells. However, as the LA does not project to the CeM directly<sup>105,127</sup>, CS-evoked responses in LA neurons have been proposed to reach the CeM via two indirect routes. The first one involves a

projection from the BLA to the CeM and is thought to provide a glutamatergic excitation onto CeM neurons. The second one consists of GABAergic inputs from CeL/C inhibitory cells (**Figure 3** in dark blue).

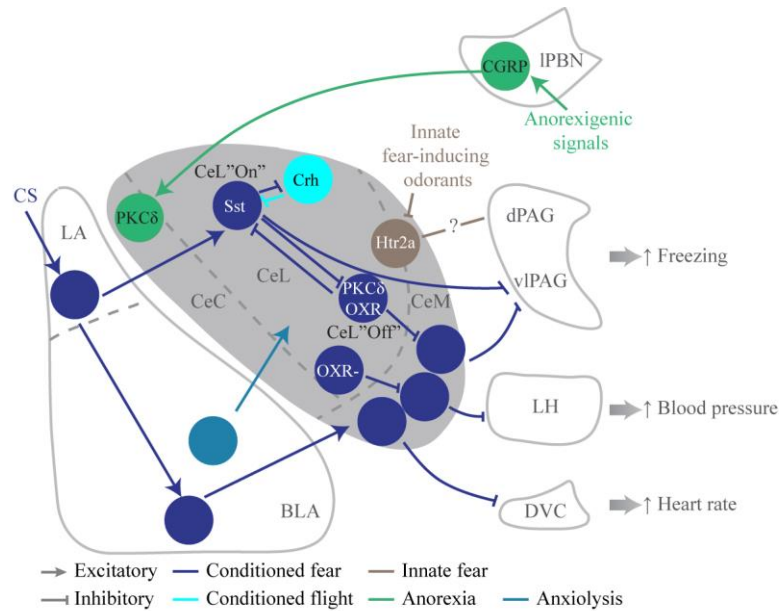


**Figure 3: Model of LA-BLA-CeA circuits for aversive behaviours including conditioned fear (dark blue), conditioned flight (cyan), innate fear (brown), anxiety (light blue), and anorexia (green).** Information about the aversive CS is relayed from LA cells onto CeM neurons by means of two different routes (dark blue). One path originates from BLA glutamatergic cells. The other involves excitation of CeL<sup>On</sup>/Sst-expressing neurons which inhibit CeL<sup>Off</sup>/PKC $\delta$ -expressing cells, therefore releasing the inhibition on CeM neurons. Increase in both CeL<sup>On</sup> and CeM neuron activities finally drives the freezing reaction via inhibition of the vIPAG. Modulation of blood pressure and heart rate occurs via projections from CeM neurons to LH and DVC respectively. In the CeL, mutual inhibition (cyan) between Sst- and Crh-expressing neurons also serves as a switch between active and passive fear responses. Alternatively, innate fear-inducing odorants inhibit the activity of Htr2a-expressing neurons (brown) which correlates with an increase in dPAG activity and innate fear behaviour, although the pathway involved remains unknown. The CeA can also mediate an anorexigenic response following exposure to cues that signal satiety or bacterial infection, a process that is dependent on projections from IPBN<sup>CGRP</sup> neurons to CeA<sup>PKC $\delta$</sup>  cells. Finally, all interactions between the LA, BLA and CeA do not merely promote aversive behaviours, as the excitation of CeL cells by BLA neurons has been shown to reduce anxiety. BLA, basolateral amygdala; CeC, central amygdala, capsular division; CeL, central amygdala, lateral division; CeM, central amygdala, medial division; DVC, dorsal vagal complex; LA, lateral amygdala; LH, lateral hypothalamus; IPBN, lateral parabrachial nucleus; dPAG, dorsal periaqueductal gray; vIPAG, ventro-lateral periaqueductal gray.

#### *From BLA to CeM*

The BLA is involved in the acquisition and expression of conditioned fear<sup>128,129</sup> and disruption of the connections between BLA and CeA abolishes conditional freezing<sup>130</sup>. Remarkably, those BLA neurons that project to the CeM specifically increase their firing rates to a CS that has been paired with an aversive event<sup>131</sup>

and optogenetic excitation of CeM-projecting BLA neurons promotes place aversion<sup>124</sup>. Together, this supports the idea that the BLA relays negative-valence information to the CeM (**Figure 3** in dark blue).

#### *CeL/C disinhibitory circuits to control CeM output*

Although CeL/C neurons have the necessary connections to control the activity of CeM effector cells<sup>102,114</sup>, they initially appear to be unlikely candidates for this function as they presumably promote inhibition of CeM neurons.

Ciocchi *et al.*,<sup>115</sup> resolved the organisation of CeL/C networks that lead to an increase of CeM firing rates. *In vivo* recordings of single units showed that in conditioned mice, exposure to the CS produces two distinct patterns of activity in CeL/C neurons. While 30% of the cells present an increase in their activity (CeL"On"), 25% show a decrease (CeL"Off"). Interestingly, the latency of activation of the CeL "On" unit was shorter than that of the inhibition of the CeL "Off" unit, indicating that CS-evoked responses first activated CeL "On" neurons, which in turn inhibited CeL "Off" cells. Additionally, CeL/C unidirectionally project to CeM and about 80% of CeM neurons exhibited an increase in their CS-evoked excitability after conditioning. This series of experiments support a model in which conditioned fear responses arise following activation of CeL "On" neurons which in turn inhibit the CeL "Off" unit. In the basal condition, CeL "Off" neurons tonically inhibit CeM output cells, so inhibition of CeL "Off" cells facilitates CS-evoked fear responses in CeM neurons through disinhibition (**Figure 3** in dark blue).

In an accompanying study, Haubensak *et al.*,<sup>32</sup> demonstrated that CeL"Off" unit corresponds to PKC $\delta$ -expressing neurons (**Figure 3** in dark blue). They showed that CeA<sup>PKC $\delta$</sup>  neurons represent the majority of the CeL/C cells that project to the CeM and, using channelrhodopsin-assisted circuit mapping technique<sup>132</sup>, revealed that they monosynaptically inhibit PAG-projecting CeM neurons. More importantly, inhibition of PKC $\delta$ + cells during the retrieval of fear memory strongly reduces the tonic activity of the CeL "Off" unit but did not affect CeL "On" cells. Consistent with this, PKC $\delta$ + neurons express the oxytocin receptor<sup>32</sup> and release of endogenous oxytocin in the CeL/C reduces conditioned freezing<sup>133</sup>.

The question of how information about the CS is conveyed onto CeL"On" neurons was addressed by a different group who found that LA neurons form functional excitatory synapses on CeA<sup>Sst</sup> cells<sup>36</sup>. In particular, not only fear conditioning enhances synaptic drive onto Sst+ at the level of LA synapses, but this experience-dependent synaptic plasticity may also be the neuronal substrate of fear memory<sup>36</sup>. Indeed, reversible silencing of Sst+ neurons in CeA during the acquisition phase of fear conditioning resulted in an attenuation of conditioned freezing, while optogenetic activation of the same neurons elicited unconditioned freezing behaviour<sup>36</sup>. Additionally, CeL/C<sup>Sst</sup> neurons do not project to the CeM and do not monosynaptically inhibit CeM neurons that project to the PAG<sup>36</sup>, in agreement with the model that PKC $\delta$ + neurons are the source of inhibition onto CeM outputs. Complementing these findings, Sst+ neurons were recently shown<sup>134,135</sup> to exhibit elevated firing rates to the CS which together, supports the

notion that Sst+ neurons correspond to the CeL "On" unit<sup>1,2</sup> (**Figure 3** in dark blue).

Nonetheless, this model was recently disputed by Kim *et al.*,<sup>25</sup> who disproved that CeA<sup>Sst</sup> neurons are mediators of the fear response. They proposed an alternative view, in which CGRPR+ in the CeC and PKC $\delta$ + neurons in the CeL represent the opposing CeL "On" and CeL "Off" units. In fact, consistent with CeL "ON" unit properties, CGRPR+ neurons elicit and are required for defensive behaviours and are activated by stimuli that promote defensive behaviours<sup>25</sup>.

#### *From CeA to hypothalamic, midbrain and brainstem structures*

The CeM is generally regarded as the main output station for the expression of conditioned fear as CeM projection neurons innervate various structures in the hypothalamus and brainstem that are thought to orchestrate the endocrine, autonomic and motor-related aspects of the fear response<sup>23,90,118</sup>. These efferents include projections to the vPAG which mediate the fear-induced freezing response<sup>90,92</sup>, to the DVC which modulates cardiovascular response<sup>97,98</sup>, and the LH which affects blood pressure<sup>90</sup> (**Figure 3** in dark blue). Remarkably Viviani *et al.*,<sup>98</sup> showed that CeM neurons projecting to two different brainstem nuclei are contacted by molecularly distinct CeL/C populations. Indeed, CeM cells that project to the PAG receive afferents from oxytocin receptor-expressing neurons, while CeM neurons projecting to the DVC are innervated by oxytocin receptor negative neurons (**Figure 3** in dark blue). Although CeM projections are more prominent, CeL/C neurons also innervate these structures<sup>102,103,136</sup>, and CeL/C efferents to the PAG (**Figure 3** in dark blue) and PVT exhibit synaptic plasticity as a result of fear conditioning<sup>137</sup>, indicating that projection neurons in the CeL/C may take part in the execution of the fear response.

In summary, here I describe two routes that lead to an increase in CeM neuron excitability, and involve excitatory inputs from BLA cells and disinhibitory inputs from CeL/C networks. Of note, one study has provided preliminary data that BLA neurons that excite CeM cells are distinct from BLA neurons that contact CeL/C cells<sup>138</sup>. Finally, the latest evidence revises the view of the CeM as the primary output station of the amygdala and indicates that distinct parallel routes from the CeM and CeL/C may contribute to fear related-behaviours<sup>137</sup>.

#### *Passive versus active fear responses*

The most common readout of fear conditioning is a freezing reaction which is defined as a passive response to an imminent and predictable threat. Nonetheless, rodents can display a diverse array of behavioural strategies depending on the proximity and intensity of the threat, such as an active escape response.

To study whether the expression of passive and active defensive responses engage the same cellular substrates in the CeA, Fadok *et al.*,<sup>134</sup> established a conditioning paradigm in which mice show a freezing response to a tone and an escape response (flight) to a white noise. Consistent with the properties of the CeL "On" unit, they found that Sst+ neurons were activated concomitantly to the freezing response but were surprisingly inhibited during the flight response.

What inputs may be responsible for this phenomenon? *In vivo* single unit-recording revealed that Crh+ neurons exhibited a preferential excitability rate during the flight response, while their activity was suppressed during the freezing response. Moreover, optogenetic inhibition of Crh+ neurons but not PKC $\delta$ + or Sst+ neurons abolished the conditioned flight behaviour, while photoactivation of these neurons was sufficient to switch the behavioural response from passive freezing towards escape defensive behaviour. Crh+ and Sst+ neurons were found to mutually inhibit each other - a circuit mechanism that could allow a shift between different behavioural programs<sup>134,135</sup> (**Figure 3** in cyan).

### 1.3.3. Beyond conditioned fear in the CeA

Fear conditioning has been extensively used to decipher the circuits underlying associative learning. Yet, fear responses can be innate and are thought to engage distinct circuits in the CeA. Additionally, when fear is generated in response to a stimulus that does not predict an aversive outcome, we refer to fear generalization; a defining feature of anxiety disorders. Finally, as animals show defensive behaviours in front of a predator, they are able to show similar avoidance responses to a potentially poisonous substance. Below, I will describe how genetically distinct populations of CeA neurons play critical roles in the aforementioned aversive states.

#### *Innate fear*

Predators or aggressive members of the same species can promote defensive behaviours which do not depend on past experience of the animal. These innate fear-induced cues can be experienced at the same time as learned fear-induced cues, raising the question of how these two stimuli compete at the level of the amygdala. Isosaka *et al.*,<sup>38</sup> modelled a natural situation in which food-deprived mice choose between overcoming their innate fear or learned fear in order to get a food reward. Learned fear was induced using a traditional fear conditioning paradigm in which the animal learned that an odour (CS) predicted an electrical shock (US) while innate fear was elicited using an optimised version of the TMT compound, a component of fox faeces. In this paradigm, mice choose to get exposed to the learned fear-induced odour rather than the innate fear-induced one, in order to approach and consume a food reward, indicating that innate fear could be prioritized over learned fear. A combination of immediate-early gene expression analysis, reversible inactivation of the CeA and drug screenings revealed that Htr2a+ neurons in the CeA might be involved in regulating the hierarchy between learned and innate fear behaviours. In fact, optogenetic inhibition of CeA<sup>Htr2a</sup> neurons resulted in an increase in the innate fear response but in a decrease in learned fear while photoexcitation of these neurons promoted the opposite behaviour. Monitoring CeA<sup>Htr2a</sup> neuron activity using the GCAMP signal as a proxy showed that CeA<sup>Htr2a</sup> neuron activity is inhibited by innate odorants only. This led to the conclusion that downregulation of CeA<sup>Htr2a</sup> neuron activity induces an increase in innate fear behaviour and a decrease in learned-

fear behaviour (**Figure 3** in brown) suggesting that a population of CeA neurons can act as a hierarchy generator between defensive responses. Subsequent experiments revealed that while the learned-freezing response is modulated by the vPAG, the innate-freezing response is controlled by the dorsal PAG (dPAG) and that inhibition of CeA<sup>Htr2a</sup> neurons induces an upregulation of immediate early gene expression in the dPAG. As anatomical connections between CeA<sup>Htr2a</sup> neurons and dPAG have not been investigated yet, the circuit leading to dPAG increase in activity remains unresolved.

### *Anxiety*

Because mice feel anxious in open spaces, anxiety is commonly studied in laboratories by measuring the time spent in the open arms of the elevated-plus maze (EPM) and the centre of the open-field (OF)<sup>139</sup>. To investigate the contribution of the BLA to CeA projections in anxiety-related behaviours Tye *et al.*,<sup>138</sup> optogenetically activated the axonal projections of BLA neurons in the CeL during EPM and OF tests. As a result, mice spent more time in the OF and the probability of open-arm entry from the maze centre was increased. Thus glutamatergic excitation of CeL neurons by BLA cells not only mediates conditioned fear expression, but can also produce an anxiolytic effect (**Figure 3** in light blue). Tye *et al.*, attributed this effect to feed-forward inhibition of CeM cells by CeL neurons.

Anxiety disorders can also be interpreted as a consequence of fear generalization in which the discrimination between a CS that has been paired with a US (CS+) and a non-paired CS (CS-) is strongly diminished. Following the idea that fear generalization is associated with an increase in tonic activity of PKC $\delta$ + neurons<sup>115</sup> Botta *et al.*,<sup>140</sup> revealed that optogenetic activation of CeA<sup>PKC $\delta$</sup>  neurons during the retrieval of fear memory leads to an increase in the ratio of freezing to CS-/CS+. Photoactivation of PKC $\delta$ + neurons also decreased the time spent in the open arm of an EPM and in the centre of the OF. Thus in the CeA, two populations of neurons<sup>138,140</sup> coexist that modulate anxiety-related behaviours in opposite directions. Further experiments will be needed in order to define how they interact.

### *Anorexia*

The consumption of appropriate food is contingent to an organism's survival. Thus, animals learn to associate the physical properties of a substance (taste, texture, odour and colour) with contextual and spatial environmental cues and the gustatory consequences of its consumption. They are then capable of using these cues during foraging to guide them to approach or avoid certain substances.

Lithium chloride (LiCl) is an agent that, when administered to rodents, mimics the consumption of bacterial toxins and promotes anorexia<sup>40</sup>. CGRP+ neurons in the IPBN have been found to mediate the effect of this anorexigenic agent<sup>57</sup>. IPBN<sup>CGRP</sup> neurons are activated by LiCl, and optogenetic activation of these neurons strongly suppresses food intake. Interestingly, while pharmacogenetic

inhibition of these cells does not affect food consumption in basal conditions, it does significantly overcome the anorexigenic effect of LiCl injection.

When investigating the relevant connections mediating this behaviour, Palmiter and colleagues observed dense IPBN<sup>CGRP</sup> innervations in the CeC. Furthermore, both selective activation and inhibition of IPBN<sup>CGRP</sup> projections in the CeA recapitulated the behaviour observed during functional manipulation of whole CGRP+ cell bodies (**Figure 3** in green).

The molecular identity of CeA cells mediating this behaviour was identified in a later study<sup>141</sup>. Cai *et al.*, showed that CeA<sup>PKCδ</sup> neurons integrate multiple anorexigenic signals and lie downstream of IPBN<sup>CGRP</sup> neurons (**Figure 3** in green). Consistent with the study of Carter *et al.*,<sup>57</sup> optogenetic activation of PKCδ+ neurons dramatically reduces food consumption, while pharmacogenetic inhibition of their activity is sufficient to rescue the effect of LiCl injection. CeA<sup>PKCδ</sup> efferents can be seen within the CeA itself and the BNST, but only reversible inactivation of whole CeA activity suppresses the inhibitory influence of CeA<sup>PKCδ</sup> activity upon food intake. This suggests that CeA<sup>PKCδ</sup> neurons may exert their influence on feeding via inhibition of a distinct population in the CeA. Consistent with these findings, functional manipulation of PKCδ-negative neurons in the CeA triggered, at least partially, an opposite behaviour on food intake.

As such, the literature to date suggests that a projection from IPBN<sup>CGRP</sup> neurons to CeA<sup>PKCδ</sup> neurons mediates feeding stop anorexia and malaise when eating conditions are unfavourable. In addition to IPBN inputs, Cai *et al.*, demonstrated that CeA<sup>PKCδ</sup> cells are innervated by IC and BLA. Convergence of inputs from these regions may serve for CS-US associations in the CeA as described in the introduction (1.3.1. Acquisition of conditioned fear) and thus promote learning that specific tastes are intrinsically aversive.

In conclusion, recent findings have substantially extended our knowledge of the CeA's functions and argue in favour of the existence of multiple parallel inhibitory circuits that regulate distinct behaviours related to aversive states.

#### 1.4. REPRESENTATION OF REWARD IN THE AMYGDALA

Over the past decades, the dominance of fear conditioning as a model to study associative learning biased the view that the amygdala primarily plays a role in fear learning. The role of the amygdala in processing positive affect came to light when the same lesions previously known to prevent conditioned responses to fear-predicting cues were also found to impair learning that a conditioned stimulus signals a rewarding outcome<sup>8,142-146</sup>.

Classical Pavlovian appetitive conditioning in which the animal learns that a conditioned stimulus (CS) predicts a reward (US) is one paradigm that is commonly used in many laboratories. The observed behaviours involve consummatory conditioned responses that are associated with the US such as

chewing, licking and approach to the food cup, in the case of a food reward. Conditioned responses that are independent of the nature of the reinforcer but are associated with the CS, such as rearing, orientation, or startle represent preparatory responses<sup>8,147</sup>. In a different setting referred as operant or instrumental conditioning, the animal learns to actively perform a task, typically press a lever or nose poke, in order to receive a reinforcer (reward). The resulting behaviours can be divided into two different phases: the approach and nose poking behaviours, which belong to the appetitive phase; and the consummatory phase of food intake.

Current evidence suggests that both the BLA and CeA are involved in these two paradigms<sup>8</sup>. However, in contrast to studies of aversive learning that rely on a serial model of BLA and CeA function, studies of reward-based behaviours suggest that these two nuclei operate in parallel to control distinct aspects of emotional learning<sup>8</sup>. For example, in the Pavlovian appetitive conditioning situation, while lesions of the BLA specifically impair consummatory responses, lesions of the CeA produce a deficit in the acquisition of preparatory responses without affecting consummatory behaviours<sup>8,142-146</sup> (**Figure 4**).

#### 1.4.1. Encoding of reward stimuli in the CeA

Early lesion studies supported a role for the CeA in preparatory conditioning and proposed that it encodes a general representation of the motivational properties of the reinforcer<sup>8,142,145,148</sup>.

Modern studies that capitalized on the temporal specificity of optogenetics have refined the role of this region in producing pleasure and reward. Robinson *et al.*,<sup>149</sup> followed by Warlow *et al.*,<sup>150</sup> have recently demonstrated that pairing optogenetic activation of the CeA with earning one reward increases the motivation to work for this particular reward over another equal one in a two choice instrumental conditioning paradigm. Interestingly, CeA photostimulation on its own was not positively reinforcing and had no effect in the absence of the external reward, indicating that the observed behaviour could not be attributed to a general increase in the motivational state. Therefore the CeA was proposed to function by increasing the incentive value of an external reward<sup>149,150</sup>, a process that could be mediated by connections with the ventromedial-prefrontal cortex (vmPFC)<sup>151</sup> (**Figure 4**).

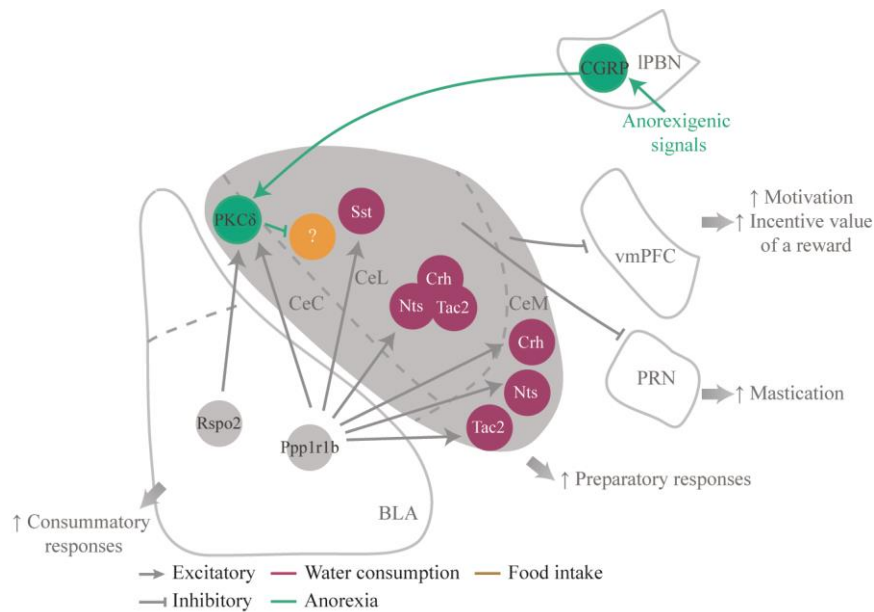


**Figure 4: Model of CeA's function in appetitive behaviours.** During an appetitive task, the BLA controls consummatory responses while the CeA is essential for the preparatory tasks. The CeA acts by increasing the motivation to work for a particular reinforcer through amplifying its incentive value; a phenomenon that appears to be dependent of CeA projections to the vmPFC. Nonetheless, a role for the CeA in the consummatory phase of appetitive behaviours cannot be ruled out, as projections to the PRN were found to promote mastication. Additionally, the CeA harbours populations of valence-selective neurons. Indeed, appetitive cues, such as food and water, drive excitation of  $CeL^{Sst}$  and  $CeL^{Crh,Nts,Tac2}$  as well as  $CeM^{Nts}$ ,  $CeM^{Sst}$  and  $CeM^{Tac2}$  neurons whose activity is intrinsically rewarding and critical for water consumption (in bordeaux). On the contrary,  $CeC^{PKC\delta}$  neurons encode negatively valenced information and their anorexigenic function (in green) occurs via inhibition of a population of  $PKC\delta$  negative neurons suggesting that an unidentified population of CeA neurons might promote food intake (in orange). All functionally defined CeA populations receive monosynaptic inputs from positively-valenced  $BLA^{Ppp1r1b}$  neurons while negatively valenced  $BLA^{Rspo2}$  neurons selectively target  $CeC^{PKC\delta}$  cells. BLA, basolateral amygdala; CeC, central amygdala, capsular division; CeL, central amygdala, lateral division; CeM, central amygdala, medial division; vmPFC, ventromedial-prefrontal cortex; PBN, lateral parabrachial nucleus; PRN, pontine reticular nucleus.

Although these studies made it clear that the CeA can intensify the motivation to work for a reward during the preparatory phase, they do not completely rule out the possibility that it might also provide a motor output for the consumption of this reward. Possible evidence for a role of the CeA in the consummatory phase comes from a study on hunting behaviour<sup>94</sup>. CeA coordinates cervical and mandibular musculatures via projections to the PRN, and optogenetic activation of CeA axons in this nucleus elicits fictive feeding behaviour and sustained mastication, although it does not promote food consumption (**Figure 4**). Thus, the CeA appears to have the necessary connections to control food intake. Whether this connection plays a role in the consummatory phase of appetitive learning, nonetheless, remains to be addressed.

#### 1.4.2. Populations of valence-selective neurons in the CeA

The finding that the CeA can mediate both appetitive and aversive behaviours raises the question of how this region processes stimuli of opposite valence. A simple hypothesis relies on the existence of valence selective neurons in the CeA so that neurons that are excited by reward-predicting cues do not respond to fear-predicting cues and vice versa.

One of the initial indications of a segregation of positive- and negative-valence signals in the CeA came from a study<sup>152</sup> that took advantage of the distinct time courses of c-fos mRNA and c-fos protein production to visualize, in the same animal, CeA cells that have been activated by two distinct cues. Using this experimental setup, Xiu *et al.*,<sup>152</sup> were able to show that CeA neurons that respond to appetitive and aversive cues are segregated in different parts of the CeA.

Yet, the work of Cai *et al.*,<sup>141</sup> on cessation of appetitive behaviour provided the first clues for the existence of a distinct subset of CeA neurons that positively regulate appetitive behaviour. As described earlier, (1.3.3. Beyond conditioned fear in the CeA) Cai *et al.*, demonstrated that signals conveying visceral malaise, nausea and satiety converge on CeA<sup>PKC $\delta$</sup>  neurons causing strong anorexia (**Figure 4**, in green). When probing the output targets responsible for this effect, they found that inhibition of a population of PKC $\delta$  negative neurons was responsible for the anorexigenic function of CeA<sup>PKC $\delta$</sup>  cells, suggesting that an unidentified population of CeA neurons may exert an opposite influence on food intake (**Figure 4**, in orange).

Building on these results, Kim *et al.*,<sup>25</sup> screened seven molecularly and spatially defined groups of CeA cells for their role in promoting appetitive behaviours. Functional characterization of these clusters using a combination of c-fos expression and optogenetic stimulation and inhibition, confirmed that PKC $\delta$ + neurons encode negative-valence information although their function might differ depending on their location in the CeA. Whereas CeC<sup>PKC $\delta$</sup>  are responsible for driving defensive behaviours, PKC $\delta$  neurons located in the CeL seem to act as inhibitors of appetitive behaviours. More importantly, they could identify subsets of CeA cells that are positive mediators of appetitive behaviours. Specifically, CeL<sup>Sst</sup> and CeL<sup>Crh,Nts,Tac2</sup> as well as CeM<sup>Nts</sup>, CeM<sup>Sst</sup> and CeM<sup>Tac2</sup> (**Figure 4**, in pink) respond to appetitive cues such as food and water. Their activity is intrinsically rewarding, as it can elicit self-reinforcement and is needed for drinking behaviour. Which brain structures may provide CeA cells with rewarding information? Kim *et al.*, laid groundwork by suggesting that valence selective neurons of the BLA<sup>153</sup> unequally project onto positive- and negative-valence CeA neurons. While positively valenced BLA<sup>Ppp1r1b</sup> neurons can monosynaptically excite all populations of CeA neurons, negatively valenced BLA<sup>Rsp02</sup> cells specifically contact CeC<sup>PKC $\delta$</sup>  neurons (**Figure 4**).

In conclusion, in addition to gating the acquisition and expression of conditioned fear, the CeA plays a role in modulating appetitive behaviours possibly by increasing the “wanting” of a reward. Whether the positive mediators of appetitive behaviours identified by Kim *et al.*, work in a similar fashion, remains

to be investigated. Finally, in contrast to the work carried out on aversive conditioning, very little is known about how rewarding information flows within the CeA. This includes the identity of the inputs that trigger an increase in activity of positive-valence CeA neurons as well as the underlying downstream structures mediating CeA function in appetitive behaviours.

### 1.5. MONOSYNAPTIC CIRCUIT TRACING USING RECOMBINANT RABIES VIRUS TECHNOLOGY

The finding that distinct groups of neurons encode signals of opposite valence in the CeA naturally leads to the question whether these populations are integrated into segregated circuits. Although a certain degree of overlap can be expected in the CeA microcircuits, identifying the pattern of inputs to functionally distinct neurons might help to predict whether they are likely to mediate rewarding or aversive behaviour. Hence, a critical step toward understanding the logic in CeA circuits is to identify the monosynaptic local and long-range inputs that target positive- and negative-valence neurons.

Conventional tracing approaches have provided valuable data regarding the organisation of connections between CeA and other brain regions. However, such methods do not allow insights into the cell-type specific connectivity profiles. Recently, the development of genetically modified rabies viruses (RABV) for the mapping of inputs to genetically defined neurons has overcome this problem<sup>154</sup>.

Wild-type RABV is a negative strand RNA virus that, when injected into the nervous system, has the ability to spread in the retrograde direction across multiple synapses; a process that is largely dependent on its glycoprotein G<sup>155</sup>. G is not necessary for the replication of the genome, nor for the transcription of the viral genes, but is required for transsynaptic spread of the viral particles. It is embedded into the membrane of the host cells and mediates budding of the viral particles out of the host cells<sup>155</sup>. Therefore, the surface of the RABV is coated with G, which determines its neurotropism and allows it to infect presynaptic nerve terminals via the G receptors<sup>155</sup>.

The development of RABV that lack their G protein (RABVΔG) has been a very important advance for studying neuronal connections, as the absence of G restricts the spread of the viral particles to one synapse only, and in the meantime allows their pseudotyping with an alternative envelope protein<sup>156</sup>. RABVΔG are usually pseudotyped with the envelope protein A (EnvA) from the avian leukosis virus, which is the direct ligand of the TVA receptor. Importantly, mammalian cells do not express TVA, permitting selective infection of EnvA-pseudotyped-RABVΔG by neurons engineered to express TVA<sup>156</sup>.

Rabies virus-based monosynaptic tracing to genetically defined populations of neurons was first established by the group of Edward Callaway<sup>154</sup>. This strategy has been extensively used for tracing the connections to single neurons<sup>157</sup>, to newborn cells<sup>158</sup>, to genetically identified cell types using Cre driver lines<sup>32,159,160</sup>,

and to cell types defined by their projection pattern<sup>161</sup>. Although different approaches can be used, typically, an adeno-associated virus (AAV) helper virus is injected in the region of interest where it induces the production of G, TVA and mCherry in the population of interest (starter cells)<sup>156</sup> (**Figure 5**). Following sufficient expression of the gene products, GFP-expressing EnvA-pseudotyped RABV $\Delta$ G is injected in the same location where it infects TVA-expressing starter cells (**Figure 5**). After multiplication in the starter cells, the presence of G permits the budding of new viral particles that have G on their surface, and their transsynaptic transport toward the input neurons (**Figure 5**). Since the RABV $\Delta$ G is not able to spread in the absence of G, the virus does not spread any further. As a result, input cells that express GFP only (green) are easily distinguishable from starter cells that are both mCherry<sup>+</sup> and GFP<sup>+</sup> (yellow) (**Figure 5**).

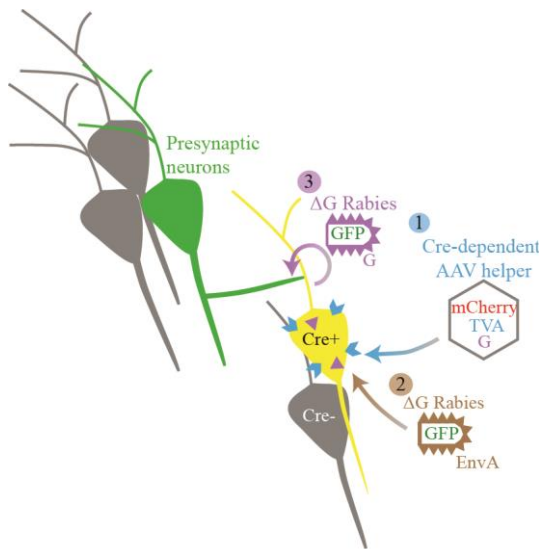


**Figure 5: Cre-dependent rabies virus-based monosynaptic tracing.** At first (1), an AAV helper virus is injected in the region of interest of a mouse that expresses Cre in a specific cell type. This virus is Cre dependent so the production of the G protein of the rabies virus, the TVA receptor, and the mCherry protein is induced in Cre<sup>+</sup> cells only. A few weeks later (2), neurons in the same region are transduced with a modified rabies virus in which the DNA sequence of the G protein is replaced by GFP (RABV $\Delta$ -GFP), and which is additionally pseudotyped with the EnvA protein, so that it can only infect the TVA-expressing cells (starter cells). RABV $\Delta$ -GFP replicates in the starter cells and trans-complementation with G allows production of new viral particles

that can spread toward the input neurons in which they drive the expression of GFP (3). However, as G is absent in the presynaptic cells, RABV $\Delta$ -GFP spreading is monosynaptically restricted. As a result, starter neurons express both mCherry and GFP (yellow), and presynaptic partners express GFP only (green).

## 1.6. AIM OF THE STUDY

The encoding of positive stimuli such as the circuits leading to the expression of appetitive behaviours are still largely unknown in the CeA. Cai *et al.*,<sup>141</sup> have recently proposed that activation of a population of PKC $\delta$ -negative CeA neurons promotes feeding behaviour (**Figure 4**). Later, Kim *et al.*,<sup>25</sup> showed that Sst+ cells among others, contribute to appetitive behaviours (**Figure 4**). However, studies to date have failed to identify the specific neuronal players and associated circuits that orchestrate feeding behaviour.

In collaboration with Amelia M. Douglass and Hakan Kucukdereli, I identified a population of PKC $\delta$  negative CeA neurons that express the Htr2a receptor. Activation of these cells promotes food consumption and is inherently rewarding. Investigating the mechanisms underlying these behaviours revealed that direct inhibition of the PBN by CeA<sup>Htr2a</sup> neurons accounted at least partially for the function of these cells.

The concept that different subsets of CeA neurons mediate opposite behaviours raises the question whether these cell units are incorporated into different circuits. Moreover, the mechanisms regulating CeA<sup>Htr2a</sup> neuron firing depending on the behavioural contexts remain to be explored.

Previous studies have identified the patterns of afferents and efferents of CeA neurons (1.2. A functional overview of CeA afferents and efferents) However, the use of conventional tracing approaches has precluded a full characterization of cell-type-specific connectivity patterns.

The aim of my thesis was to study the organisation of CeA local networks and to identify the neuronal players upstream of CeA<sup>Htr2a</sup>, CeA<sup>PKC $\delta$</sup>  and CeA<sup>Sst</sup> neurons using monosynaptic retrograde transsynaptic tracing based on a modified rabies virus. I intended to answer the following questions: first of all, do CeA<sup>Htr2a</sup> neurons overlap with other functionally described CeA units; how do they interact with these units; and how does this integrate with what is known to date about the circuits mediating aversive and appetitive behaviours in the CeA. I then wished to identify brain-wide putative sources of excitatory inputs that would account for an increase in CeA<sup>Htr2a</sup> activity during food intake. As they function via inhibition of the PBN, I wanted to study whether PBN-projecting CeA<sup>Htr2a</sup> neurons integrate a specific subset of these inputs. Finally, based on the pattern of their monosynaptic inputs, I hoped to shed light on the question of whether CeA<sup>Htr2a</sup> neurons may have the necessary connections required to mediate learning that environmental stimuli predict a rewarding outcome, or whether they simply act as effectors of the appetitive tasks.



## 2. RESULTS



### 3.1. PHENOTYPIC CHARACTERIZATION OF $CEA^{HTR2A}$ NEURONS

#### 3.1.1. Molecular profile of $CeA^{Htr2a}$ neurons

As an initial step toward dissecting the circuitry through which  $CeA^{Htr2a}$  neurons regulate food consumption, I investigated the overlap of  $Htr2a+$  cells with other functionally-defined populations of  $CeA$  neurons namely,  $PKC\delta^{+25,32,140,141}$ ,  $Sst^{+25,36,134}$ ,  $Tac2^{+25,141}$  and  $Crh^{+25,134,141}$ .

To gain genetic access to  $Htr2a+$  neurons, *Htr2a-Cre* mice, in which Cre is selectively expressed in the  $CeA$ , were crossed with a *LacZ* or *tdTomato* reporter line to identify Cre+ cells. First, Cre expression was compared with that of endogenous  $Htr2a$  using *in situ* hybridization for *LacZ* and  $Htr2a$  mRNA.  $86.6\% \pm 4.5\%$  of  $LacZ+$  cells contained  $Htr2a$  mRNA, confirming that Cre expression recapitulated the pattern of endogenous  $Htr2a$  expression in the  $CeL/C$  (**Figure 6a, b and g**).

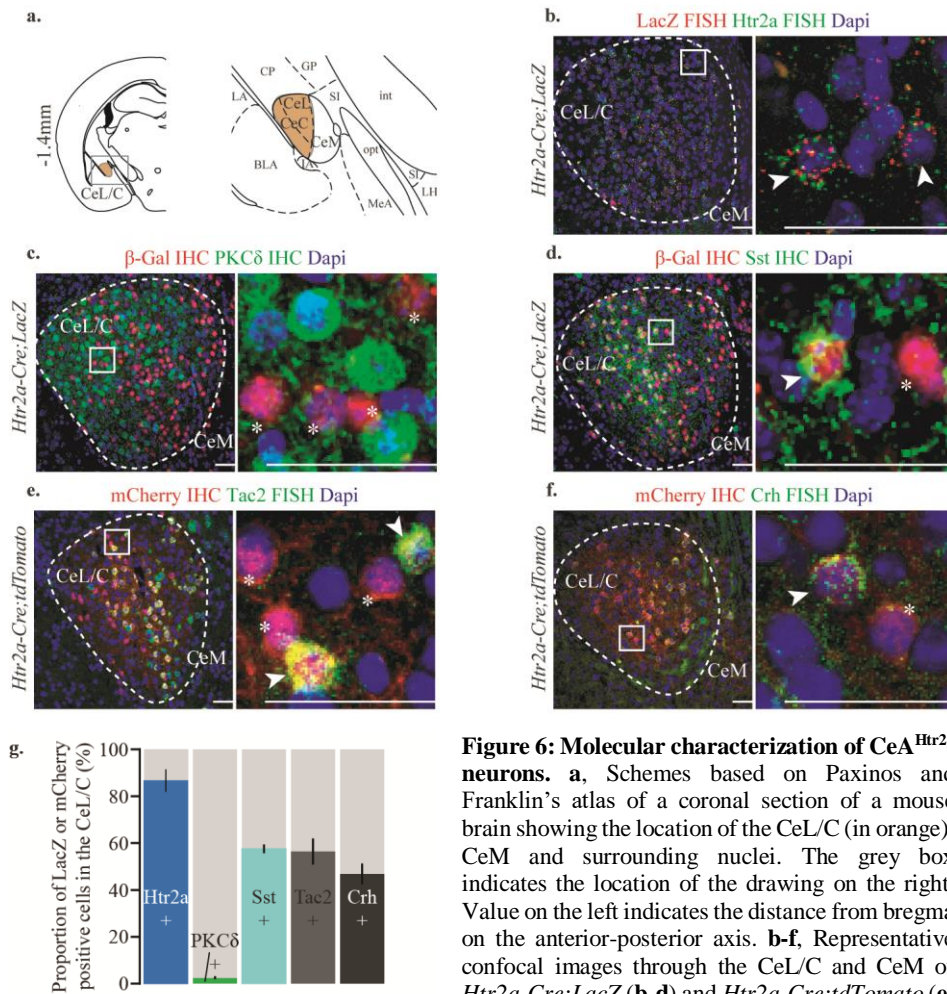


**Figure 6: Molecular characterization of  $CeA^{Htr2a}$  neurons.** **a**, Schemes based on Paxinos and Franklin's atlas of a coronal section of a mouse brain showing the location of the  $CeL/C$  (in orange),  $CeM$  and surrounding nuclei. The grey box indicates the location of the drawing on the right. Value on the left indicates the distance from bregma on the anterior-posterior axis. **b-f**, Representative confocal images through the  $CeL/C$  and  $CeM$  of *Htr2a-Cre;LacZ* (**b-d**) and *Htr2a-Cre;tdTomato* (**e-f**).

f) mice labelled for LacZ and Htr2a mRNAs (b),  $\beta$ -Gal and PKC $\delta$  proteins (c),  $\beta$ -Gal and Sst proteins (d), mCherry protein and Tac2 mRNAs (e) and mCherry protein and Crh mRNA (f) (each representative of 3 mice). White boxes indicate the location of the high-magnification panel on the right. White arrowheads indicate double positive cells. Asterisks indicate neurons expressing only LacZ (b-d) or tdTomato (e-f). g, Proportion of LacZ<sup>+</sup> or mCherry<sup>+</sup> neurons in the CeL/C co-expressing Htr2a, PKC $\delta$ , Sst, Tac2 and Crh markers (n = 3 mice per marker). CeL/C, central lateral and capsular amygdala; CeM, central medial amygdala; BLA, basolateral amygdala; CP, caudoputamen; GP, globus pallidus; int, internal capsule; LA, lateral amygdala; LH, lateral hypothalamus; MeA, medial amygdala; opt, optic tract; SI, substantia innominate. Bar graphs show mean  $\pm$  SEM. Scale bars: 50  $\mu$ m.

Next, immunohistochemistry and, or *in situ* hybridization methods were used to evaluate colabelling of Cre<sup>+</sup> cells with PKC $\delta$ <sup>+</sup>, Sst<sup>+</sup>, Tac2<sup>+</sup> and Crh<sup>+</sup> neurons. Quantifications indicated that CeL/C<sup>Htr2a</sup> neurons show minimal overlap with CeL/C<sup>PKC $\delta$</sup>  neurons as only 2.4%  $\pm$  0.4% of Htr2a<sup>+</sup> cells express the PKC $\delta$  protein (Figure 6c and g). This result is consistent with the data from another study<sup>38</sup>. 57.5%  $\pm$  1.4% of CeL/C<sup>Htr2a</sup> neurons express the Sst protein (Figure 6d and g), which is lower than previously described<sup>38</sup>. A similar degree of overlap was also observed with Tac2<sup>+</sup> and Crh<sup>+</sup> neurons as 56.4%  $\pm$  5.1% of Htr2a<sup>+</sup> are Tac2<sup>+</sup> (Figure 6e and g) and 46.8%  $\pm$  4.0% of Htr2a<sup>+</sup> neurons are Crh<sup>+</sup> (Figure 6f and g) in the CeL/C.

These data indicate that CeL/C<sup>Htr2a</sup> cells are distinct from CeL/C<sup>PKC $\delta$</sup>  aversive population but are comprised of subsets of Sst<sup>+</sup>, Tac2<sup>+</sup> and Crh<sup>+</sup> neurons which have been previously described to mediate appetitive behaviours<sup>25</sup>. The following experiments focus on CeA<sup>Htr2a</sup>, CeA<sup>PKC $\delta$</sup>  and CeA<sup>Sst</sup> populations only.

### 3.1.2. Spatial segregation of CeA<sup>Htr2a</sup> and CeA<sup>PKC $\delta$</sup> neurons

Along with the functional diversity of CeA cellular units, a recent study has pointed out a functional distinction between the capsular part and the lateral part of the CeA<sup>25</sup>, which might additionally exhibit a distinct underlying connectivity profile, at least with regards to their inputs from the parabrachial nucleus (PBN)<sup>59</sup>.

This encouraged me to analyse the spatial distribution of Htr2a<sup>+</sup>, PKC $\delta$ <sup>+</sup> and Sst<sup>+</sup> neurons in the CeL/C of an *Htr2a-Cre;LacZ* mouse. Digital recognition of cell bodies was done of neurons immunolabelled for LacZ (as a marker for Htr2a<sup>+</sup> neurons), PKC $\delta$  and Sst proteins (Figure 7a). However, poor staining for Sst protein precluded digital reconstruction of Sst<sup>+</sup> cell bodies and for this reason, only the 3D coordinates of Htr2a<sup>+</sup> and PKC $\delta$ <sup>+</sup> cells could be extracted (Figure 7b).

Although the distribution profiles suggested that PKC $\delta$ <sup>+</sup> and Htr2a<sup>+</sup> neurons were evenly distributed along the rostro-caudal (Figure 7c, f and g) and dorso-ventral axes (Figure 7d, f and g), analysis of the lateral-medial distribution revealed that PKC $\delta$ <sup>+</sup> neurons were confined toward the lateral part of the CeA (*i.e.* CeC nucleus) (Figure 7e-g). This is consistent with previously published studies demonstrating that CGRP-expressing neurons of the lateral PBN (IPBN)

specifically project onto PKC $\delta$ + neurons in the CeC<sup>141,37,25</sup>. Htr2a+ neurons, on the other hand, were located more medially (*i.e.* CeL division) (**Figure 7e-g**), suggesting that these two populations might receive different types of sensory information.

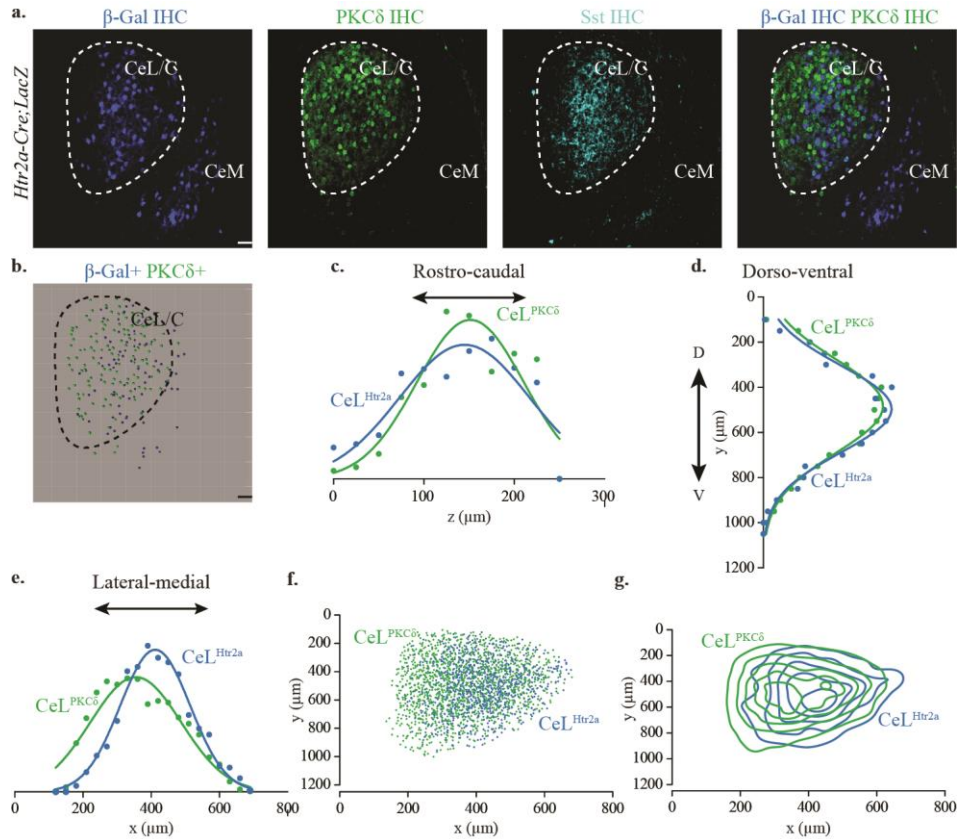


**Figure 7: Spatial distribution of CeL/C<sup>Htr2a</sup> and CeL/C<sup>PKC $\delta$</sup>  neurons.** **a**, Confocal images through a coronal plane of the CeL/C and CeM of an *Htr2a-Cre;LacZ* mouse brain immunostained for  $\beta$ -Gal as a marker for Htr2a-Cre+ neurons, and PKC $\delta$  and Sst proteins. **b**, Corresponding digital reconstruction of Htr2a+ (blue dots) and PKC $\delta$ + (green dots) cell bodies of the CeL/C shown in **a**. **c-e**, Frequency distributions as percentage and Gaussian fits of all CeL/C<sup>Htr2a</sup> (blue) and CeL/C<sup>PKC $\delta$</sup>  (green) neurons along the rostral-caudal (z axis) (**c**), dorso-ventral (y axis) (**d**) and lateral-medial (x axis) (**e**) axes ( $n = 1$  *Htr2a-Cre;LacZ* mouse). **f**, Digital coordinates along the lateral-medial (x axis) and dorso-ventral (y axis) axes of all reconstructed CeL/C<sup>Htr2a</sup> and CeL/C<sup>PKC $\delta$</sup>  cell bodies ( $n = 1$  mouse). **g**, Contour plot depicting Kernel density estimates of CeL/C<sup>Htr2a</sup> and CeL/C<sup>PKC $\delta$</sup>  neuronal distributions along the x and y axes ( $n = 1$  mouse). Scale bars: 50  $\mu$ m.

## 3.2. ORGANISATION OF CEAL INHIBITORY MICROCIRCUITS

### 3.2.1. Strategy to identify monosynaptic inputs to CeA<sup>Htr2a</sup>, CeA<sup>PKCδ</sup> and CeA<sup>Sst</sup> neuronal populations

To understand how functionally distinct populations locally interact within the CeA, I performed Cre-dependent rabies virus-based monosynaptic tracing<sup>156,159</sup>. *Htr2a-cre*, *Prkcd-cre* or *Sst-Cre* mice were transduced in the CeA with first two AAV to induce expression of TVA-mCherry and the rabies virus envelope glycoprotein (RG) in Cre-expressing neurons, and second with an EnvA-pseudotyped, glycoprotein (RG)-deleted, and GFP-expressing rabies virus (**Figure 8a**).

I found that TVA receptor expression, labelled by mCherry fluorescence, was restricted to Cre-expressing neurons in *Htr2a-Cre* and *Sst-Cre* transduced animals and to PKCδ protein-expressing neurons in *Prkcd-Cre* transduced mice (**Figure 8b-d**). In addition, identification of starter neurons based on coexpression of TVA-mCherry and RABV-eGFP revealed that between animals, about 50 to 63% of the whole CeL/C<sup>Htr2a</sup>, 16 to 46% of the whole CeL/C<sup>Sst</sup> and 20 to 69% of the whole CeL/C<sup>PKCδ</sup> populations were transduced using this strategy (**Figure 8e**).

I found PKCδ starter neurons to be exclusively present in the CeL/C in accordance with PKCδ protein expression pattern<sup>32</sup> (**Figure 8f**). 71 to 82% of Htr2a and 77 to 85% of Sst starter cells were confined to the CeL/C, the remainder being located in the CeM and, or BLA (**Figure 8f**). In all tracing experiments, a small number of starter neurons could be seen in one or several of the neighbouring nuclei, namely the globus pallidus (GP), caudoputamen (CP), substantia innominate (SI) and the very lateral part of the LH (**Figure 8g**). However, these neurons accounted for only a small portion of the total starter cells.

To further assess the specificity of the tracing approach used, I repeated the previously described approach in wild-type mice with no Cre expression (**Figure 8h**). This resulted in transsynaptic labelling of a small number of neurons (about 25) at the level of the injection site only. This non-specific infection might be the result of leaky expression of the TVA receptor, which could not be detected by mCherry fluorescence visualization but still permitted infection of the EnvA-pseudotyped rabies virus<sup>156,159</sup>. Alternatively, few particles of non-EnvA-pseudotyped rabies virus might have contaminated the viral preparations.

Together, these results demonstrate a specific and high degree of transduction of Htr2a-, Sst- and PKCδ- expressing neurons mainly restricted to the CeA and confirm that most RABV-eGFP+ neurons only, in the CeA, constitute local monosynaptic inputs. Hence, these experiments validate the strategy used to study inter-connectivity between CeA<sup>Htr2a</sup>, CeA<sup>PKCδ</sup> and CeA<sup>Sst</sup> neuronal populations.



### 3.2.2. Interaction between CeA<sup>Htr2a</sup>, CeA<sup>PKCδ</sup> and CeA<sup>Sst</sup> neuronal populations

One hypothesis that could explain how CeA neurons control appetitive and aversive behaviours in an opposing fashion would be that functionally defined cell types mutually inhibit each other within the CeA network<sup>134</sup>. To address this, I investigated how CeA<sup>Htr2a</sup> and CeA<sup>Sst</sup> populations locally interact with CeA<sup>PKCδ</sup> neurons.

I combined Cre-dependent rabies virus–based monosynaptic tracing in *Htr2a-Cre*, *Sst-Cre* and *Prkcd-Cre* animals, as described in **Figure 8a**, with immunohistochemistry or *in situ* hybridization methods and determined whether monosynaptic inputs (RABV-eGFP+ only neurons) expressed Htr2a, Sst and PKCδ markers.

Monosynaptic inputs (RABV-eGFP+ only neurons) to CeA<sup>Htr2a</sup>, CeA<sup>Sst</sup> and CeA<sup>PKCδ</sup> were extensively found in the CeA (**Figure 9**, **Figure 10** and **Figure 11**). Identification of local presynaptic partners to CeA<sup>Htr2a</sup> neurons revealed that CeL/C<sup>PKCδ</sup> cells accounted for about 22.2% ± 1.8% of all CeL/C monosynaptic inputs (**Figure 9a** and **c**), while 34.3% ± 4.5% originated from other Htr2a+ cells in the CeL/C (**Figure 9b-c**).

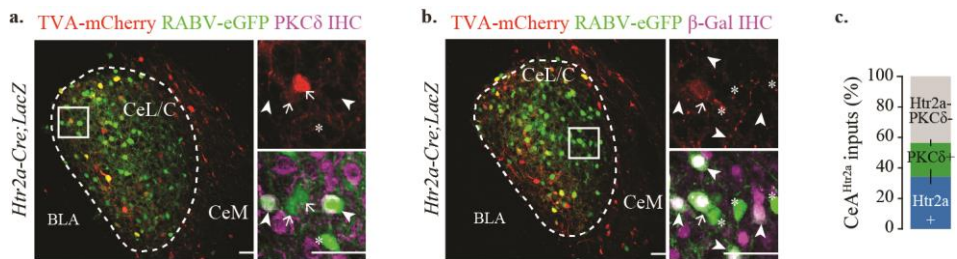


**Figure 9: Local inputs to CeA<sup>Htr2a</sup> neurons.** **a, b**, Representative confocal images of coronal sections through the CeL/C and CeM of a CeA<sup>Htr2a</sup> traced brain. The magnified views on the right represent the area in the white box. Arrows indicate starter neurons (TVA-mCherry+ and RABV-eGFP+). Asterisks denote input neurons (RABV-eGFP+ only). Arrowheads indicate input neurons (RABV-eGFP+ only) that express PKCδ protein (**a**) or β-Gal protein as a marker for Htr2a-Cre+ neurons (**b**) (representative of 3 *Htr2a-Cre;LacZ* mice). **c**, Proportion of inputs to CeA<sup>Htr2a</sup> neurons from CeL/C<sup>Htr2a</sup> cells or CeL/C<sup>PKCδ</sup> neurons (n = 3 *Htr2a-Cre;LacZ* mice, see **Figure 8e** and **f**) (Number of RABV-eGFP+ input counted cells per mouse quantified for PKCδ IHC and β-Gal IHC (as a marker for Sst-Cre+ neurons): [108-285] and [132-374] respectively). Bar graphs show mean ± SEM. Scale bars: 50 μm.

Similarly, 24.2% ± 2.8% of all local monosynaptic inputs to CeA<sup>Sst</sup> came from CeL/C<sup>PKCδ</sup> neurons (**Figure 10a** and **c**) and afferents from neurons of the same kind accounted for 43.2% ± 3.6% (**Figure 10b-c**).

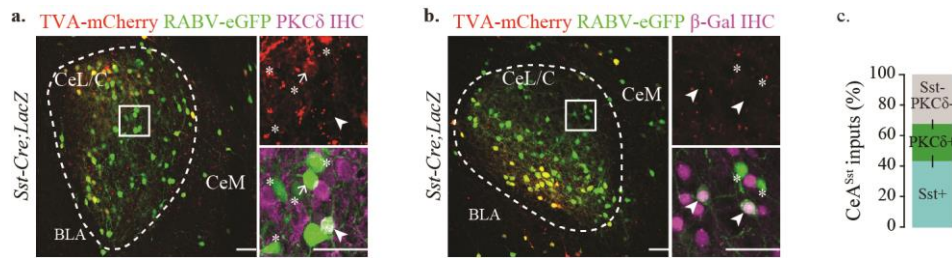


**Figure 10: Local inputs to CeA<sup>Sst</sup> neurons.** **a, b** Representative confocal images of coronal sections through the CeL/C and CeM of a CeA<sup>Sst</sup> traced brain. The magnified views on the right represent the area in the white box. Arrows indicate starter neurons (TVA-mCherry+ and RABV-eGFP+). Asterisks denote input neurons (RABV-eGFP+ only). Arrowheads indicate input neurons (RABV-eGFP+ only) labelled for PKC $\delta$  protein (**a**) or  $\beta$ -Gal protein as a marker for Sst-Cre+ neurons (**b**) (representative of 4 *Sst-Cre;LacZ* mice). **c**, Proportion of inputs to CeA<sup>Sst</sup> neurons from CeL/C<sup>Sst</sup> cells or CeL/C<sup>PKC $\delta$</sup>  neurons. (n = 4 *Sst-Cre;LacZ* mice, see **Figure 8e** and **f**) (Number of RABV-eGFP+ input cells counted per mouse quantified for PKC $\delta$  IHC and  $\beta$ -Gal IHC (as a marker for Sst-Cre+ neurons): [353-408] and [246-290] respectively). Bar graphs show mean  $\pm$  SEM. Scale bars: 50  $\mu$ m.

Additionally, I confirmed that CeL/C<sup>Htr2a</sup> cells provide monosynaptic inputs to CeA<sup>PKC $\delta$</sup>  neurons, albeit difficult to quantify using a fluorescent *in situ* hybridization method that labels single mRNA molecules (**Figure 11a**). Sst+ neurons densely innervated CeA<sup>PKC $\delta$</sup>  cells (44.5%  $\pm$  1.8% of all RABV-eGFP+ only cells are Sst+). Interconnectivity within CeA<sup>PKC $\delta$</sup>  cells, on the other hand, was very low (9.1%  $\pm$  2.7% of all RABV-eGFP+ only cells are PKC $\delta$ + ) (**Figure 11c-d**).

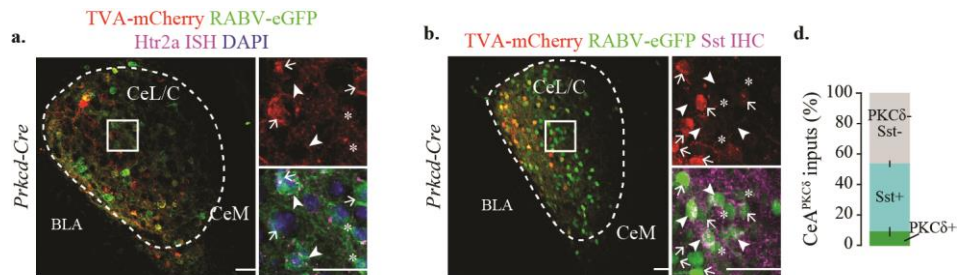


**Figure 11: Local inputs to CeA<sup>PKC $\delta$</sup>  neurons.** **a-c**, Representative confocal images of coronal sections through the CeL/C and CeM of a CeA<sup>PKC $\delta$</sup>  traced brain. The magnified views on the right represent the area in the white box. Arrows indicate starter neurons (TVA-mCherry+ and RABV-eGFP+). Asterisks denote input neurons (RABV-eGFP+ only). Arrowheads indicate input neurons (RABV-eGFP+ only) labelled for Htr2a mRNA. (**a**), Sst protein (**b**) or PKC $\delta$  protein (**c**) (representative of 4 *Prkcd-Cre* mice). **d**, Proportion of inputs to CeA<sup>PKC $\delta$</sup>  neurons from CeL/C<sup>PKC $\delta$</sup>  cells or CeL/C<sup>Sst</sup> neurons. (n = 4 *Prkcd-Cre* mice, see **Figure 8e** and **f**) (Number of RABV-eGFP+ input cells counted per mouse quantified for Sst IHC and PKC $\delta$  IHC: [260-323] and [223-286] respectively.) Bar graphs show mean  $\pm$  SEM. Scale bars: 50  $\mu$ m.

### 3.2.3. Identification of local inputs to PBN-projecting CeA neurons

Experiments conducted in our group (Amelia M. Douglass - data not shown) have demonstrated that optogenetic activation of CeA<sup>Htr2a</sup> axonal projections in the PBN can recapitulate both the increase in food intake and rewarding behaviour observed during activation of CeA<sup>Htr2a</sup> cell bodies. Furthermore, the fact that CeA<sup>PKCδ</sup> cells have been proposed to suppress feeding via local inhibition of a population of PKCδ- neurons prompted me to explore whether CeA<sup>PKCδ</sup> neurons are poised to inhibit PBN-projecting CeA cells.

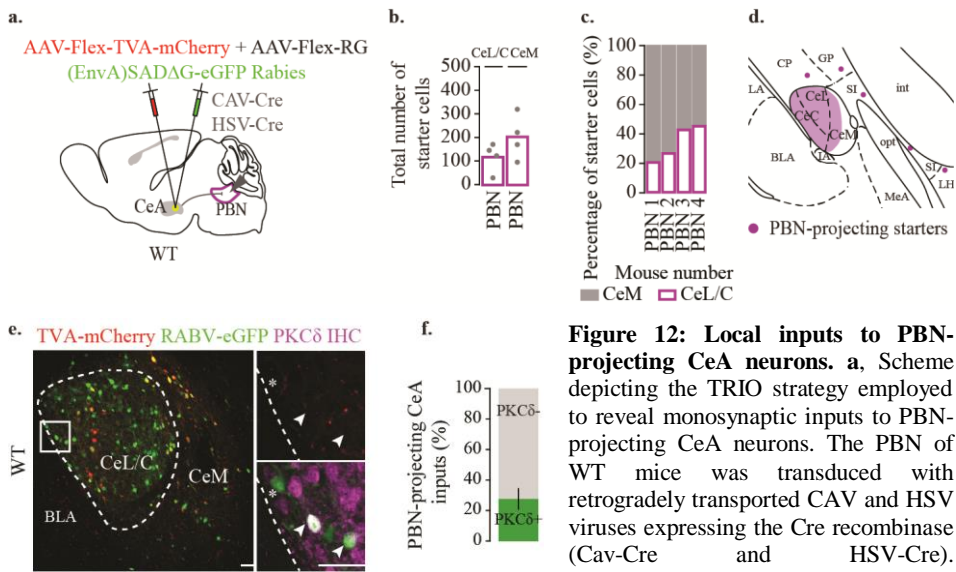


**Figure 12: Local inputs to PBN-projecting CeA neurons.** **a**, Scheme depicting the TRIO strategy employed to reveal monosynaptic inputs to PBN-projecting CeA neurons. The PBN of WT mice was transduced with retrogradely transported CAV and HSV viruses expressing the Cre recombinase (Cav-Cre and HSV-Cre). Simultaneously, Cre-dependent helper

adeno-associated viruses expressing the avian sarcoma leucosis virus glycoprotein EnvA receptor (TVA) (AAV-FLEX-TVA-mCherry) and rabies virus envelope glycoprotein (RG) (AAV-FLEX-RG) were injected in the CeA in combination with a modified rabies virus (EnvA)SADAG-eGFP. **b**, Number of starter neurons in the CeL/C and CeM of PBN-projecting CeA tracing experiments quantified in **f**. Bar graphs show mean and each dot is a separate tracing experiment. **c**, Proportion of starter neurons in the CeL/C and CeM per mouse quantified in **f**. **d**, Drawing based on Paxinos and Franklin's atlas of a coronal section through the CeL/C, CeM and surrounding nuclei showing the approximate location of PBN-projecting CeA starter cells. The majority of them were located in the CeL/C and CeM and a minority in the neighboring nuclei such as CP, SI, GP and LH. **e**, Representative confocal images of coronal sections through the CeL/C and CeM of a PBN-projecting CeA tracing brain. The white box delineates the location of the magnified views on the right. Arrowheads indicate input neurons (RABV-eGFP+ only) that express PKCδ protein (representative of 4 WT mice). **f**, Proportion of inputs to PBN-projecting CeA neurons from CeL/C<sup>PKCδ</sup> neurons (n = 4 WT mice, see **b** and **c**) (Number of RABV-eGFP+ input cells counted per mouse quantified for PKCδ IHC: [67-200]). For abbreviations of brain subregions, see legend of **Figure 6**. Bar graphs show mean ± SEM. Scale bars: 50 μm.

To test this, I used the “tracing the relationship between input and output” (TRIO) strategy<sup>161</sup> which permits identification of monosynaptic partners to a selected subset of CeA cells based on their projections to the PBN. It consists of using

Cre-dependent monosynaptic rabies tracing in the CeA (as depicted in **Figure 8a**) where Cre expression is restricted to PBN-projecting CeA neurons by transducing the PBN of WT mice with retrogradely transported canine adenovirus (CAV) and herpes simplex virus (HSV) viruses that express the Cre recombinase (**Figure 12a**).

Analysis of starter cell distribution showed that the average number of starter cells present in the whole CeA was approximately six times lower in the PBN-projecting CeA tracing experiments as compared to the CeA<sup>Htr2a</sup> tracing experiments (**Figure 12b**). 22 to 46% of all CeA starters were confined to the CeL/C, while the majority of them were located in the CeM (**Figure 12c**). As reported for CeA<sup>Htr2a</sup>, CeA<sup>Sst</sup> and CeA<sup>PKCδ</sup> experiments, Cre-expressing cells could be found in surrounding nuclei leading to the presence of a small number of starter neurons in these regions (**Figure 12d**).

Identification of RABV-eGFP+ only labelled cells using immunostaining against PKCδ protein revealed that CeL/C<sup>PKCδ</sup> neurons contributed 27.7% ± 6.6% of whole CeA inputs to PBN-projecting CeA neurons (**Figure 12e-f**).

These findings collectively support a model (**Figure 13**) in which CeA<sup>Htr2a</sup> and CeA<sup>Sst</sup> form reciprocal inhibitory connections with CeA<sup>PKCδ</sup> neurons, a circuit motif that could allow functionally distinct CeA neurons to modulate appetitive and aversive behaviours depending on environmental conditions. Likewise, my results demonstrate that CeA<sup>PKCδ</sup> neurons have the necessary connections to control PBN-projecting CeA neuron activity, hence supporting an inhibitory role on food intake. Interestingly, connections from CeA<sup>Sst</sup> to CeA<sup>PKCδ</sup> cells are more prominent than the other way around, indicating a possible hierarchy in the organisation of the microcircuit. Finally, these experiments pinpoint a high connection rate between Htr2a-Htr2a and Sst-Sst expressing neurons, possibly reflecting heterogeneity among these two CeA units.

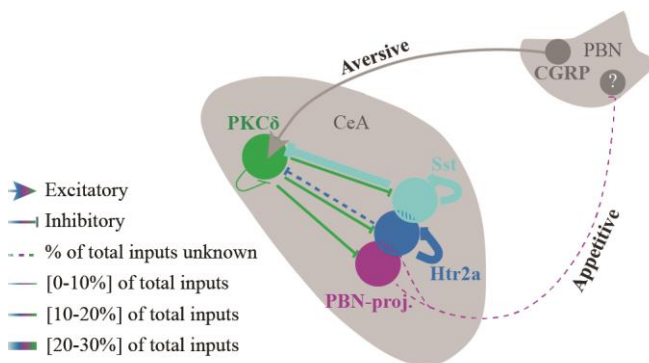


**Figure 13: Model of CeA microcircuits.** The scheme illustrates how four molecularly distinct CeA populations interact locally. In summary, CeA<sup>Htr2a</sup>, CeA<sup>Sst</sup> and PBN-projecting (PBN-proj.) CeA neurons form partially overlapping populations of CeA neurons while CeA<sup>PKCδ</sup> neurons are distinct. CGRP+ projections from PBN neurons specifically

target CeA<sup>PKCδ</sup> neurons while only CeA<sup>Htr2a</sup> and CeA<sup>SST</sup> cells project to the PBN. CeA<sup>Htr2a</sup> and CeA<sup>Sst</sup> mutually inhibit each other with CeA<sup>PKCδ</sup> neurons. Inputs from CeA<sup>Sst</sup> to CeA<sup>PKCδ</sup> involve many CeA<sup>Sst</sup> cells, while inputs from CeA<sup>PKCδ</sup> to CeA<sup>Sst</sup> did not involve many CeA<sup>PKCδ</sup> neurons. CeA<sup>Htr2a</sup> and CeA<sup>Sst</sup> form connections with neurons belonging to the same molecular kind while CeA<sup>PKCδ</sup> cells form very little connections in between themselves. Finally, CeA<sup>PKCδ</sup> neurons are able to inhibit PBN-projecting CeA neurons.

### 3.3. IDENTIFICATION OF WHOLE-BRAIN INPUTS TO $\text{CeA}^{\text{HTR2A}}$ , $\text{CeA}^{\text{PKC}\delta}$ AND $\text{CeA}^{\text{SST}}$ NEURONS

Dissection of CeA microcircuits organisation showed that distinct CeA populations mutually inhibit each other, a mechanism that could allow for a rapid switch between different behavioural programs. However, it does not explain how  $\text{CeA}^{\text{Htr2a}}$  neuron activity increases during an appetitive task.

To resolve the circuits leading to  $\text{CeA}^{\text{Htr2a}}$  neuron activation, it is essential to identify candidate sources of excitatory inputs and to investigate differences in the kind of information that  $\text{CeA}^{\text{Htr2a}}$ ,  $\text{CeA}^{\text{PKC}\delta}$  and  $\text{CeA}^{\text{Sst}}$  neurons receive.

To do so, I expanded the monosynaptic tracing strategy used in **Figure 8** to **Figure 11** to whole-brain mapping of inputs to Htr2a+, PKC $\delta$ + and SST+ neurons of the CeA. Five to six animals per group were chosen and my analysis of the tracing efficiency revealed that 13 to 69% of the whole CeL/C<sup>Htr2a</sup>, 34 to 55% of the whole CeL/C<sup>Sst</sup> and 30 to 71% of the whole CeL/C<sup>PKC $\delta$</sup>  populations were transduced (**Figure 14a**). As previously observed, all PKC $\delta$  starter cells were restricted to the CeL/C nucleus (**Figure 14b**). As for  $\text{CeA}^{\text{Htr2a}}$  and  $\text{CeA}^{\text{Sst}}$  tracing experiments, the majority of starter neurons were confined to the CeL/C, the remainder being located in the CeM and or BLA (**Figure 14b**). The numbers of transsynaptically labelled neurons were roughly proportional to the numbers of starter neurons. On average,  $\text{CeA}^{\text{PKC}\delta}$  tracing experiments yielded higher numbers of long-range inputs as compared to  $\text{CeA}^{\text{Htr2a}}$  and  $\text{CeA}^{\text{Sst}}$  tracing experiments (**Figure 14c**).

The location of monosynaptic inputs was determined based on the Allen Institute's reference atlas<sup>162</sup> and in consultation with Paxinos and Franklin's atlas<sup>163</sup>. 25 subregions embedded in 10 brain areas were identified as providing long range inputs to  $\text{CeA}^{\text{Htr2a}}$ ,  $\text{CeA}^{\text{Sst}}$  and  $\text{CeA}^{\text{PKC}\delta}$  neurons (**Figure 14d-e** and **Figure 15a**). This analysis excluded some regions that were part of the amygdala complex as well as nuclei adjacent to the injection sites where a small number of starter cells could be found (see: 5.9.3. Whole brain monosynaptic inputs to CeAHtr2a, CeAPKC $\delta$ , CeASst, PBN-projecting CeA and PBN-projecting CeAHtr2a neurons and **Figure 8g**). To correct for variability between animals, the number of input neurons in each brain area or subregion was normalized to the total number of input cells per quantified brain (**Figure 14d-e** and **Figure 15a**).

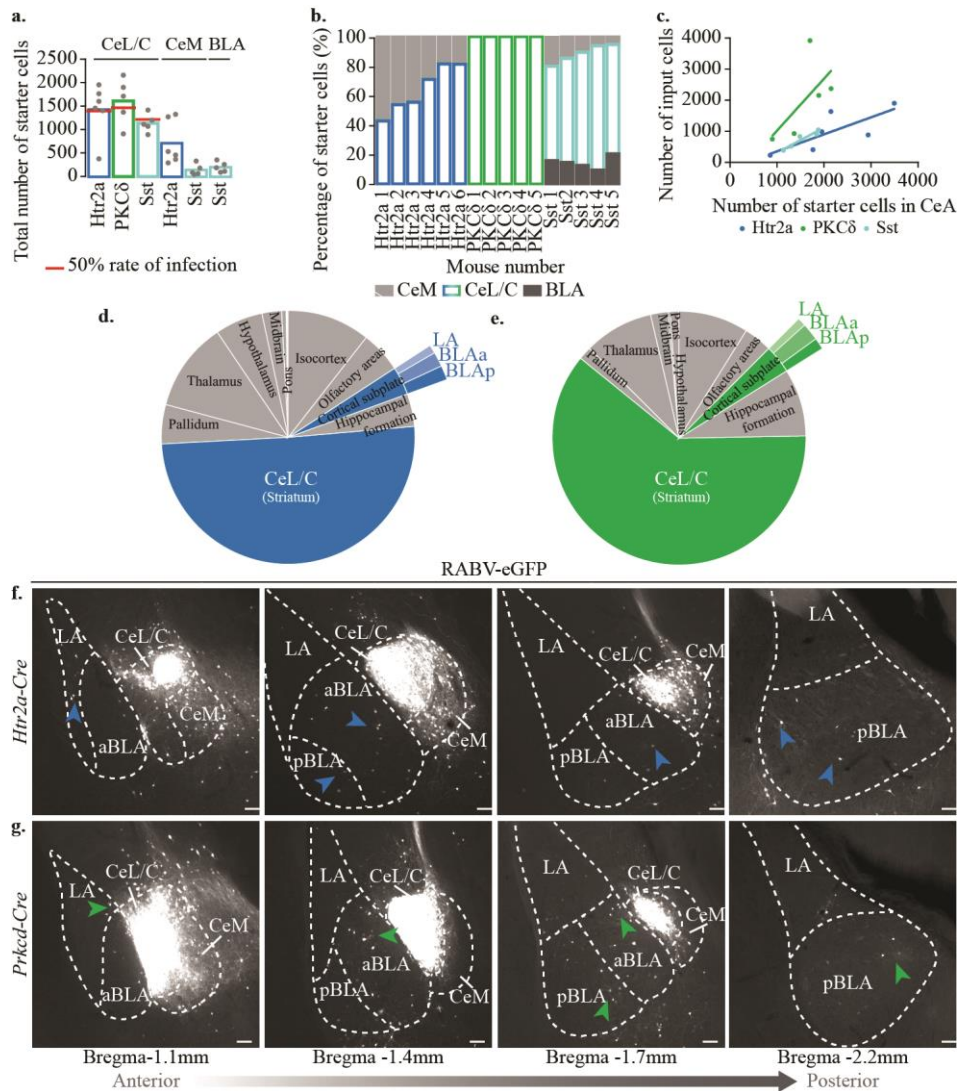


**Figure 14 : Identification of whole brain inputs to CeA<sup>Htr2a</sup>, CeA<sup>PKCδ</sup> and CeA<sup>Sst</sup> neurons.** a, Number of starter neurons in the CeL/C, CeM and BLA of CeA<sup>Htr2a</sup>, CeA<sup>PKCδ</sup> and CeA<sup>Sst</sup> tracing experiments quantified in **d** and **e**, **Figure 15a**, **Figure 17d**, **Figure 18a, c and d-f**. The red bar delineates the number of CeA<sup>Htr2a</sup>, CeA<sup>PKCδ</sup> and CeA<sup>Sst</sup> neurons needed to transduce in order to target 50% of the respective populations. Bar graphs show mean and each dot is a separate tracing experiment. **b**, Proportion of starter neurons in the CeL/C, CeM and BLA per mouse quantified in **d** and **e**, **Figure 15a**, **Figure 17d**, **Figure 18a, c and d-f**. **c**, Number of long range input cells in 21 selected subregions as a function of number of CeA<sup>Htr2a</sup>, CeA<sup>PKCδ</sup>, or CeA<sup>Sst</sup> starter cells. **d**, **e**, Proportion of inputs to CeA<sup>Htr2a</sup> (**d**) or CeA<sup>PKCδ</sup> (**e**) coming from the isocortex, olfactory areas, cortical subplate including LA, aBLA and pBLA, hippocampal formation, CeL/C, pallidum, thalamus, hypothalamus, midbrain and pons. Sunburst graphs show mean (n=6 *Htr2a-Cre* and 5 *Prkcd-Cre* brains, see a-b). **f**, **g**, Representative epifluorescent images of coronal sections through the CeL/C, CeM, LA, aBLA and pBLA nuclei of CeA<sup>Htr2a</sup> (**f**) or CeA<sup>PKCδ</sup> (**g**) traced brains. Selected images show the nuclei from anterior (left) to posterior (right) with distances from bregma indicated at the bottom of **g**. Arrowheads indicate RABV-eGFP+ cells in the LA, aBLA or pBLA nuclei identified as presynaptic partners to CeA<sup>Htr2a</sup> neurons (**f**, in blue) or CeA<sup>PKCδ</sup> (**g**, in green) (representative of 6 *Htr2a-Cre* and 5 *Prkcd-Cre* mice, see a-b). aBLA, basolateral amygdala, anterior part; pBLA, basolateral amygdala, posterior part. Scale bars: 100 μm.

### 3.3.1. Contribution of LA and BLA inputs to CeA<sup>Htr2a</sup> and CeA<sup>PKC $\delta$</sup> neurons

In the traditional view of amygdala circuits, information flows from LA and BLA nuclei toward the CeA<sup>109</sup>. Additionally, a recent study showed that CeA neurons mediating appetitive behaviours receive direct inputs from BLA neurons coding for positive-valence stimuli<sup>25</sup>.

This prompted me to explore the contribution of LA and BLA (anterior: aBLA and posterior part: pBLA) projections to CeA neurons. As the presence of Sst starter neurons in the BLA of all CeA<sup>Sst</sup> tracing brains would bias the results, only LA and BLA inputs to CeA<sup>Htr2a</sup> and CeA<sup>PKC $\delta$</sup>  were quantified (**Figure 14d-g**).

This analysis highlighted that most presynaptic partners to CeA<sup>Htr2a</sup> and CeA<sup>PKC $\delta$</sup>  neurons were located within the CeA itself which provides about 49% and 60% of all inputs to CeA<sup>Htr2a</sup> and CeA<sup>PKC $\delta$</sup>  cells, respectively (**Figure 14d-g**). LA, aBLA and pBLA projections all together represented 3.5% of all afferents to both cell types which was much less than the proportion of inputs coming from, for instance, the isocortex (**Figure 14d-e**). This provides new insights into amygdala circuits, arguing against the previous model supporting serial information processing and illustrates that CeA might function independently of the LA and BLA complex.

### 3.3.2. Quantitative analysis of CeA<sup>Htr2a</sup>, CeA<sup>Sst</sup> and CeA<sup>PKC $\delta$</sup> input distribution

Across the whole brain, the most abundant labelling was found in the isocortex and thalamus for CeA<sup>Htr2a</sup> and CeA<sup>PKC $\delta$</sup>  tracing experiments (**Figure 14d-e**, **Figure 15a** and **b**). In comparison, the hypothalamus and hippocampus contributed most of the long-range inputs to CeA<sup>Sst</sup> neurons (**Figure 15a** and **b**). Within the brain areas mentioned above, afferents to all cell types came only from a subset of subregions.

#### *Isocortex and olfactory areas*

Although RABV-eGFP+ neurons could be found throughout the somatosensory, auditory, perirhinal, ectorhinal and temporal associations areas of the cortex (Cx) (**Figure 15a**), labelled neurons were mostly concentrated in the posterior insula cortex (IC) (between +0.4mm anterior and - 1mm posterior from bregma), including the layer 5 of the visceral and gustatory areas (**Figure 15a** and **b<sub>1</sub>**). The piriform cortex (Pir.) also contained a large number of labelled neurons (**Figure 15a**). Overall, I found striking differences in the distribution of monosynaptic inputs to all three cell types, as the isocortex and olfactory areas were heavily labelled in CeA<sup>PKC $\delta$</sup>  and CeA<sup>Htr2a</sup> tracing experiments but devoid in CeA<sup>Sst</sup> tracing brains (**Figure 15a** and **b<sub>1</sub>**).

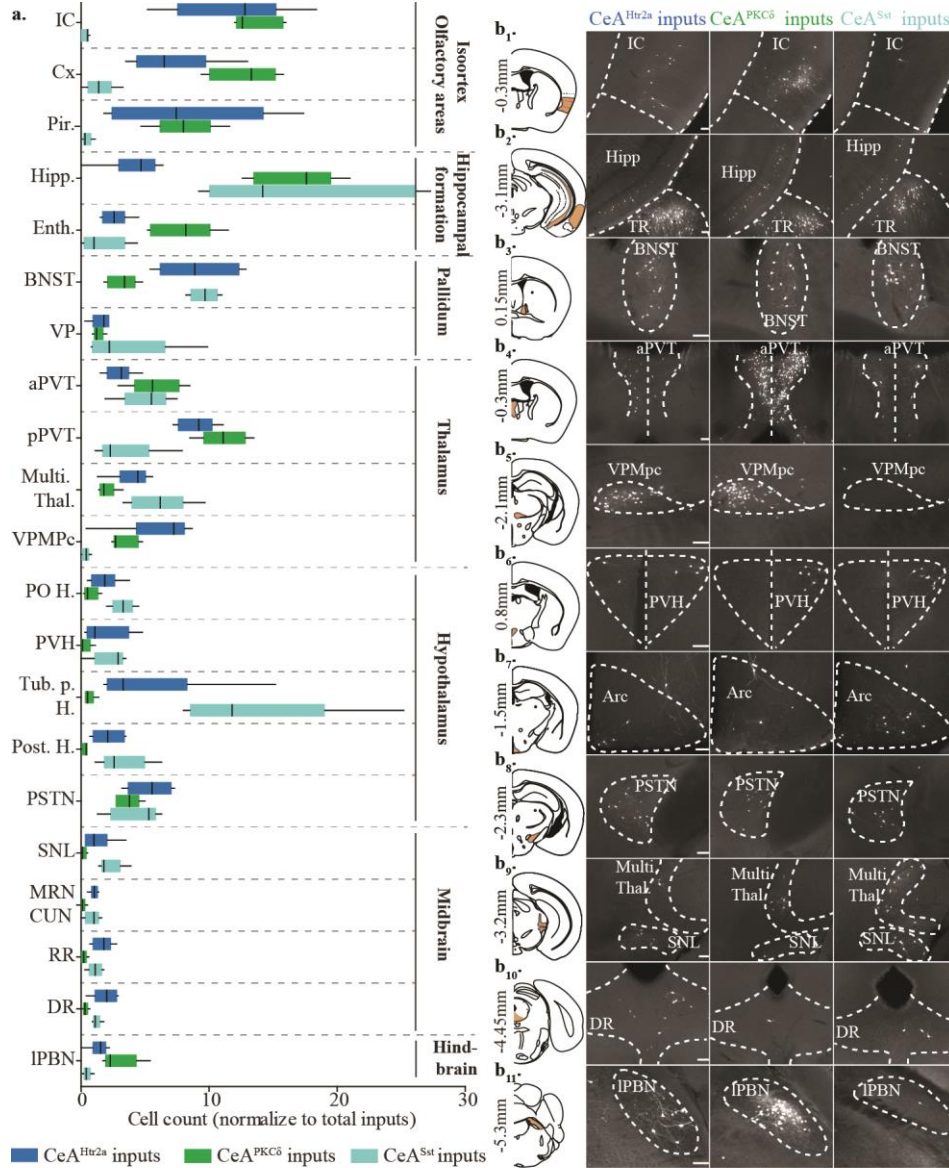


**Figure 15: Long-range presynaptic partners of CeA<sup>Htr2a</sup>, CeA<sup>PKCδ</sup> and CeA<sup>Sst</sup> neurons. a.** Monosynaptic inputs to CeA<sup>Htr2a</sup>, CeA<sup>PKCδ</sup> and CeA<sup>Sst</sup> neurons from 21 brain subregions shown as the proportion of the total input cells counted per quantified brain. Box-whisker plots display median, interquartile range and 5th–95th percentiles of the distribution (n=6 *Htr2a-Cre*, 5 *Prkcd-Cre* and 5 *Sst-Cre* brains see Figure 13a-c). **b.** Representative epifluorescent pictures of coronal sections showing the distribution of monosynaptic partners (RABV-eGFP+ cells) to CeA<sup>Htr2a</sup>, CeA<sup>PKCδ</sup> and CeA<sup>Sst</sup> neurons in the IC (b<sub>1</sub>), Hipp (b<sub>2</sub>), BNST (b<sub>3</sub>), aPVT (b<sub>4</sub>), VPMpc (b<sub>5</sub>), PVH (b<sub>6</sub>), Arc (b<sub>7</sub>), PSTN (b<sub>8</sub>), Multi. Thal. (b<sub>9</sub>), SNL (b<sub>9</sub>), DR (b<sub>10</sub>) and IPBN (b<sub>11</sub>). Coronal section planes of a schematic brain are shown on the left with distances (anterior-posterior axis) from bregma (representative of 6 *Htr2a-Cre*, 5 *Prkcd-Cre* and 5 *Sst-Cre* brains). IC, insula cortex; Cx, cortex; Pir., piriform cortex; Hipp., hippocampus; Enth., entorhinal cortex; TR, postpiriform transition nucleus; BNST, bed nucleus of the stria terminalis; VP, ventral pallidum; aPVT, anterior paraventricular thalamus; pPVT, posterior paraventricular thalamus; Multi. Thal., multimodal thalamus; VPMpc, ventral posteromedial nucleus of the thalamus, parvocellular part; PO H.,

preoptic hypothalamus; PVH, paraventricular hypothalamus; Arc, arcuate nucleus; Tub. p. H., tuberal posterior hypothalamus; Post. H., posterior hypothalamus; PSTN, parasubthalamic nucleus; SNL, substantia nigra, lateral part; MRN, midbrain reticular nucleus; CUN, cuneiform nucleus; RR, midbrain reticular nucleus, retrorubral area; DR, dorsal raphe; IPBN, lateral parabrachial nucleus. Scale bars: 100  $\mu$ m.

### *Hippocampal formation*

In the hippocampal formation, the densest labelling was observed in the hippocampus and subiculum (Hipp.) (**Figure 15a** and **b<sub>2</sub>**) and the entorhinal cortex (Enth.) (**Figure 15a**). The hippocampus and subiculum showed a notable trend toward projecting to CeA<sup>PKC $\delta$</sup>  and CeA<sup>Sst</sup> neurons (**Figure 15a**). The Enth., however, sent biased inputs onto CeA<sup>PKC $\delta$</sup>  neurons compared to CeA<sup>Htr2a</sup> and CeA<sup>Sst</sup> cells (**Figure 15a**).

### *Pallidum*

All three CeA cell types received a substantial number of projections from the bed nucleus of the stria terminalis (BNST) (**Figure 15a** and **b<sub>3</sub>**) and from scattered neurons in the ventral pallidum (VP) (**Figure 15a**).

### *Thalamus*

I found that the thalamic nucleus with most RABV-eGFP+ neurons was the paraventricular thalamus (PVT) (both anterior and posterior part). This nucleus contributed to a larger proportion of inputs to CeA<sup>PKC $\delta$</sup>  neurons (**Figure 15a** and **b<sub>4</sub>**). The multimodal thalamic nuclei (Multi. Thal.) sent afferents to the three cell types with a slight bias to CeA<sup>Sst</sup> neurons (**Figure 15a** and **b<sub>9</sub>**). Conversely, the gustatory thalamus (VPMpc, ventral posteromedial nucleus of the thalamus, parvicellular part) provided many inputs to CeA<sup>Htr2a</sup> and CeA<sup>PKC $\delta$</sup>  neurons but no inputs to CeA<sup>Sst</sup> neurons (**Figure 15a** and **b<sub>5</sub>**).

### *Hypothalamus*

In the hypothalamus the most prominent labelling was observed in the tuberal posterior hypothalamus (Tub. p. H., including the arcuate nucleus (Arc)), partly due to its large volume (**Figure 15a** and **b<sub>7</sub>**). Although the parasubthalamic nucleus (PSTN) was unique in that it provided dense afferents to the three cell types (**Figure 15a** and **b<sub>8</sub>**), all other hypothalamic nuclei predominantly projected onto CeA<sup>Sst</sup> and CeA<sup>Htr2a</sup> neurons (**Figure 15a** and **b<sub>6-8</sub>**).

### *Midbrain*

In the midbrain, moderate labelling was found in the substantia nigra lateralis (SNL), midbrain reticular nucleus (MRN), cuneiform nucleus (CUN) midbrain reticular nucleus, retrorubral area (RR), and dorsal raphe (DR) (**Figure 15a** and **b<sub>9-10</sub>**) nuclei. Together, midbrain nuclei provided preferential inputs to CeA<sup>Htr2a</sup> and CeA<sup>Sst</sup> neurons (**Figure 15a** and **b<sub>9-10</sub>**).

## Hindbrain

Most nuclei in the hindbrain were either devoid of cells or sporadically labelled. The exception was the IPBN which showed distinct patches of RABV-eGFP+ cells in CeA<sup>PKC $\delta$</sup>  traced brains that were more scattered in CeA<sup>Htr2a</sup> brains and were absent in the CeA<sup>Sst</sup> experiments (**Figure 15a** and **b<sub>11</sub>**).

As a whole, this experiment allowed for comparisons of the presynaptic partners of CeA<sup>Htr2a</sup>, CeA<sup>Sst</sup> and CeA<sup>PKC $\delta$</sup>  cells and revealed considerable differences in the pattern of inputs targeting these neurons. For instance, I found that the components of the gustatory<sup>39</sup>, visceral<sup>39</sup>, nociceptive<sup>164</sup> and olfactory systems<sup>66</sup> (IC, VPMpc, IPBN and Pir.) preferentially project onto CeA<sup>PKC $\delta$</sup>  and CeA<sup>Htr2a</sup> neurons (**Figure 15a** and **Figure 16**). On the other hand, hypothalamic nuclei critical for the homeostatic regulation of basic physiological needs, such as food intake<sup>165</sup> (PVH and Arc in the Tub. p. H.), send disproportionately higher projections to CeA<sup>Htr2a</sup> and CeA<sup>Sst</sup> neurons in comparison to CeA<sup>PKC $\delta$</sup>  cells (**Figure 15a** and **Figure 16**). Finally, CeA<sup>Htr2a</sup> and CeA<sup>Sst</sup> exclusively, receive inputs from regions of the midbrain such as the SNL, RR and DR which have been shown to harbour populations of dopaminergic<sup>166</sup> and serotonergic<sup>167</sup> neurons respectively (**Figure 15a** and **Figure 16**).

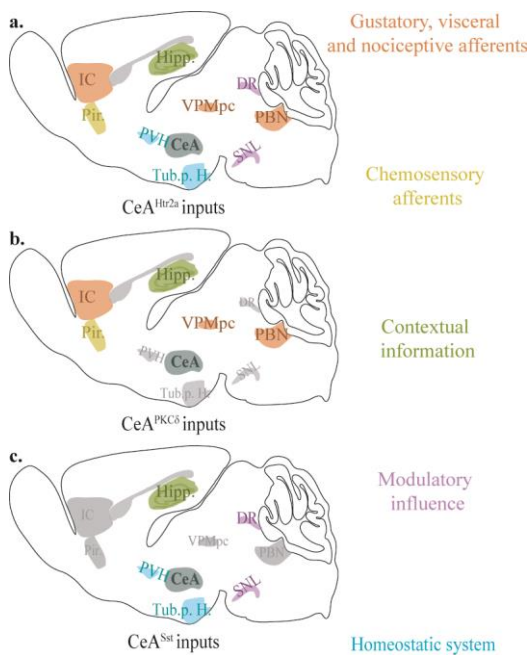


**Figure 16: Summary of whole brain inputs to CeA<sup>Htr2a</sup>, CeA<sup>PKC $\delta$</sup> , and CeA<sup>Sst</sup> neurons.** Examples of presynaptic partners of CeA<sup>Htr2a</sup> (a.), CeA<sup>PKC $\delta$</sup>  (b.) and CeA<sup>Sst</sup> (c.) neurons in schematic sagittal sections. All three genetically-defined populations are provided with afferents from the hippocampus (Hipp.), presumably conveying spatial and temporal contextual information. CeA<sup>Htr2a</sup> and CeA<sup>PKC $\delta$</sup>  neurons receive inputs from the major ascending pathways of the gustatory, viscerosensitive and nociceptive systems (IPBN, VPMpc and IC). Both cell types are also targeted by descending sensory information from the olfactory cortex (Pir). Homeostatic control of feeding behaviour is regulated in part by the arcuate nucleus (Arc, included in the Tub. p. H.) and its projection to the paraventricular hypothalamus (PVH), which both send information to CeA<sup>Htr2a</sup> and CeA<sup>Sst</sup> cells. The midbrain substantia nigra lateralis (SNL) and dorsal raphe

(DR) nuclei which contain dopaminergic and serotonergic populations, respectively, provide inputs to CeA<sup>Htr2a</sup> and CeA<sup>Sst</sup> cells.

### 3.3.3. Characterization of transsynaptically labelled neurons in the IPBN

Previous studies have identified a circuit for appetite suppression involving CGRP+ neurons in the IPBN and their projections to PKC $\delta$ + neurons in the capsular part of the CeA<sup>57,141</sup>. As quantifications in **Figure 15a** indicated that CeA<sup>Htr2a</sup> neurons also receive monosynaptic inputs from this region, I examined whether IPBN<sup>CGRP</sup> neurons provided greater inputs to CeA<sup>PKC $\delta$</sup>  as compared to CeA<sup>Htr2a</sup> cells.

A closer look at the distribution of transsynaptically labelled neurons showed that IPBN inputs to CeA<sup>PKC $\delta$</sup>  neurons segregated and formed clusters in one specific area of the IPBN called the external lateral division of the IPBN (PBle) which is defined by a high level of CGRP+ cells<sup>56,57</sup> (**Figure 17a-b**). IPBN inputs to CeA<sup>Htr2a</sup> neurons were also found in the PBle but were more dispersed and less frequent (**Figure 17c**). Immunolabelling for CGRP protein revealed that 60.4  $\pm$  4.4% of IPBN inputs to CeA<sup>PKC $\delta$</sup>  neurons expressed the CGRP protein versus 16.4  $\pm$  7.1% for CeA<sup>Htr2a</sup> cells (**Figure 17d**).

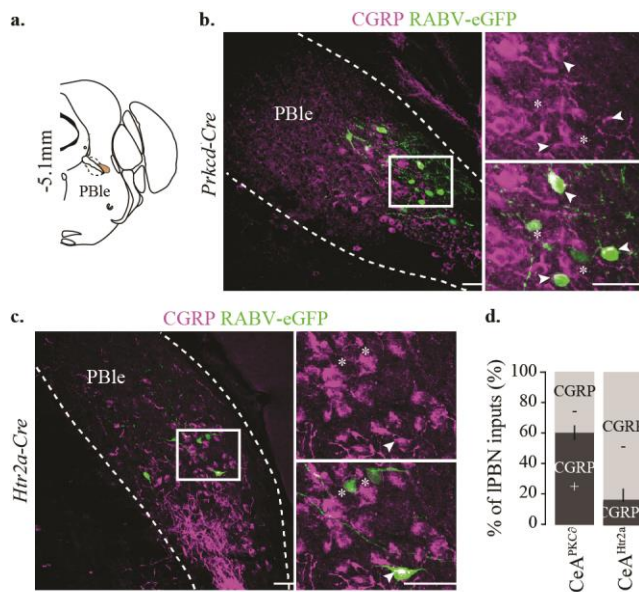


**Figure 17: Cell-type-specific IPBN inputs onto CeA<sup>Htr2a</sup> and CeA<sup>PKC $\delta$</sup>  neurons.** **a**, Scheme of a coronal section of a mouse brain showing the location of the PBle (in orange). Value on the left indicates the distance from bregma on the anterior-posterior axis. **b**, **c**, Representative confocal images of coronal sections through the PBle of CeA<sup>PKC $\delta$</sup>  (**b**) and CeA<sup>Htr2a</sup> (**c**) traced brains. White boxes indicate the location of the high-magnification panel on the right. Arrowheads indicate input neurons (RABV-eGFP+ only) that express the CGRP protein. Asterisks denote input neurons (RABV-eGFP+

only) that are CGRP-negative. **d**, Proportion of IPBN inputs to CeA<sup>Htr2a</sup> or CeA<sup>PKC $\delta$</sup>  neurons that express the CGRP protein (n = 4 *Htr2a-Cre* and 5 *Prkcd-Cre* mice see **Figure 14a-c**) (Number of RABV-eGFP+ input cells counted per mouse quantified for *Prkcd-Cre* mice: [6-63] and for *Htr2a-Cre* mice: [3-81]). PBle, external lateral division of the IPBN. Bar graphs show mean  $\pm$  SEM. Scale bars: 50  $\mu$ m.

This is consistent with previously published data<sup>141</sup> and corroborates the results presented in **Figure 7** showing that CeA<sup>Htr2a</sup> neurons are only sparsely present in the CeC where CGRP axons end. Although the nature of most of CeA<sup>Htr2a</sup> inputs

in the IPBN remain to be identified, this experiment further implies that CeA<sup>Htr2a</sup> and CeA<sup>PKC $\delta$</sup>  neurons might receive different kinds of sensory information.

### 3.3.4. Covariance analysis between input regions to CeA<sup>Htr2a</sup> neurons

In my analysis of long-range presynaptic partners to CeA<sup>Htr2a</sup> and CeA<sup>Sst</sup> neurons (**Figure 15a**), I observed that the proportion of input neurons within each quantified subregion varied noticeably between animals.

I therefore calculated a coefficient of variation (CV) for each subregion and each tracing experiment as a measure of the inter-mouse variability. The graph (**Figure 18a**) shows that CVs for CeA<sup>PKC $\delta$</sup>  tracings are generally lower compared to CVs for CeA<sup>Htr2a</sup> and CeA<sup>Sst</sup> tracings, indicating that the proportion of input cells within each quantified subregion varies less between CeA<sup>PKC $\delta$</sup>  than CeA<sup>Htr2a</sup> and CeA<sup>Sst</sup> experiments. Besides, the graph illustrates that within each experiment, the proportion of inputs in some subregions tended to be more variable than in others. For CeA<sup>Htr2a</sup> tracings for example, the PVH, Tub. p. H. and SNL, displayed higher variability than the BNST, aPVT and PSTN (**Figure 18a**).

I then asked whether this variability would reflect that starter cells in all CeA<sup>Htr2a</sup> experiments originated from different subpopulations of CeA<sup>Htr2a</sup> neurons, each of them exhibiting a distinct input pattern. One could imagine a situation in which CeA<sup>Htr2a</sup> neurons are composed of spatially segregated sub-populations, each of them receiving afferents from a distinct combination of brain regions (**Figure 18b<sub>1</sub>** and **b<sub>2</sub>**). In such circumstances, a tracing experiment achieving a higher number of starter cells in one subpopulation compared to the others would show a higher proportion of input neurons in a specific combination of regions (**Figure 18b<sub>1</sub>** and **b<sub>2</sub>**). If the experiment was repeated several times, tracing results representative of all samples drawn from CeA<sup>Htr2a</sup> neurons would be obtained. A pattern should then appear in which the number of input neurons in some combination of regions would be highly correlated but would show no correlation with other group of regions (**Figure 18b<sub>3</sub>** and **b<sub>4</sub>**).

Using the six CeA<sup>Htr2a</sup> tracing experiments, I calculated Pearson's correlation coefficients between all the 21 input regions quantified, and hierarchically clustered the data. Interestingly, the heatmap (**Figure 18c**) exposed at least two distinct clusters with the IC and VPMpc showing a strong positive correlation and, together with the Enth. and Cx, forming a separate cluster from the hypothalamic nuclei, MRN, CUN, RR, SNL and BNST (**Figure 18c-f**).

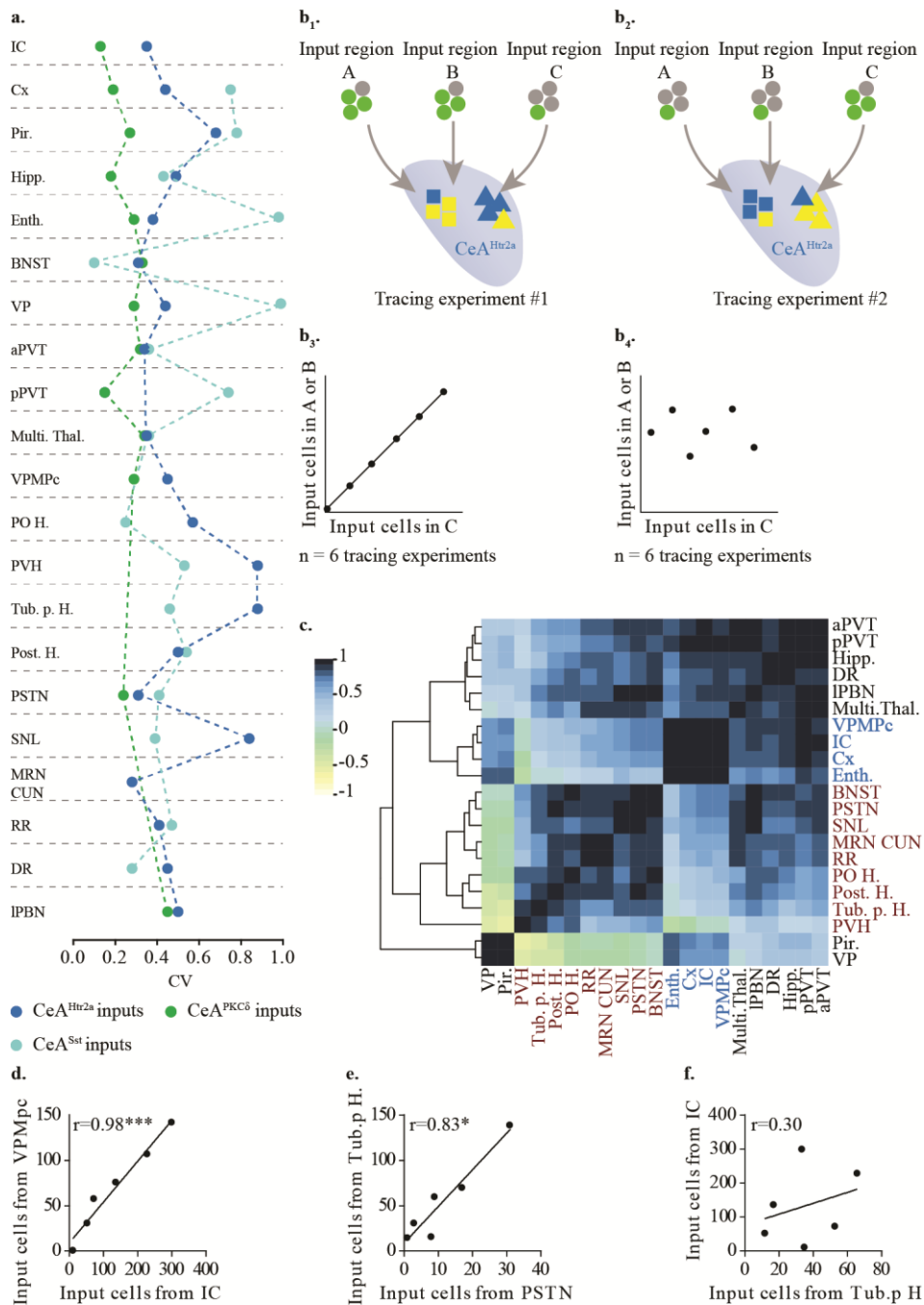


**Figure 18: Inter-mouse variability in CeA<sup>Htr2a</sup>, CeA<sup>PKC $\delta$</sup>  and CeA<sup>Sst</sup> tracing experiments.** **a**, Coefficient of variation (CV) calculated for each region giving more than 1% of the total inputs to CeA<sup>Htr2a</sup>, CeA<sup>PKC $\delta$</sup>  and CeA<sup>Sst</sup> neurons. Dotted lines connecting dots between subregions are drawn to help show that values of CV for CeA<sup>Htr2a</sup> and CeA<sup>Sst</sup> tracing experiments are higher than for the CeA<sup>PKC $\delta$</sup>  experiments (n=6 *Htr2a-Cre*, 5 *Prkcd-Cre* and 5 *Sst-Cre* brains, see **Figure 14a-c**). **b**, Schemes illustrate two hypothetical populations of CeA<sup>Htr2a</sup> neurons that exhibit spatial segregation. One population is represented with squares and the other one with triangles (**b<sub>1</sub>** and **b<sub>2</sub>**).

population receives inputs from regions A and B while the triangle population receives inputs from region C (**b<sub>1</sub>** and **b<sub>2</sub>**). Tracing experiment #1 (**b<sub>1</sub>**) achieves a higher number of starter cells (in yellow) in the square population compared to the triangle one leading to a higher number of monosynaptic inputs (in green) in regions A and B over region C. Tracing experiment #2 (**b<sub>2</sub>**) achieves a higher number of starter cells in the triangle population compared to the square one leading to a higher number of monosynaptic inputs in region C over regions A and B. Plotting the number of input cells in region A versus in region B for 6 different tracing experiments shows a strong positive correlation between the two variables (**b<sub>3</sub>**), while plotting the number of inputs cells in region A or B versus in region C shows no correlation between the two variables (**b<sub>4</sub>**). **c**, Heatmap of hierarchically clustered Pearson's correlation coefficients calculated between all combinations of the 21 subregions giving inputs to CeA<sup>Htr2a</sup> neurons (n= 6 *Htr2a*-Cre brain see **Figure 14a-c**). The colour scale indicates the degree of correlation. Dark blue denotes a strong positive correlation between subregions while light blue and green show no correlation between subregions. Subregions written in dark red or blue belong to two distinct clusters. **d-f**, Example graphs showing that the number of input cells in the VPMpc is positively correlated with the number of input cells in the IC (**d**) as is the number of input cells in the Tub. p. H. versus the PSTN (**e**). The number of input cells in the Tub. p. H. shows no correlation with the number of input cells in the IC (**f**). Each dot is a separate experiment. Values shown are Pearson correlation coefficients with p values from a two-tailed unpaired t-test (n= 6 *Htr2a*-Cre brain see **Figure 14a-c**). For abbreviations of brain subregions, see legend of **Figure 15**. Significance levels are indicated as follows: no stars: not significant, \*P < 0.05; \*\*\*P < 0.001.

Together, these findings reveal that CeA<sup>Htr2a</sup> neurons receiving inputs from the IC and VPMpc receive very few inputs from the hypothalamic nuclei or the SNL and suggest that CeA<sup>Htr2a</sup> are composed of at least two distinct subpopulations based on their input pattern. These subgroups of CeA<sup>Htr2a</sup> neurons may be spatially segregated in the CeA.

### 3.4. ORGANISATION OF MONOSYNAPTIC INPUTS TO PBN-PROJECTING CEA<sup>HTR2A</sup> AND PBN-PROJECTING CEA NEURONS

Manipulation of CeA<sup>Htr2a</sup> neuronal activity in combination with behavioural studies, have shown that CeA<sup>Htr2a</sup> neurons exert their function, at least in part, by inhibiting neurons in the PBN (Amelia M. Douglass - data not shown). The need to identify which signals are integrated at the level of PBN-projecting CeA<sup>Htr2A</sup> neurons prompted me to map the specific inputs they receive and to compare them to whole brain inputs to CeA<sup>Htr2a</sup> and PBN-projecting CeA neurons.

The results of the tracing experiments for CeA<sup>Htr2a</sup> neuron population presented in **Figure 19** are the same as those in **Figure 14** to **Figure 18** (blue coloured inputs). To determine the long-range presynaptic partners of PBN-projecting CeA neurons (magenta-coloured inputs), I used the approach depicted in **Figure 12a**. To comparatively evaluate which of these inputs specifically target PBN-projecting Htr2a+ neurons (dark red-coloured inputs), I used a modified version of the TRIO approach called cell-type-specific TRIO (cTRIO)<sup>161</sup> (**Figure 19a**). It relies on using Flp-dependent monosynaptic rabies tracing in the CeA where Flp expression is restricted to PBN-projecting CeA<sup>Htr2a</sup> neurons. To achieve this, the PBN of *Htr2a-Cre* mice is transduced with retrogradely transported and Cre-dependent CAV-Flp and HSV-Flp viruses.

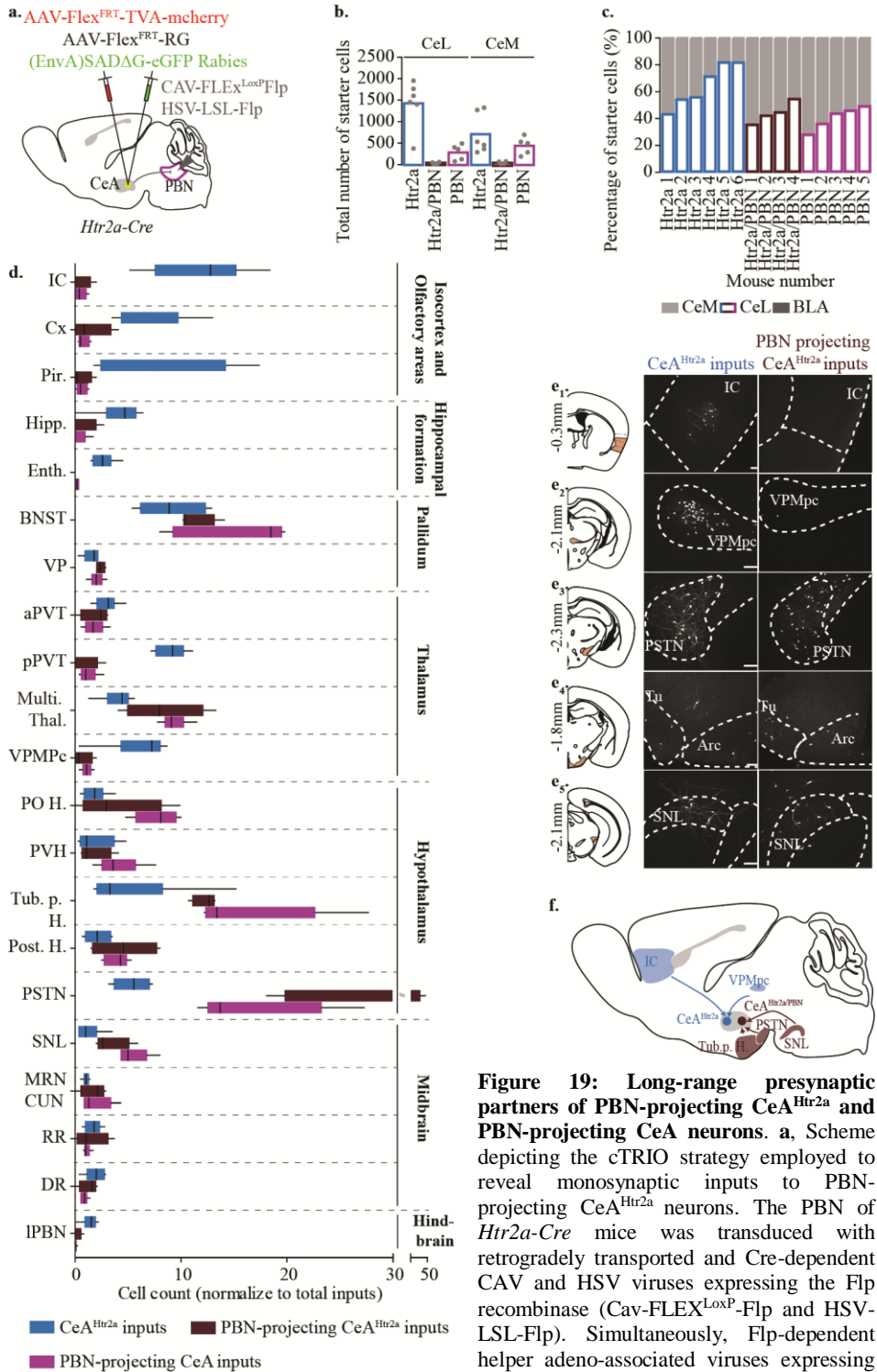


**Figure 19: Long-range presynaptic partners of PBN-projecting CeA<sup>Htr2a</sup> and PBN-projecting CeA neurons.** **a.** Scheme depicting the cTRIO strategy employed to reveal monosynaptic inputs to PBN-projecting CeA<sup>Htr2a</sup> neurons. The PBN of *Htr2a-Cre* mice was transduced with retrogradely transported and Cre-dependent CAV and HSV viruses expressing the Flp recombinase (Cav-FLEX<sup>LoxP</sup>-Flp and HSV-LSL-Flp). Simultaneously, Flp-dependent helper adeno-associated viruses expressing the avian sarcoma leucosis virus glycoprotein

EnvA receptor (TVA) (AAV-FLEX<sup>FRT</sup>-TVA-mCherry) and rabies virus envelope glycoprotein (RG) (AAV-FLEX<sup>FRT</sup>-RG) were injected in the CeA in combination with a modified rabies virus

(EnvA)SADΔG–eGFP. **b**, Number of starter neurons in the CeL/C, CeM and BLA of CeA<sup>Htr2a</sup>, PBN-projecting CeA<sup>Htr2a</sup> and PBN projecting CeA tracing experiments quantified in **d**. CeA<sup>Htr2a</sup> tracing experiments shown in the whole **Figure 19** are the same as in **Figure 14** to **Figure 18**. Bar graphs show mean and each dot is a separate tracing experiment. **c**, Proportion of starter neurons in the CeL/C, CeM and BLA per mouse quantified in **d**. **d**, Monosynaptic inputs to CeA<sup>Htr2a</sup>, PBN-projecting CeA<sup>Htr2a</sup> and PBN-projecting CeA neurons from 21 brain subregions shown as a proportion of the total input cells per quantified brain. Box–whisker plots display median, interquartile range and 5th–95th percentiles of the distribution (n=6 *Htr2a-Cre* brains for CeA<sup>Htr2a</sup> tracing, 4 *Htr2a-Cre* brains for PBN-projecting CeA<sup>Htr2a</sup> tracing and 5 WT brains for PBN-projecting CeA tracing see **b-c**). **e**, Representative confocal images of coronal sections showing the distribution of monosynaptic partners (RABV-eGFP+ cells) to CeA<sup>Htr2a</sup> and PBN-projecting CeA<sup>Htr2a</sup> neurons in the IC (**e**<sub>1</sub>), VPMpc (**e**<sub>2</sub>), PSTN (**e**<sub>3</sub>), tuberal hypothalamus (Tu) (**e**<sub>4</sub>), Arc (**e**<sub>4</sub>) and SNL (**e**<sub>5</sub>). Coronal section planes of a schematic brain are shown on the left with distances (anterior-posterior axis) from bregma (representative of 6 CeA<sup>Htr2a</sup> and 4 PBN-projecting CeA<sup>Htr2a</sup> tracing experiments). **f**, Examples of presynaptic partners to CeA<sup>Htr2a</sup> neurons in a schematic sagittal section. CeA<sup>Htr2a</sup> neurons that project to the PBN (in dark red) receive inputs from the Tub. p. H., PSTN, SN and RR. A distinct subset of CeA<sup>Htr2a</sup> neurons receive inputs from the IC and VPMpc (in blue). For abbreviations of brain subregions, see legend of **Figure 15**. Scale bars: 100 μm.

The distribution of Htr2a/PBN starters resembled the pattern of Htr2a and PBN-projecting starters (**Figure 8g** and **Figure 12d**). Yet in the whole CeA, the average number of Htr2a/PBN starter cells was approximately 13 times lower than the number of Htr2a starters (**Figure 19b**) and they were more numerous in the CeM compared to the CeL/C (**Figure 19c**).

The methodology used to register the location of labelled neurons was identical to that described previously (see: 3.3. Identification of whole-brain inputs to CeAHtr2a, CeAPKCδ and CeASst neurons). As PBN-projecting CeA<sup>Htr2a</sup> and PBN-projecting CeA neurons showed a very similar pattern of inputs, I will from this point on refer to the results obtained from PBN-projecting CeA<sup>Htr2a</sup> tracing experiments only.

Overall, PBN-projecting CeA<sup>Htr2a</sup> neurons and whole CeA<sup>Htr2a</sup> cell population received afferents from similar brain regions (meaning that no additional subregion was identified) but preferential distributions in anatomical subdivisions were observed. I therefore further examined quantitative differences in the proportion of inputs within subregions. Notably, I looked for subregions that showed enrichment in the proportion of inputs to PBN-projecting CeA<sup>Htr2a</sup> neurons compared to the whole CeA<sup>Htr2a</sup> population.

#### *Isocortex, olfactory areas and hippocampal formation*

I found the isocortex, olfactory areas and hippocampal formation to be almost devoid of RABV-eGFP+ neurons in PBN-projecting CeA<sup>Htr2a</sup> tracing experiments (**Figure 19d** and **e**<sub>1</sub>) while these input areas were among the most prominent for the total population of CeA<sup>Htr2a</sup> cells.

#### *Pallidum*

In the pallidum, both BNST and VP contributed to higher proportion of inputs to PBN-projecting CeA<sup>Htr2a</sup> neurons as compared to the whole CeA<sup>Htr2a</sup> population (**Figure 19d**).

### *Thalamus*

In the thalamus, the PVT (both aPVT and pPVT) (**Figure 19d**) and VPMpc (**Figure 19d** and **e<sub>2</sub>**) provided only sparse afferents to PBN-projecting CeA<sup>Htr2a</sup> neurons. In contrast, they received abundant inputs from the multimodal thalamic nuclei (**Figure 19d**).

### *Hypothalamus and midbrain*

Inputs to PBN-projecting CeA<sup>Htr2a</sup> cells were highly enriched in all hypothalamic nuclei with the exception of the PVH (**Figure 19d** and **e<sub>3,4</sub>**).

### *Midbrain*

While the SNL (**Figure 19d** and **e<sub>5</sub>**) and MRN/CUN nuclei (**Figure 19d**) send disproportionately higher inputs to PBN-projecting CeA<sup>Htr2a</sup> neurons, the other midbrain nuclei showed only sparse labelling (**Figure 19d**).

### *Hindbrain*

RABV-eGFP+ cells were absent in the IPBN of PBN-projecting CeA<sup>Htr2a</sup> neurons (**Figure 19d**).

These experiments demonstrated that Htr2a+ neurons projecting to the PBN exhibit biases in their input selection as they receive preferential afferents from nuclei that are part of the homeostatic such as Arc<sup>165</sup> (included in the Tub. p. H.) and neuromodulatory systems<sup>166</sup> (SNL) (**Figure 19f**). Interestingly, apart from the BNST and PSTN, these afferents were previously highlighted as providing less pronounced inputs to CeA<sup>PKC $\delta$</sup>  neurons (**Figure 15a** and **Figure 16**). Remarkably, seven out of nine of the brain areas that showed an enrichment in the proportion of inputs to PBN-projecting CeA<sup>Htr2a</sup> neurons belonged to one distinct cluster (in dark red) in our covariance analysis (**Figure 18c**). In light of this finding, I propose that CeA<sup>Htr2a</sup> neurons projecting to the PBN constitute a subpopulation of CeA<sup>Htr2a</sup> neurons based on the inputs they receive.

## 3.5. IDENTIFICATION OF CE A<sup>HTR2A</sup> OUTPUT PATHWAYS

My efforts to characterize the presynaptic partners to CeA<sup>Htr2a</sup> neurons projecting to the PBN revealed that one subpopulation of CeA<sup>Htr2a</sup> neurons can be identified based on their projections to the PBN (**Figure 19**). However, another subpopulation of CeA<sup>Htr2a</sup> neurons that receives information from the IC and VPMpc remains unidentified (**Figure 18**). One possibility exists that it belongs to a different group of projection neurons.

To analyse the extent of CeA<sup>Htr2a</sup> axonal terminals, I transduced the CeA of *Htr2a-Cre mice* with AAV conditionally expressing the mCherry protein or a Synaptophysin-Myc fusion protein upon Cre recombination (**Figure 20a**).

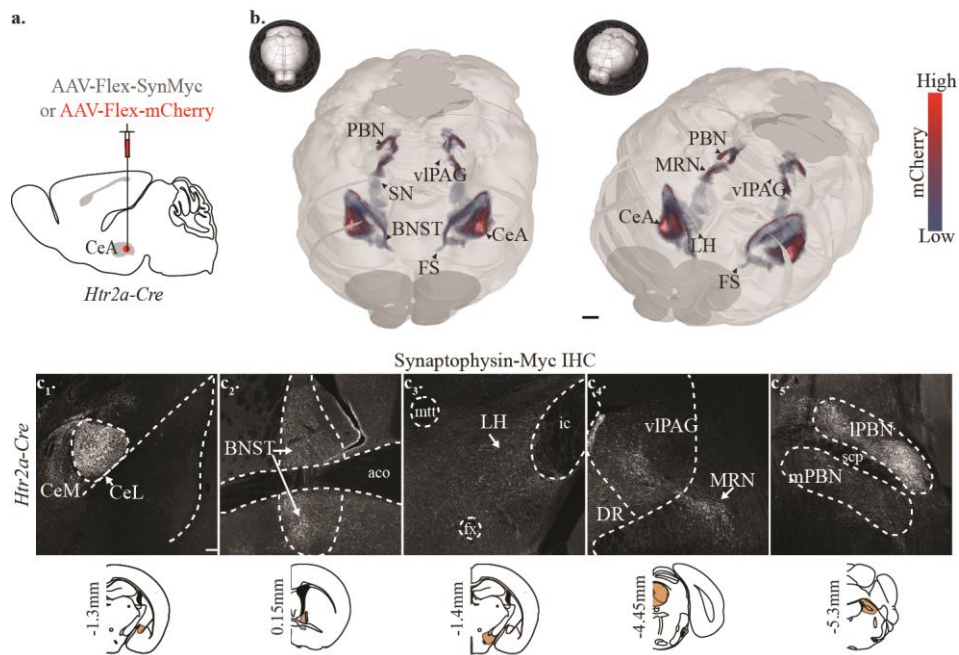


**Figure 20: Axonal projections of CeA<sup>Htr2a</sup> neurons.** **a**, Scheme representing the strategy used to highlight CeA<sup>Htr2a</sup> axonal terminals by transducing the CeA of *Htr2a-Cre* with either Cre-dependent AAV-mCherry (**b**) or Cre-dependent AAV-SynMyc (**c**). **b**, Dorsal (left) and lateral (right) views of a 3D reconstructed whole *Htr2a-Cre* mouse brain transduced in the CeA with AAV-Flex-mCherry. CeA<sup>Htr2a</sup> axonal projections are seen in the CeL, CeM, FS, BNST, LH, SN, MRN, vIPAG and PBN. The color scale indicates the intensity of the mCherry fluorescence. **c**, Representative confocal images of coronal sections of an *Htr2a-Cre* mouse brain transduced in the CeA with AAV-Flex-SynMyc and immunostained against myc protein. CeA<sup>Htr2a</sup> axonal terminals are found in the CeL (**c**<sub>1</sub>), CeM (**c**<sub>1</sub>), BNST (**c**<sub>2</sub>), LH (**c**<sub>3</sub>), DR (**c**<sub>4</sub>), vIPAG (**c**<sub>4</sub>), MRN (**c**<sub>4</sub>), IPBN (**c**<sub>5</sub>) and mPBN (**c**<sub>5</sub>) (representative of 3 *Htr2a-Cre* mice). Coronal section planes of a schematic brain are shown at the bottom with distances (anterior-posterior axis) from bregma. FS, fundus striatum; BNST, bed nucleus of the stria terminalis; aco, anterior commissure; LH, lateral hypothalamus; mt, mammillothalamic tract; fx: fornix; ic: internal capsule; SN, substantia nigra; DR, dorsal raphe; vIPAG, ventro-lateral periaqueductal gray; MRN, midbrain reticular nucleus; IPBN, lateral parabrachial nucleus; mPBN, medial parabrachial nucleus; scp: superior cerebellar peduncles. Scale bars: 1mm in **b** and 100  $\mu$ m in **c** and **d**.

Three-dimensional reconstruction of CeA<sup>Htr2a</sup> axonal projections through the whole mouse brain (**Figure 20b**) together with analysis of Synaptophysin-Myc protein accumulation (**Figure 20c<sub>1-5</sub>**) revealed that CeA<sup>Htr2a</sup> axons extend rostrally to the BNST (**Figure 20b** and **c**<sub>2</sub>) and the fundus of striatum (FS) (**Figure 20b**), dorsally to the PVT (data not shown) medially toward the LH (**Figure 20b** and **c**<sub>3</sub>) and caudally to SN (**Figure 20b**), MRN, DR, vIPAG (**Figure 20b** and **c**<sub>4</sub>), PBN (**Figure 20c**<sub>5</sub>), PRN (data not shown) and the NTS (data not shown). This is consistent with what is known to date about CeA efferents (see: 1.2.2. Long range efferents of the CeA).

### 3.6. DIFFERENTIAL DISTRIBUTION OF CEA PROJECTION NEURONS

With the same objective of identifying a subgroup of CeA<sup>Htr2a</sup> projection neurons that receives afferents from the IC and VPMpc, I speculated that projection cells populating the same territory of the CeA may receive inputs from the same candidate pairs of regions. Conversely, projection neurons segregated in different part of the CeA may receive inputs from distinct areas. This assumption encouraged me to investigate the spatial organisation of projection neurons in the CeL/C.

As depicted in **Figure 20**, CeA<sup>Htr2a</sup> neuron send axons to several brain areas. To identify the neuronal ensembles projecting to the BNST, PVT, LH, SN, MRN, vlPAG and PBN, I targeted retrogradely transported CTB conjugated with different fluorescent molecules to the aforementioned output regions. This experiment revealed that neurons present in both the CeL/C and CeM project to the BNST, LH, PAG and PBN (**Figure 21a-e**). CTB injections in the SN and MRN, on the other hand, yielded retrogradely labelled cells in the CeM division only (data not shown). Moreover, I failed to identify labelled cells in the whole CeA after CTB injections in the PVT (data not shown).

On average, injection of CTB conjugates in the BNST led to the highest number of retrogradely labelled neurons in the CeL/C followed by PBN, LH and PAG (**Figure 21c-e**). Considering the PBN as the region located the furthest away from the CeA, this result might reflect the real proportional distribution of these neurons and not be due to technical limitations leading to a higher retrograde labelling of neurons projecting to neighbouring nuclei. However, injections were not always successful with regard to complete coverage of the output regions, especially in the case of the LH, which might have led to an underestimation of the number of retrogradely labelled cells.

To analyse the three-dimensional distribution, x–y–z coordinates were assigned to labelled projection neurons (**Figure 21f**). Rostro-Caudal distribution profiles showed that all four projection neurons are evenly distributed along the rostro-caudal axis (**Figure 21g**). Dorso-ventral distributions revealed that PBN-projecting CeL/C neurons were located in a slightly more dorsal position than LH- and PAG-projecting CeL/C neurons (**Figure 21h, j and k**). However, I observed the most pronounced divergence along the medio-lateral dimension, with PBN projecting CeL/C neurons located more laterally compared to LH, and PAG- projecting CeL/C neurons (**Figure 21i-k**). Overall, BNST-projecting neurons seemed to be more evenly distributed in the CeL/C (**Figure 21g-i**).

In conclusion, these data highlight that projection neurons occupy two different, yet overlapping parts of the CeL/C. PBN-projecting neurons are located in a dorsal-lateral fashion while PAG- and LH- projecting cells segregate more toward the ventral-medial part. These differences in their spatial distribution allude to a distinct underlying input pattern.

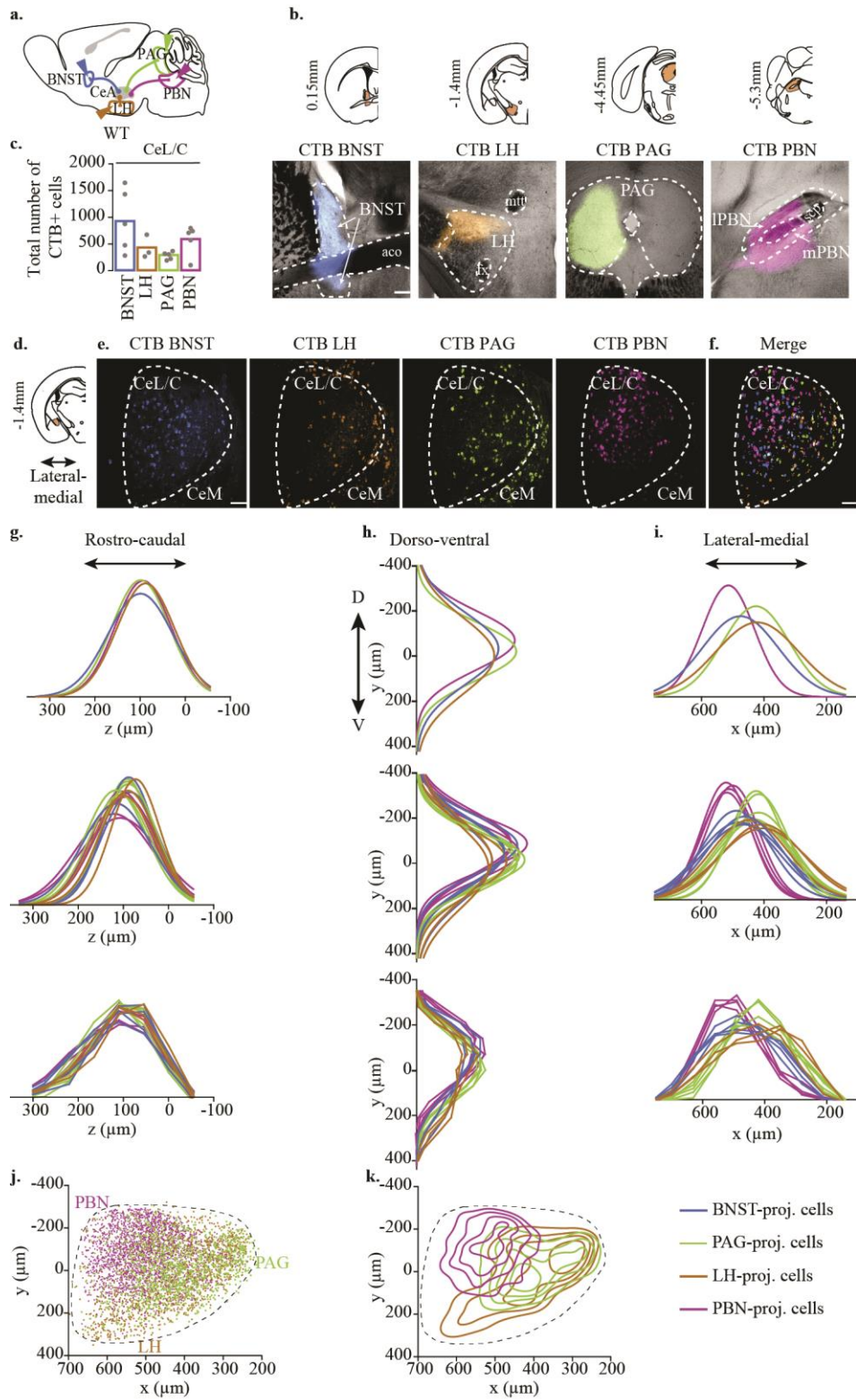


**Figure 21: Spatial segregation of CeL/C projection neurons.** **a**, Scheme illustrating the approach used to reveal spatial segregation among CeL/C projection neurons. Various CTB conjugates were injected into the BNST and, or LH and, or PAG and, or PBN of WT mice. **b**, Representative epifluorescent images showing the location of the CTB injections in the BNST, LH, PAG and PBN. Coronal section planes of a schematic brain are shown on top with distances (anterior-posterior axis) from bregma (representative of 5 mice for BNST, 3 mice for LH, 5 mice for PAG and 5 mice for PBN injections). **c**, Total number of retrogradely labelled CTB cells in the CeL/C of WT mice injected in the BNST, LH, PAG, or PBN. Bar graph shows mean and each dot is a separate experiment. **d**, Scheme of a coronal section of a mouse brain showing the location of the CeL/C (in orange). Value on the left indicates the distance from bregma on the anterior-posterior axis. **e**, Representative confocal images showing retrogradely labelled CTB cells in the CeL/C of WT mice injected in the BNST and, or LH and, or PAG and, or PBN. **f**, Corresponding digital reconstructions of BNST- (blue), LH- (orange), PAG- (green) and PBN- (magenta) projecting cell bodies. **g-i**, Frequency distribution as percent of BNST- (blue), LH- (orange), PAG- (green) and PBN- (magenta) projecting neurons of the CeL/C amygdala along the rostro-caudal (z axis) (**g**), dorso-ventral (y axis) (**h**) and lateral-medial (x axis) (**i**) axes. The top graphs show the Gaussian fits of the average traces. The middle graphs show the Gaussian fits of the single traces. The bottom graphs show the smoothed raw data of the single traces (n= 5 mice for BNST, 3 mice for LH, 5 mice for PAG and 5 mice for PBN injections). **j**, Digital coordinates along the lateral-medial (x axis) and dorso-ventral (y axis) axes of all reconstructed PAG- and PBN-projecting CeA neurons (n= 5 mice for PAG and 5 mice for PBN injections). **k**, Contour plots depicting Kernel density estimates of PAG- and PBN-projecting neuron distributions along the x and y axes (n= 5 mice for PAG and 5 mice for PBN injections). For abbreviations of brain subregions, see legend of **Figure 20**. Scale bars: 200  $\mu\text{m}$  in **c** and 100  $\mu\text{m}$  in **d**.

### 3.7. INPUT-OUTPUT RELATIONSHIP OF CE A PROJECTION NEURONS

To resolve the question of whether CeA neurons defined by their output targets receive afferents from different brain areas, I expanded the TRIO strategy<sup>161</sup> used to reveal local and long-range partners to PBN-projecting CeA neurons (**Figure 12** and **Figure 19**) to the three other major output stations of the CeA (**Figure 22a**).

In the CeA, the starter cell locations (**Figure 22b** and **e1-4**) were consistent with the topographical organisation of CeA projection neurons defined in **Figure 21**. Starter cell contamination was observed in the BLA, MeA, CP, GP, SI and LH depending on the tracing experiments (**Figure 22b**). Contrary to what was observed in **Figure 21**, tracings of LH-projecting CeA neurons harboured the largest number of starter cells in the CeL/C followed by tracings of BNST-, PBN- and PAG-projecting CeA cells. (**Figure 22c**). Proportionally, LH- and most of BNST-projecting starters were more abundant in the CeL/C part, while PBN- and PAG-projecting starters were more frequent in the CeM (**Figure 22d**).

Since my main objective was finding a class of projection neurons that receives afferents from the IC, I restricted my input analysis to quantification of RABV-eGFP+ neurons present in this region only. This compelled me to find another quantitative method to compare the proportion of IC inputs to BNST-, LH-, PAG- and PBN- projecting CeA neurons.

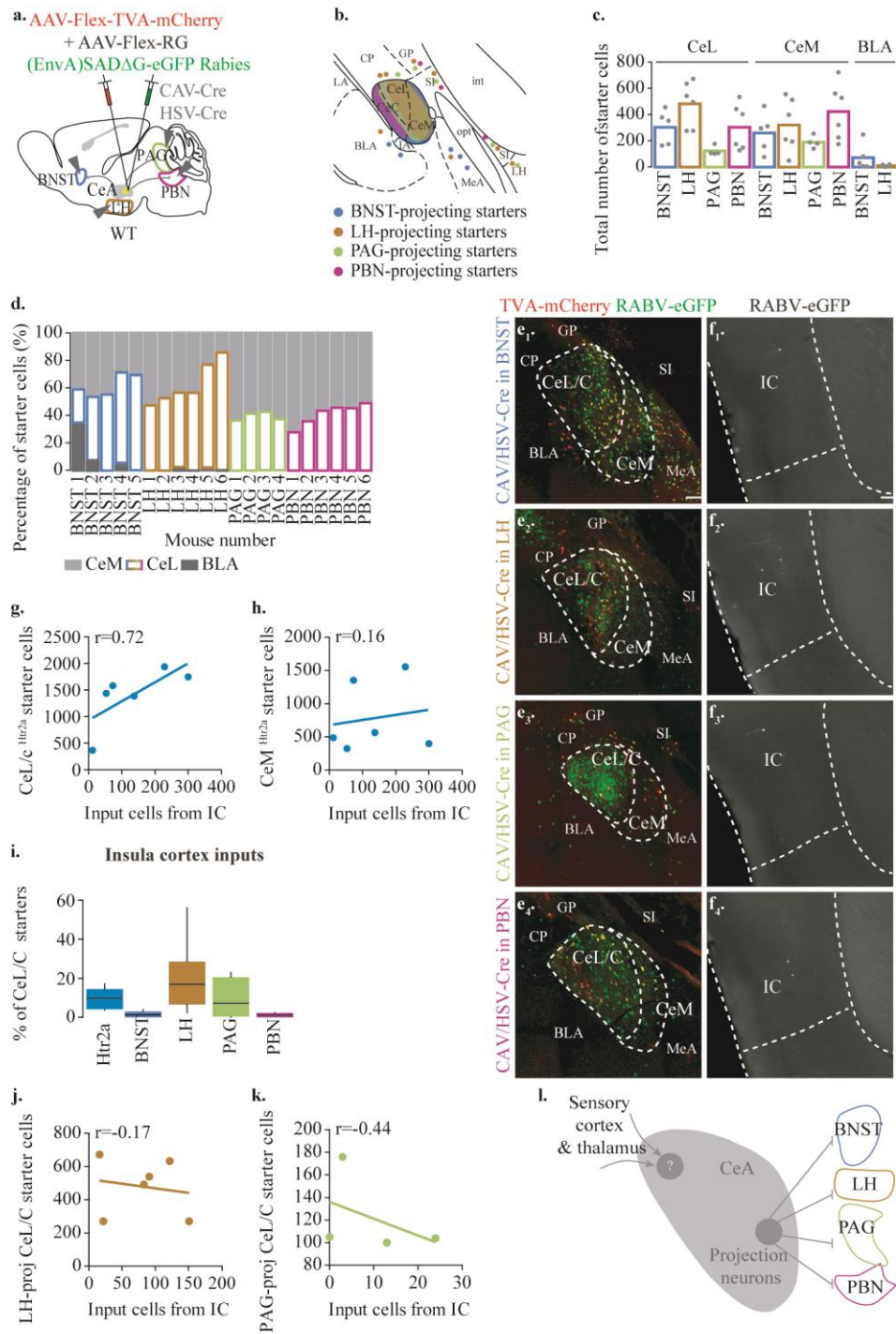


**Figure 22: Cortical input mapping of CeA projection neurons.** **a**, Scheme depicting the TRIO strategy employed to reveal monosynaptic inputs to CeA projection neurons. The BNST, or LH, or PAG, or PBN of WT mice was transduced with retrogradely transported CAV and HSV viruses expressing the Cre recombinase (Cav-Cre and HSV-Cre). Simultaneously, Cre-dependent helper adeno-associated viruses expressing the avian sarcoma leucosis virus glycoprotein EnvA receptor

(TVA) (AAV-FLEX-TVA-mCherry) and rabies virus envelope glycoprotein (RG) (AAV-FLEX-RG) were injected in the CeA in combination with a modified rabies virus (EnvA)SADΔG-eGFP. **b**, Drawing based on Paxinos and Franklin's atlas of a coronal section through the CeL/C, CeM and surrounding nuclei showing the approximate location of BNST-, LH-, PAG- and PBN-projecting CeA starter cells. BNST-projecting starters were found in CeA, BLA, MeA and SI. LH-projecting starters were found in CeA, BLA, CP, GP, MeA, SI and LH. PAG-projecting starters were found in CeA, CP, GP, SI and LH. PBN-projecting starters were found in CeA, GP and SI. **c**, Number of starter neurons in the CeL/C and CeM of BNST-, LH-, PAG- and PBN-projecting CeA tracing experiments quantified in **i-k**. Bar graph shows mean and each dot is a separate tracing experiment. **d**, Proportion of starter neurons in the CeL/C and CeM per mouse quantified in **i-k**. **e**, Representative confocal images of coronal sections through the CeL/C, CeM and surrounding nuclei of BNST- (**e<sub>1</sub>**), LH- (**e<sub>2</sub>**), PAG- (**e<sub>3</sub>**) and PBN-projecting CeA tracing brain (**e<sub>4</sub>**) (representative of 5 BNST-, 6 LH-, 4-PAG and 6 PBN-projecting CeA tracing experiments, see **b-d**). **f**, Representative epifluorescent images of coronal sections showing the distribution of monosynaptic partners (RABV-eGFP+ cells) to BNST- (**e<sub>1</sub>**), LH- (**e<sub>2</sub>**), PAG- (**e<sub>3</sub>**) and PBN-projecting CeA neurons in the IC (**e<sub>4</sub>**) (representative of 5 BNST-, 6 LH-, 4-PAG and 6 PBN-projecting CeA tracing experiments, see **b-d**). **g, h**, graphs showing that the number of input cells in the IC is positively correlated with the number of Htr2a starter cells in the CeL/C (**g**), but is not correlated with the number Htr2a starter cells in the CeM (**h**). Each dot is a separate experiment. Values shown are Pearson correlation coefficients with p values from a two-tailed unpaired t-test (n = 6 Htr2a-Cre brain see **Figure 14a-c**). **i**, IC monosynaptic inputs to CeA<sup>Htr2a</sup>, BNST-, LH-, PAG and PBN-projecting CeA neurons shown as the proportion of starter cells counted in the CeL/C per quantified brain. Box-whisker plot displays median, interquartile range and 5th-95th percentiles of the distribution (n = 6 CeA<sup>Htr2a</sup>, 5 BNST-, 6 LH-, 4-PAG and 6 PBN-projecting CeA tracing experiments, see **b-d**). **j, k**, The number of IC input cells to LH- (**j**) or PAG- (**k**) projecting CeA neurons shows no correlation with the number of LH- (**j**) or PAG- (**k**) projecting starter cells in the CeL/C. Each dot is a separate experiment. Values shown are Pearson correlation coefficients with p values from a two-tailed unpaired t-test (n = 6 LH- and 4 PAG-projecting CeA tracing experiments, see **b-d**). **l**, The scheme illustrates an organising principle of CeA afferents and efferents. Sensory information from the cortex and gustatory thalamus does not preferentially target CeA projection neurons but rather a yet unidentified population of cells that may not send axons outside of the CeA For abbreviations of brain subregions, see legend of **Figure 6** and **Figure 20**. Scale bars: 100 μm.

Identification of long-range presynaptic partners to CeA<sup>Htr2a</sup> neurons showed that 12.0% ± 1.9% of their inputs came from the IC (**Figure 15a**) and a more detailed analysis revealed that the number of RABV-eGFP+ cells in the IC is positively correlated with the number of Htr2a starter cells in the CeL/C (**Figure 22g**) but not in the CeM (**Figure 22h**). This suggested that IC inputs synapsed onto neurons present in the CeL/C division and thus, I could normalize the number of labelled neurons in the IC to the number of starter cells in the CeL/C.

Overall, the IC of BNST, LH, PAG and PBN tracing experiments exhibited very little labelling (**Figure 22f<sub>1</sub>-f<sub>4</sub>**) in comparison to CeA<sup>Htr2a</sup> or CeA<sup>PKCδ</sup> traced brains (**Figure 15b<sub>1</sub>**). In the case of LH and PAG tracing experiments nonetheless, scattered input neurons could be found throughout the anterior-posterior IC (data not shown).

Quantifications reflected these observations as IC inputs seemed to preferentially target LH- and PAG- projecting CeA neurons compared to BNST- and PBN-projecting CeA neurons as well as CeA<sup>Htr2a</sup> cells (**Figure 22i**). However, plotting the number of RABV-eGFP+ cells in the IC as a function of the number of LH- (**Figure 22j**) or PAG-projecting starter cells in the CeL/C (**Figure 22k**) did not

show such a positive correlation as observed for CeA<sup>Htr2a</sup> experiments (**Figure 22g**). This argues that the number of labelled neurons in the IC is not dependent on the number of LH- and PAG-projecting starter cells present in the CeL/C part. IC inputs observed in LH- and PAG- projecting experiments could then project onto neurons outside of the CeA or, in other words, transsynaptic labelling of IC neurons may have occurred because of starter cell contamination in the neighbouring nuclei.

In conclusion, these data suggest that the IC does not preferentially target CeA projection neurons (**Figure 22i**). On the contrary, the IC may project onto another class of CeA neurons with a field of efferents that does not extend outside of the CeA (**Figure 22i**). Hence, these results provide a foundation for further analysis to determine whether the subset of CeA<sup>Htr2a</sup> neurons that receive inputs from sensory cortices and thalamus represents a population of interneurons.



## 4. DISCUSSION



#### 4.1. SUMMARY OF FINDINGS

In the course of my thesis work, I took advantage of a set of viral-genetic tools to quantitatively analyse the connectivity profile of a population of central amygdala (CeA) neurons that express the serotonin receptor 2a. CeA<sup>Htr2a</sup> neurons have been shown by Amelia M. Douglass (data not shown) to promote food intake and self-reinforcement by means of projection to the parabrachial nucleus (PBN), and to functionally antagonize the activity of PKC $\delta$ -expressing cells. In light of this, I found that CeA<sup>Htr2a</sup> neurons mark a population of PKC $\delta$ -negative cells and overlap with a number of CeA markers that have been previously described to influence appetitive behaviours. Rabies virus-based input mapping suggests that CeA<sup>Htr2a</sup> and CeA<sup>PKC $\delta$</sup>  mutually inhibit each other, likely promoting an imbalance in their tonic activity *in vivo*, which might underlie distinct behavioural strategies. CeA<sup>Htr2a</sup> and CeA<sup>PKC $\delta$</sup>  neurons were found to gather sensory information from gustatory, visceral, nociceptive and olfactory systems, together with contextual information from the hippocampus. In addition, CeA<sup>Htr2a</sup> neurons are provided with inputs from homeostatic centres and neuromodulatory systems. Interestingly, different presynaptic partners appear to target distinct subpopulations of CeA<sup>Htr2a</sup> neurons, suggesting functional specialization within this population. Subsequent analysis of the input-output relationships revealed that CeA subcircuits might exhibit a certain organising principle. Indeed, while PBN-projecting CeA neurons receive substantial inputs from hypothalamic and midbrain nuclei, they were found to receive disproportionately smaller inputs from the sensory cortices (including the insula cortex: IC) and thalamus. Further investigations into the four principal classes of CeA projection neurons demonstrated that they occupy different parts of the CeA, arguing in favour of distinct underlying input patterns. Nonetheless, my preliminary results demonstrated that none of these populations of projection neurons might be monosynaptically contacted by the IC. Taken together, this work lays the groundwork for further investigations into the organisation of CeA circuits for appetitive and aversive behaviours.

#### 4.2. CEA<sup>HTR2A</sup> NEURONS MAY FUNCTION IN PARALLEL TO THE LA AND BLA NUCLEI

Although challenged by studies on appetitive conditioning<sup>8</sup>, the traditional model of the amygdala's function suggests that sensory information enters the amygdala complex in the lateral nucleus (LA) and is transmitted to the CeA via projections from both LA and basolateral (BLA) nuclei<sup>109</sup>. Remarkably, recent work by Kim *et al.*,<sup>25</sup> suggested that information about the valence of a stimulus is relayed onto CeA neurons by two distinct populations of BLA cells.

When investigating the long-range presynaptic partners of CeA neurons, I found that the IC and gustatory thalamus contributed to a much larger proportion of whole inputs to both CeA<sup>Htr2a</sup> and CeA<sup>PKC $\delta$</sup>  cells as compared to the LA and BLA.

This alone indicates that the traditional view of sensory information reaching the CeA via a first relay in LA and BLA is too narrow and argues in favour of parallel and independent controls of aversive and appetitive behaviours by these amygdala nuclei.

Indeed, CeA<sup>Htr2a</sup> neurons appear as a hub integrating sensory afferents from the cortex, thalamus, hippocampus and brainstem, as well as inputs from homeostatic centres and neuromodulatory systems in the hypothalamus and midbrain respectively. How these afferents might influence different aspect of the rewarding behaviour will be further discussed in the subsequent sections.

#### 4.3. CE<sup>A</sup><sup>HTR2A</sup> NEURONS REPRESENT A HETEROGENEOUS POPULATION

Although functionally homogeneous, as it is the first CeA population described that positively modulates food intake, anatomical evidence points toward heterogeneity in the CeA<sup>Htr2a</sup> population. For instance, analysis of local connectivity demonstrated that inputs to CeA<sup>Htr2a</sup> cells were likely to be from other Htr2a-expressing neurons, a wiring motif that was also observed between Sst-expressing neurons but not among CeA<sup>PKC $\delta$</sup>  cells. While interconnectivity could be important in preventing runaway excitation, another plausible interpretation would be that CeA<sup>Htr2a</sup> and CeA<sup>Sst</sup> neurons are composed of several subpopulations that are reciprocally connected. Additionally, if each of these CeA<sup>Sst</sup> subpopulations monosynaptically inhibits CeA<sup>PKC $\delta$</sup>  neurons, this would explain why CeA<sup>Sst</sup> inputs onto CeA<sup>PKC $\delta$</sup>  cells are more numerous than CeA<sup>PKC $\delta$</sup>  inputs onto CeA<sup>Sst</sup> neurons.

Hierarchical clustering of the brain regions that give inputs to CeA<sup>Htr2a</sup> neurons based on their covariance, provided the strongest evidence of heterogeneity within this population. It revealed that CeA<sup>Htr2a</sup> neurons can be seen as composite of several subpopulations that exhibit specific input patterns. At this stage, a definite number of these subsets is hard to estimate, however, it appears that while some of them show a substantial degree of overlap in their input pattern, others receive information from a completely distinct set of brain structures. Along those lines, *in vivo* calcium imaging experiments (conducted by Amelia M. Douglass and Hakan Kucukdereli – data not shown) demonstrated that the latency at which CeA<sup>Htr2a</sup> neurons begin firing upon the start of food intake is highly variable, suggesting that their activation is likely driven by diverse inputs. Could this be attributed to a discrepancy in the transduction of CeL<sup>Htr2a</sup> versus CeM<sup>Htr2a</sup> neurons, as these two divisions supposedly exhibit distinct underlying connectivities<sup>65,168</sup>? This is an appealing interpretation and certainly accounts for some of the variances observed in the input pattern of CeA<sup>Htr2a</sup> neurons. Nonetheless, it cannot justify the full range of differences, as all divisions of the CeA appear to receive inputs from the cortex, thalamus, hypothalamus and brainstem<sup>65,168</sup>.

In the subsequent sections, I will further discuss what roles these distinct subsets might play in appetitive behaviours.

#### 4.4. CEA<sup>HTR2A</sup> NEURONS HAVE THE NECESSARY CONNECTIONS TO INFLUENCE APPETITIVE BEHAVIOURS

Behavioural experiments conducted by Amelia M. Douglass demonstrated that Htr2a-expressing cells in the CeA promote both food consumption and self-reinforcement via inhibition of the PBN. Yet, the question remains as to what inputs trigger activation of PBN-projecting CeA<sup>Htr2a</sup> neurons during an appetitive task.

My analysis of long-range presynaptic partners revealed that those CeA<sup>Htr2a</sup> cells projecting to the PBN only receive a subset of the whole inputs to CeA<sup>Htr2a</sup> neurons. Interestingly, in my hierarchically clustered map, nine out of ten of these brain areas belong to one distinct cluster, and eight out of these nine were shown to provide substantial innervation onto CeA<sup>Htr2a</sup> neurons, but weak or almost non-existent innervation onto CeA<sup>PKCδ</sup> cells. These eight regions included hypothalamic nuclei as well as midbrain structures such as the substantia nigra lateralis (SNL) that harbours populations of dopaminergic neurons.

Hypothalamic inputs onto CeA cells have not yet been investigated very thoroughly and were thus far considered as feedback afferents from effector centres (see: 1.2.1. Long-range afferents to the CeA). Yet, I could identify the arcuate nucleus (Arc) – a region that is not one of the downstream targets of the CeA – as a hypothalamic structure giving inputs to PBN-projecting CeA<sup>Htr2a</sup> neurons. Circuits involving agouti-related protein (AGRP) and pro-opiomelanocortin (POMC) expressing cells in this nucleus have been extensively studied for their role in homeostatic control of body weight<sup>165,169</sup>. Arc<sup>AGRP</sup> and Arc<sup>POMC</sup> neurons sense circulating hormones that signal energy deficits (ghrelin) or body fat levels (leptin and insulin) and influence food intake through projections to several brain areas<sup>165,169</sup>. Not surprisingly, the energetic level of an animal can strongly influence its performance in instrumental conditioning. Indeed, food deprived animals will work much harder to obtain a food reward than satiated ones<sup>170</sup>. This phenomenon is thought to occur because animals will assign higher incentive value to nutrients that are consumed when they are hungry compared to when they are not<sup>171</sup>. As described in the introduction (see: 1.4.1. Encoding of reward stimuli in the CeA), the CeA can mediate an increase in the motivation to work for one particular reward by strengthening its incentive salience properties<sup>149,150</sup>. So, it is attractive to think that afferents from the Arc that carry information about the current nutritive state of an animal might help CeA<sup>Htr2a</sup> neurons in this task and would facilitate the consumption of less palatable food during energy deficit. This interaction between homeostatic and hedonic control of food intake is a very exciting area for future research as the literature so far has mainly treated these two processes as independent<sup>172</sup>.

In addition to hypothalamic nuclei, PBN-projecting CeA<sup>Htr2a</sup> neurons appear to be targeted by the SNL nucleus, which constitutes an important source of dopaminergic neurons<sup>166</sup>. Dopamine has long been implicated as a critical component of motivated behaviours. Indeed, dopamine intrinsically promotes reward, as animals will self-stimulate for dopamine release<sup>172,173</sup>. It is also implicated with the motivation to execute the behaviours necessary to obtain and consume food<sup>172</sup>, and has been proposed to function by accrediting incentive salience to reward-related stimuli<sup>174,175</sup>. As ingestion of palatable foods has been shown to increase dopamine release in CeA<sup>176,177</sup>, it would be of great interest to determine whether the role of the CeA in rewarding behaviour might be dependent on dopamine release.

With regard to the structures downstream of CeA<sup>Htr2a</sup> neurons that participate in appetitive behaviours, projections to the PBN have been shown to carry a positive-valence signal as well as to facilitate food intake. However, the processes underlying these effects remain unresolved. For instance, do CeA<sup>Htr2a</sup> cells act by inhibiting CGRP-expressing neurons in the lateral PBN (lPBN) that encode a negative-valence signal and therefore block the excitation onto CeA<sup>PKCδ</sup> cells? Alternatively, can they shape the response profile of PBN cells<sup>87,88</sup> in a way that it increases the “wanting” of particular tastes? Molecular and physiological characterization of PBN neurons that receive monosynaptic inputs from CeA<sup>Htr2a</sup> would help to shed light on these questions.

Nevertheless, examination of the output pathways should not be restricted to the study of the PBN, as distinct CeA<sup>Htr2a</sup> efferents might differentially contribute to feeding and reward related behaviours. Indeed, my analysis of whole brain projections of CeA<sup>Htr2a</sup> neurons revealed that they send axons to the pontine reticular nucleus (PRN), a nucleus which has been recently involved in controlling jaw movements<sup>94</sup>.

Additionally, CeA<sup>Htr2a</sup> axons were found in the substantia nigra (SN), which is known to influence dopamine release<sup>166</sup> and therefore act concomitantly on several brain circuits that mediate motivated behaviours including food seeking and consumption<sup>172</sup>.

Finally, CeA<sup>Htr2a</sup> innervate the lateral hypothalamus (LH) but the identity of the postsynaptic cells is unknown. Further investigations could address whether this connection acts in parallel to bed nucleus of the stria terminalis (BNST) to LH projections to inhibit LH glutamatergic neurons whose activity is known to encode a negative-valence signal and inhibit food intake<sup>178</sup>.

#### 4.5. CEA NEURONS MAY FORM STIMULUS-VALENCE ASSOCIATIONS NECESSARY FOR BOTH AVERSIVE AND APPETITIVE LEARNING.

Perhaps the most surprising outcome of my covariance analysis study is that CeA<sup>Htr2a</sup> neurons that receive inputs from the cortex, including the IC, and the

gustatory thalamus, form a very distinct cluster and largely do not overlap with CeA<sup>Htr2a</sup> neurons that are innervated by hypothalamic and neuromodulatory centres. Furthermore, my preliminary results suggest that those subsets that receive strong inputs from the IC might not belong to the four principal populations of CeA projection neurons. This finding raises the possibility that sensory information coming from the cortex and thalamus might preferentially terminate onto cells that extend axons only locally within the CeA. To my knowledge, the existence of a population of CeA interneurons has not been demonstrated. Immunostaining against classical markers of striatal interneurons such as Sst and NPY is in vain as they mark, at least partially, populations of projection neurons in the CeA<sup>23,25,179,180</sup>. Nonetheless, recordings performed in slice preparations recently revealed that a small number of CeA cells (8%) exhibit electrophysiological properties that resemble the ones of BLA interneurons<sup>181</sup>. In addition, an anatomical study provided hints that calbindin- and calretinin-expressing cells in this region may represent populations of interneurons as they have morphological characteristics typical of inhibitory interneurons<sup>182</sup>. Based on my tracing studies, we expect CeA interneurons to express Htr2a and PKC $\delta$ , as both populations receive inputs from the IC and gustatory thalamus.

Assuming that sensory information from the IC and gustatory thalamus targets CeA neurons that only project within the CeA, could this segregation in the distribution of information onto a subset of CeA neurons follow a certain logic? In the BLA complex, it is thought that CS-US associations occur in neurons that receive convergent afferents from the sensory cortex and thalamus (conveying CS information) and nociceptive system (transmitting US information) in the case of aversive learning<sup>1</sup>. If the same logic applies to CeA neurons, then we would expect that the subpopulation of CeA cells that integrates inputs from the IC, gustatory thalamus and PBN is able to form its own stimulus-value associations and undergo synaptic plasticity mechanisms that are necessary to establish memory.

Supporting this view, IC cortex inputs onto CeA cells have recently been shown to mediate learning that environmental cues predict an unpleasant taste<sup>64</sup>. Similarly, CGRP+ neurons in the IPBN encode visceral, energy balance and pain information and projections from IPBN<sup>CGRP</sup> neurons to CeA neurons have been proposed to convey a negative-valence signal that is essential to drive aversive learning<sup>37,57</sup>. Remarkably, both CeA<sup>Htr2a</sup> and CeA<sup>PKC $\delta$</sup>  neurons receive afferents from the hippocampal formation, suggesting that they might additionally integrate spatial and contextual information<sup>71</sup> and their connections with the posterior paraventricular thalamus (pPVT) might support the retrieval and maintenance of these memories<sup>125,126</sup>.

Therefore, based on anatomical evidence from my work, together with previously published behavioural studies<sup>37,57,64</sup>, I propose that a population of CeA interneurons that receives convergent inputs from the IC, gustatory thalamus and CGRP-expressing IPBN neurons is responsible for learning about negative-valence stimuli. Because these afferents emanate from gustatory and visceral associated structures, I suggest that aversive CeA-mediated learning is primarily essential to link physical properties of potentially harmful substances to

contextual and spatial environmental cues and the resulting symptoms of their consumption.

In spite of this, we could imagine that a distinct population of CeA interneurons may mediate appetitive learning so that an animal learns that environmental cues predict a rewarding outcome such as food availability or that a particular taste, odour or texture is associated with a positive outcome. In favour of this, I found that both CeA<sup>Htr2a</sup> neurons that promote appetitive behaviours and CeA<sup>PKC $\delta$</sup>  neurons that elicit aversive behaviours receive inputs from the IC, gustatory thalamus and IPBN, suggesting that distinct subsets of neurons in these structures might target these two CeA populations. This is partially illustrated by the fact that  $60.4 \pm 4.4\%$  of IPBN inputs to CeA<sup>PKC $\delta$</sup>  neurons originate from CGRP+ cells, while the latter provide only  $16.4 \pm 7.1\%$  of CeA<sup>Htr2a</sup> inputs.

Alternatively, information about the positive US may be relayed by dopamine that is known to encode prediction errors and therefore serve as a teaching signal for reward learning<sup>183,184</sup>. In light of this, the SNL and midbrain reticular nucleus, retrorubral area (RR) that harbour populations of dopaminergic neurons preferentially project onto CeA<sup>Htr2a</sup> neurons compared to CeA<sup>PKC $\delta$</sup>  cells.

Finally, considerable evidence suggests that the IC can represent both positive and negative values<sup>39,185–187</sup>. Yet, in a recent study<sup>64</sup>, optogenetic silencing of IC to CeA projections only led to impairment in the avoidance response to a predicted unpleasant taste but left the approach behaviour to a predicted pleasant taste intact. At this point, the role of defined subsets of CeA neurons in mediating stimulus-valence association during appetitive learning remains uncertain and needs more detailed interrogations.

#### 4.6. PARALLEL COLLABORATIVE CIRCUITS IN THE CEA MAY CONTROL BEHAVIOUR

In addition to providing efferents to brain areas involved in rewarding behaviours, CeA<sup>Htr2a</sup> neurons send axon collaterals to a number of other forebrain and brainstem structures, which have previously been implicated in controlling conditioned-fear expression. Among them, the ventro-lateral periaqueductal gray (vIPAG) is a key site for mediating the freezing reaction in response to a threat<sup>92</sup>.

This raises the question whether pleasure and displeasure would be underpinned by CeA circuits that are organised in a somewhat overlapping manner. As described earlier (see: 1.3.3. Beyond conditioned fear in the CeA), projections from the BLA to the CeA can both exert an anxiolytic influence<sup>138</sup> and encode a negative valence signal<sup>124,131</sup>, illustrating that one single pathway can affect opposing behaviours. Therefore, it is conceivable that the same connections that were once thought to regulate conditioned fear may also control rewarding behaviour. As an example, the sight of a high incentive reward can also trigger an increase in heart rate and blood pressure<sup>188</sup>, supporting a model in which

physiological responses to positive and negative emotions may be processed by neural systems that partially overlap.

Yet, some connections must be exclusive to either the appetitive or aversive behaviour, and the fact that projection neurons do not occupy the same territory in the CeL could make them more likely to be connected with positively or negatively valenced elements. This would be an interesting question to pursue. Furthermore, local antagonistic connections between two opposing units might serve to maintain an imbalance in their tonic activity that would contribute to different behavioural programs. For instance, we have seen that CeA<sup>Htr2a</sup> neurons and CeA<sup>PKC $\delta$</sup>  cells mutually inhibit each other, a circuit mechanism that could allow for a rapid switch between reinforcement and inhibition of food intake.

Overall, this suggests that the CeA is a collective of collaborative neuronal circuits that act together to modulate pleasant or unpleasant behaviour depending on the environmental conditions and the internal state of the animal. The focus should now be on how distinct sensory information is computed locally to give rise to diverse functional effects.

#### 4.7. LIMITATIONS OF THE RABIES VIRUS–BASED MONOSYNAPTIC TRACING TECHNOLOGY

Trans-synaptic tracing using modified rabies virus has proven itself extremely valuable to map connections in between defined populations of neurons<sup>156</sup>. Yet, it is important here to mention its associated caveats and limitations.

First, at the level of the local connectivity, leaky expression of TVA, G- and mCherry proteins outside of Cre+ cells has been observed<sup>159</sup>. Although this leaky expression does not allow sufficient production of the G protein necessary for trans-complementation and transsynaptic spread, a very low level of TVA expression can however permit an efficient interaction with the EnvA protein, resulting in RABV infection and subsequent expression of genes from the viral genome. Since the level of mCherry protein in these cells is not detectable, these neurons are undistinguishable from presynaptic partners. To overcome this problem, a new form of the TVA receptor that exhibits a lower affinity with its EnvA ligand has been produced<sup>189</sup>. This mutant does not show Cre-independent labelling and therefore could be implemented in our laboratory for further analysis of CeA local connectivity.

A second issue that should be considered is the difficulty in analysing interconnectivity between Cre+ neurons. Indeed, transsynaptic spread to a neuron that was initially infected with the AAV helper but not with the RABV would result in further trans-complementation with G and spread of the virions across an additional synaptic step. This likely resulted in an underestimation of the proportion of inputs originating from the same population in my microcircuit analysis.

In addition, although this study is the first to provide a comprehensive whole-brain atlas of the monosynaptic inputs to CeA<sup>Htr2a</sup> neurons, some of the presynaptic partners of CeA<sup>PKC $\delta$</sup>  and CeA<sup>Sst</sup> cells have already been published<sup>64,134,141</sup>. While the results from this work and others are very consistent considering CeA<sup>PKC $\delta$</sup>  tracing experiments, divergences exist with respect to the identity of long-range inputs to CeA<sup>Sst</sup> neurons. Indeed, although I have never observed RABV+ neurons in the IC of CeA<sup>Sst</sup> tracing brains, two groups<sup>64,134</sup> have reported CeA<sup>Sst</sup> neurons as downstream targets of the IC. Several explanations could account for these discrepancies. First, the use of a different Cre-driver line in Schiff *et al.*, study might lead to disparate results. Second, Sst+ cells are widely represented in the BLA which lies next to the CeA. If BLA<sup>Sst</sup> neurons receive IC inputs, then a high infection rate of these cells would strongly compromise the data analysis. Additional methods would be needed to solve this issue.

Importantly, as the mechanism through which the RABV is transsynaptically transported to the input neurons is not entirely understood, the possibility still stands that the RABV exhibits a specificity towards infecting certain types of neurons or a resistance towards others as it was recently described for myelinated and unmyelinated sensory neurons in the dorsal root ganglia of the spinal cord<sup>190</sup>. This would strongly bias the interpretation of studies using trans-synaptic rabies virus-based tracing.

Finally, it is yet not clear whether the use of RABV overcomes the limitations that are usually encountered with other retrograde tools such as infection of axons in passage<sup>156</sup>.

Overall, this study of local and long-range presynaptic partners of defined populations of CeA neurons has reliably revealed trends as well as biases that likely mask the real organisation of CeA circuits. In the future, complementary techniques such as channelrhodopsin-assisted circuit mapping<sup>132</sup> could be used to support this work.

#### 4.8. CONCLUSIONS AND OUTLOOK

The aim of my thesis was to provide a high level of detail in the wiring diagram, including both the pattern of inputs and outputs, of a population of CeA neurons that has been shown to positively regulate food intake.

Based on results from my work and a rich literature on CeA neuronal assemblies, a picture of CeA microcircuits has emerged (**Figure 23**) in which sensory information from the IC and gustatory thalamus might specifically terminate onto a population of interneurons. CeA interneurons would in turn process this information to provide a positive- or negative-valence tag to the physical properties of particular nutrients and the contextual cues associated with their ingestion. Through local computations, the encoding cells would then use this tag to modulate the activity of projection neurons in the CeA to engage the appropriate behaviour. Importantly, as CeA networks are exclusively composed of inhibitory neurons, I propose that encoding cells and executing cells are

separated by more than one synapse. Indeed, in basal condition, an intermediate population might inhibit the projection neurons and disinhibition of these intermediate cells by the encoding ones would release the tonic inhibition onto the output neurons and facilitate their excitation by external components, such as neuromodulators.

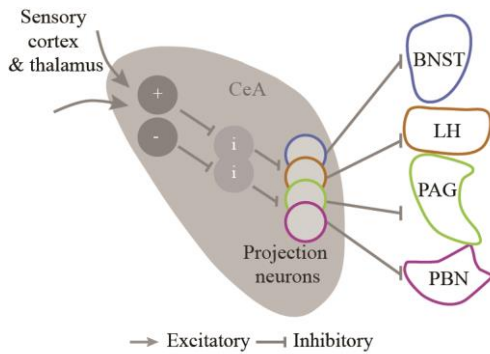


**Figure 23: Schematic model of the organisation of CeA microcircuits.** In the CeA, two populations of encoding interneurons encode positively or negatively valenced cues (+ and -) and control the activity of projection neurons via intermediate cells (i) that tonically inhibit the latter. Activation of encoding cells inhibits the intermediate cells, thereby releasing the inhibition on the projection neurons, which facilitates their activation by external players such as neuromodulators.

Of great interest would be to characterize the identity of the CeA neurons that lie downstream of the IC and find further evidence that they exhibit the anatomical and functional properties of interneurons. In order to do so, one strategy could consist of acutely activating the axonal projections of IC neurons in the CeA. Subsequent analysis of immediate early gene expression (such as c-fos) in combination with immunostaining for various CeA markers would provide details about the molecular identity of CeA neurons that receive inputs from the cortex. A similar approach could be pursued after injection of retrogradely transported beads in one or several output regions in order to assess the likeliness that c-fos positive CeA cells overlap with retrogradely labelled CeA neurons. Complementing this set of experiments, channelrhodopsin-assisted circuit mapping<sup>132</sup> in brain slices could confirm the functionality of the identified connections and define whether CeA neurons that receive afferents from the IC undergo learning-dependent plasticity.

Once molecular markers have been identified, intersecting combinations of specific Cre driver lines could be used to further assess the function of these cells. For instance, recording calcium transients could demonstrate whether the activity of these neurons can encode both the conditioned (CS) and unconditioned stimulus (US). Remarkably, we could identify whether neurons that encode aversive stimuli are distinct from the ones that encode appetitive stimuli. Functional manipulation of this population using optogenetics and pharmacogenetic tools would finally confirm whether memory traces are stored in the CeA. Collectively, this array of experiments would provide new insights into how associative memories are stored in the CeA. Of note, we should keep in mind that neuronal coding in the amygdala might be dependent on both up- and down-regulation<sup>191</sup> of cell activity and merely focusing on CeA neurons that are excited during learning and retrieval might only partially reveal how CeA ensembles encode memories.

In order to understand the division of labour within the CeA, functionality must be mapped onto each CeA projection neuron using well-designed behavioural tasks. Importantly, it is unlikely that all neurons that project to the same nucleus share the same function. For this reason, more specific targeting will be needed and together with state of the art tracing methods, would permit the visualisation of where the circuits for the execution of appetitive and aversive behaviours overlap and separate.

Finally, as we look to the future of research on CeA circuits, I believe that understanding how neuromodulators influence the encoding of positive and negative valence cues should deserve special attention. For instance, what is the role of dopamine in both appetitive and consummatory parts of CeA-mediated rewarding behaviours as well as whether it can act as a teaching signal for learning about positive-valence stimuli. In addition, CeA<sup>Htr2a</sup> neurons appear to be specific target of the dorsal raphe (DR) nucleus that contains the largest group of serotonin-producing neurons in the brain. Although the identity of the input neurons in the DR has not been investigated in this study, it was previously shown that glemanserin which is a selective antagonist of the Htr2a receptor can decrease the activity of Htr2a-Cre positive neurons in the CeA, suggesting that serotonin increases the firing of these cells<sup>38</sup>. Thus far, serotonin has been described as a negative regulator of food intake<sup>192</sup>. Yet, a study has demonstrated that blocking the Htr2a receptor in fly can decrease food consumption suggesting a positive role of serotonin and this receptor on feeding behaviour<sup>193</sup>.

In conclusion, my findings provide a new angle on the architecture of CeA circuits that control appetitive and aversive behaviours. Further delineation of CeA cell populations based on their molecular profiles, developmental origin, response properties, and connectivity pattern is required in order to understand how neuronal signals in the CeA come to affect behaviour.

## 5. METHODS



## 5.1. ANIMALS

*Htr2a-Cre* BAC (STOCK Tg[Htr2a-cre] KM208Gsat/Mmucd) and *Prkcd-Cre* BAC (Tg(Prkcd-glc-1/CFP,-cre)EH124Gsat) transgenic lines were obtained from the Mutant Mouse Regional Resource Center (<https://www.mmrrc.org/>). *Sst-Cre* (Ssttm2.1(cre)Zjh) transgenic mice were acquired from the Jackson Laboratory (<https://www.jax.org/>). *Td-Tomato* (B6.Cg-Gt(ROSA)26Sortm9(CAG-tdTomato)Hze/J) and *Rosa26R* mouse lines have been previously described. WT mice were from the C57BL/6NRj strain (Janvier Labs - <http://www.janvier-labs.com>). All experiments were conducted using 2-4 month old males and females mice backcrossed onto a C57BL/6NRj background.

## 5.2. VIRAL CONSTRUCTS

AAV1-EF1 $\alpha$ -FLEX-TVAmCherry and AAV1-CAG-FLEX-RG were purchased from the University of North Carolina Vector Core (<https://www.med.unc.edu/genetherapy/vectorcore>). AAV8-CAG-FlexFRT-G and AAV5-CAG-FlexFRT-TC were obtained from the Gene Vector and Virus Core of Stanford University School of Medicine (<http://med.stanford.edu/gvvc/>). For mapping of monosynaptic inputs to CeA<sup>Htr2a</sup>, CeA<sup>PKC $\delta$</sup>  and CeA<sup>Sst</sup> neurons, I used the EnvA G-deleted rabies-eGFP produced at the Gene Transfer Targeting and Therapeutics Core of the Salk Institute for Biological Studies (<http://www.salk.edu/science/core-facilities/gene-transfer-targeting-and-therapeutics-core/>). EnvA G-deleted rabies-eGFP used for TRIO and cTRIO experiments has been previously described<sup>154</sup>. We obtained the CAV2-Cre and CAV2-FlexLoxp-Flp from the Montpellier Vectorology Platform of the UMS Biocampus (<http://www.igmm.cnrs.fr/spip.php?rubrique166>). HSV-hEF1 $\alpha$ -Cre and HSV-hEF1 $\alpha$ -LS1L-IRESflpo were supplied by the Viral Gene Transfer Core of the Massachusetts Institute of Technology (<https://mcgovern.mit.edu/technology/viral-core-facility>). AAV-Flex-SynMyc<sup>194</sup> was a gift from S. Arber (FMI, Basel). AAV-Flex-mcherry<sup>195</sup> was a gift from M. Schwarz (Max Planck Institute for Medical Research, Heidelberg).

## 5.3. STEREOTAXIC SURGERIES

Mice were anaesthetized using isoflurane (Cp-pharma) (induction, 3%; maintenance, 1.5%) in oxygen-enriched air and head-fixed on a stereotaxic frame (Model 1900 – Kopf Instruments). Their body temperature was maintained at 37°C using a heating pad. Carprofen (Rimadyl – Zoetis) (5 mg/kg body weight), as an analgesic, was given via subcutaneous injection. Viral particles were delivered using glass pipettes (708707 - BLAUBRAND intraMARK) connected to a Picospritzer III (Parker Hannifin Corporation) and controlled by a Master-8

pulse stimulator (A.M.P.I) at a flow rate of 50 nL/min. After delivery of the virus, the pipette remained in the brain for 5 min to prevent spread of the virus.

### 5.3.1. Negative control experiments for monosynaptic tracing

0.2-0.4  $\mu$ L of AAV1-EF1 $\alpha$ -FLEX-TVAmCherry and AAV1-CA-FLEX-RG mixed at a ratio of 1:4 were unilaterally or bilaterally injected in the CeA of WT mice (stereotaxic coordinates from bregma in **Table 1**). Fourteen days later, mice were injected in the CeA using the exact same coordinates with 0.2-0.4  $\mu$ L of EnvA G-deleted rabies-eGFP virus. After recovery, mice were housed for seven days before euthanasia.

### 5.3.2. Identification of monosynaptic inputs to CeA<sup>Htr2a</sup>, CeA<sup>PKC $\delta$</sup> and CeA<sup>Sst</sup> neurons

0.2-0.4  $\mu$ L of AAV1-EF1 $\alpha$ -FLEX-TVAmCherry and AAV1-CA-FLEX-RG mixed at a ratio of 1:4 were unilaterally or bilaterally injected in the CeA of *Htr2a-Cre* or *Prkcd-Cre* or *Sst-Cre* mice (stereotaxic coordinates from bregma in **Table 1**). Fourteen days later, mice were injected in the CeA using the exact same coordinates with 0.2-0.4  $\mu$ L of EnvA G-deleted rabies-eGFP virus. After recovery, mice were housed for seven days before euthanasia.

### 5.3.3. Identification of monosynaptic inputs to BNST, LH, PAG and PBN-projecting CeA neurons (TRIO experiments)

0.2-0.4  $\mu$ L of AAV1-EF1 $\alpha$ -FLEX-TVAmCherry and AAV1-CA-FLEX-RG mixed at a ratio of 1:4 were unilaterally or bilaterally injected in the CeA of WT mice (stereotaxic coordinates from bregma in **Table 1**). In the same surgery, 0.4  $\mu$ L of CAV2-Cre and HSV-hEF1 $\alpha$ -Cre mixed at a ratio of 1:1 were also injected unilaterally or bilaterally in the BNST, or LH, or PAG, or PBN (stereotaxic coordinates from bregma in **Table 1**). Fourteen days later, mice were injected in the CeA using the exact same coordinates as described above with 0.2-0.4  $\mu$ L of EnvA G-deleted rabies-eGFP virus. After recovery, mice were housed for seven days before euthanasia.

### 5.3.4. Identification of monosynaptic inputs to PBN-projecting CeA<sup>Htr2a</sup> neurons (cTRIO experiments)

0.4  $\mu$ L of AAV8-CAG-Flex<sup>FRT</sup>-G and AAV5-CAG-Flex<sup>FRT</sup>-TC mixed at a ratio of 1:1 were unilaterally or bilaterally injected in the CeA of *Htr2a-Cre* mice (stereotaxic coordinates from bregma in **Table 1**). In the same surgery, 0.4  $\mu$ L of CAV2-Flex<sup>L<sup>oxp</sup></sup>-Flp and HSV-hEF1 $\alpha$ -LS1L-IRES-flpo mixed at a ratio of 1:1

were also injected in the PBN (stereotaxic coordinates from bregma in **Table 1**). Fourteen days later, mice were injected in the CeA using the exact same coordinates with 0.2-0.4  $\mu$ L of EnvA G-deleted rabies-eGFP virus. After recovery, mice were housed for seven days before euthanasia.

### 5.3.5. Analysis of spatial segregation of CeA projection neurons

WT mice were injected in the BNST and or LH and or PAG and or PBN (stereotaxic coordinates from bregma in **Table 1**) with 300nL of Cholera Toxin Subunit B (CTB) conjugated with Alexa fluor 488 or 555 or 647 (C34775, C34776, C34778 – Invitrogen). After recovery, mice were housed for seven days before euthanasia.

### 5.3.6. Axonal projections of CeA<sup>Htr2a</sup> and CeA<sup>PKC $\delta$</sup> neurons

*Htr2a-Cre* or *Prkcd-Cre* mice were unilaterally or bilaterally injected in the CeA (stereotaxic coordinates from bregma in **Table 1**) with AAV-Flex-SynMyc or AAV-Flex-mcherry. After recovery, mice were housed for seven days before euthanasia.

<b>Injection site</b>	<b>Tracing experiments</b>	<b>Rostro-caudal (in mm)</b>	<b>Medio-lateral (in mm)</b>	<b>Dorso-ventral (in mm)</b>
<b>CeA</b>	Inputs to CeA <sup>Htr2a</sup> Inputs to CeA <sup>Pkcδ</sup> Inputs to CeA <sup>Sst</sup> Inputs to PBN-projecting CeA <sup>Htr2a</sup> Negative control for monosynaptic tracing Axonal projections of CeA <sup>Htr2a</sup> and CeA <sup>PKCδ</sup>	-1.25	+/-2.9	-4.9 to 4.8
<b>CeA</b>	Inputs to BNST-projecting	-1.2	+/-2.85	-4.7
<b>CeA</b>	Inputs to LH-projecting	-1.2	+/-2.86	-4.8
<b>CeA</b>	Inputs to PAG-projecting	-1.25	+/-2.86	-4.8
<b>CeA</b>	Inputs to PBN-projecting	-1.3	+/-2.9	-4.8
<b>BNST</b>	Inputs to BNST-projecting Spatial segregation of BNST-projecting	+0.56	+/-0.92	-4.95 to 4.65
<b>LH</b>	Inputs to LH-projecting Spatial segregation of LH-projecting	-1.25	+/-1.15	-5.2
<b>PAG</b>	Inputs to PAG-projecting Spatial segregation of PAG-projecting	-4.2 to 4.4	+/-0.55	-2.84
<b>PBN</b>	Inputs to PBN-projecting Spatial segregation of PBN-projecting CeA <sup>Htr2a</sup>	-5.3	+/- 1.35 to 1.45	-3.9 to -3.8

**Table 1:** Stereotaxic coordinates from bregma

#### 5.4. HISTOLOGY

Animals were anesthetized with ketamine/xylazine (Medistar and Serumwerk) (100 mg/kg and 16 mg/kg respectively) and transcardially perfused with phosphate-buffered saline (PBS), followed by 4% paraformaldehyde (PFA) (1004005 – Merck) (w/v) in PBS. Extracted brains were postfixed at 4 °C in 4%

PFA (w/v) in PBS for 12 h. Brain tissues for *in situ* hybridization were cryoprotected sequentially in 15% and 30% sucrose (S0389 – Sigma-Aldrich) (w/v) in PBS at 4°C and embedded in O.C.T (Sakura Finetek). 15 µm coronal cryo-sections were cut using a cryostat (CM30505 - Leica), mounted on Superfrost Plus slides (Thermo Fisher Scientific - Menzel-Gläser), dried in air for 20 min at RT and stored at –80 °C for later use. All other brain samples were embedded in 4% agarose (01280 – Biomol) (w/v) in PBS and sliced using a Vibratome (VT1000S - Leica) into 50- to 100-µm free-floating coronal sections.

## 5.5. BRAIN TISSUE CLEARING

The protocol was adapted from a previously published protocol<sup>196</sup>. *Htr2a-Cre* mice that had been stereotaxically injected in the CeA with an AAV-mCherry virus to reveal CeA<sup>Htr2a</sup> axonal projections, were anesthetized with ketamine/xylazine (Medistar and Serumwerk) (100 mg/kg and 16 mg/kg respectively) and perfused through the ascending aorta at a speed of 4 mL/min with 20 mL of ice cold PBS followed by 20 mL of ice-cold hydrogel monomer solution containing 2% acrylamide (161-0140, Bio-Rad), 0.025% bisacrylamide (1610142, Bio-Rad), 4% PFA and 0.25% VA-044 initiator (w/v) (27776-21-2, Wako) in PBS. After perfusion, brains were placed in 20 mL of ice-cold hydrogel monomer solution and incubated for 3 days at 4 °C. Brain tissues immersed in hydrogel monomer solution were then incubated for 3 h at 37 °C to allow the solution to polymerize. The embedded samples were extracted from the gel and 2 mm sections were cut using a vibratome (VT1000S - Leica) Sections were then washed with a clearing solution: 4% SDS (0183 – Carl Roth) and 200 mM boric acid (1.00165, Millipore), pH 8.5, until they became transparent (approximately 2 weeks). When transparency was achieved, sections were rinsed for at least 3 days in PBS and 0.1% Triton X-100 (6683 – Carl Roth) at 37 °C to remove residual SDS. Sections were finally incubated in a refractive-index-matching solution (RapiClear, RI = 1.47, SunJin Lab) for 8 h (up to 1 day) at RT before to be mounted in fresh RapiClear between two coverslips separated by iSpacers (IS003 1mm - SunJin Lab).

## 5.6. FLUORESCENCE IN SITU HYBRIDIZATION (FISH)

Fixed frozen sections from *Htr2a-cre;LacZ*, *Htr2a-cre; tdTomato* mice or *Prkcd-Cre* mice that were transduced in the CeA with AAV helper viruses and recombinant rabies virus to identify monosynaptic inputs to CeA<sup>PKCδ</sup> neurons underwent two-color FISH. The assay was performed by using the proprietary probes and methods of Advanced Cell Diagnostics (ACD Technical notes 320535 for sample preparation and 320293 for multiplex fluorescence labeling, <http://www.acdbio.com/technical-support/downloads/>).

Briefly, sections were washed with PBS to remove O.C.T. They were then boiled for 5 min in Pretreat 2 buffer and immediately afterwards washed 2 times in

distilled water and 1 time in 100% ethanol (32205 – Sigma-Aldrich) at RT. Sections were then air dried before incubation with Pretreat 4 for 30 min at 40 °C in a HybEZ humidified incubator (ACDBio). Sections were rinsed 2 times at RT with distilled water before hybridization with probes. Single- or dual-probe labelling were performed using probes for *Htr2a* (Mm-Htr2a-C1, 401291), *LacZ* (Ecoli-lacZ-C3, 313451-C3), *Tac2* (Mm-Tac2-C2, 446391) and *Crh* (Mm-CRH-C2, 316091) mRNA. The C1 probe was ready to use. When used in combination with C1, the C2 and C3 probes were diluted 50 times in C1 probe. When used alone, the C2 and C3 probes were diluted 50 times in the probe diluent buffer. Probes were heated in a 40 °C water bath for 10 min before use. Probe mix was applied to the tissue sections, which were placed in a 40 °C HybEZ humidified incubator for 2 h. Sections were rinsed in ACD Wash Buffer (2 × 2 min at RT) and underwent sequential incubations with the proprietary ACD reagents AMP1-FL (30 min at RT), AMP2-FL (15 min at RT), AMP3-FL (30 min at RT) and Amp 4 Alt B-FL AMP4-FL (15 min at RT) with two washes (2 min) between each step. Brain sections from *Htr2a-cre;LacZ* mice were then labelled with DAPI for 30 seconds (Sigma-Aldrich) and immediately coverslipped using Fluorescent Mounting Medium (S3023 - Dako).

Brain sections from *Htr2a;tdTomato* mice or from *Prkcd-Cre* mice that were transduced in the CeA with AAV helper viruses and recombinant rabies virus to identify monosynaptic inputs to CeA<sup>PKC $\delta$</sup>  neurons were blocked for 2 h at RT with 0.2% BSA (A7030 – Sigma-Aldrich) and 5% donkey serum (017-000-121 – Jackson Immunoresearch) (w/v) in PBS. Sections were then incubated at 4 °C overnight with mouse anti-GFP (1:500) (632381, Clontech) and/or rabbit anti-mCherry (1:500) (ab167453, Abcam) in 0.1% Triton X-100 (66831 – Carl Roth) and 0.2% BSA (w/v) in PBS. After three washes of 15 min each in PBS, they were incubated for 2 h at RT with the following secondary antibodies: donkey anti-rabbit/mouse Alexa Fluor 488 or Cy3 or Alexa Fluor 647 (1:300) (anti-rabbit, 711-545-152, 711-165-152, 711-495-152; anti-mouse, 715-545-151, 715-165-151, 715-605-151 – Jackson Immunoresearch) in 0.1% Triton X-100 and 0.2% BSA (w/v) in PBS. Sections were finally washed three times for 15 min each with PBS, labelled with DAPI for 30 seconds (Sigma-Aldrich) and immediately coverslipped using Fluorescent Mounting Medium (S3023 - Dako).

## 5.7. IMMUNOHISTOCHEMISTRY (IHC)

50  $\mu$ m free-floating coronal sections cut using a Vibratome (VT1000S – Leica) were incubated in 50 mM ammonium chloride (NH<sub>4</sub>Cl) (1.01145 – Merck) for 15 min to reduce auto-fluorescence of the brain tissues. Sections were then permeabilized for 30 min at RT with 0.5% TritonX-100 (66831 – Carl Roth) in PBS and blocked for 2 hr at RT with 0.2% BSA (A7030 – Sigma-Aldrich) and 5% donkey serum (017-000-121 – Jackson Immunoresearch) (w/v) in PBS. Sections were incubated with primary antibodies diluted in 0.2% BSA (w/v) in PBS at 4 °C overnight. The following primary antibodies were used: mouse anti-PKC $\delta$  (1:100) (610398, BD Biosciences), chicken anti-LacZ (1:200) (ab9361,

Abcam), rabbit anti-Sst (1:1000) (T-4103, Peninsula Laboratories International), goat anti-CGRP (1:500) (Abcam, ab36001) and rabbit anti-myc (ab9106, Abcam). Sections were washed three times 15 min with 0.1% TritonX-100 in PBS and incubated for 2 h at RT with secondary antibody diluted 1:300 in 0.2% BSA (w/v) in PBS. The following secondary antibodies were used: donkey anti-rabbit/mouse/goat/chicken Alexa Fluor 488 or Cy3 or Alexa Fluor 647 (anti-rabbit, 711-545-152, 711-165-152, 711-495-152; anti-mouse, 715-545-151, 715-165-151, 715-605-151; anti-goat, 705-545-147, 705-165-157, 705-175-147; anti-chicken, 703-545-155, 703-165-155, 703-605-155 – Jackson Immunoresearch). Sections were washed two times 15 min with 0.1% Triton X-100 in PBS and incubated with DAPI (1/2000) (Sigma - Aldrich) in PBS. After 15 min wash in PBS, sections were finally coverslipped using Fluorescent Mounting Medium (S3023 - Dako).

## 5.8. MICROSCOPY AND IMAGE PROCESSING

A Leica SP8 confocal microscope and a 20×/0.75 IMM objective (Leica) were used to acquire Fluorescence z-stack images. Epifluorescence images were obtained with an upright epifluorescence microscope (Zeiss) with 5×/0.15 or 10×/0.3 objectives (Zeiss). Entire coronal sections of a mouse brain or full view of CeA and surrounding nuclei were acquired using the tile scan and automated mosaic merge functions of Leica LAS AF software. Images were minimally processed with ImageJ software (NIH) to adjust for brightness and contrast for optimal representation of the data. A median filter was used to decrease noise.

## 5.9. DATA ANALYSIS

### 5.9.1. Molecular characterization of CeA<sup>Htr2a</sup> neurons

For colocalization analyses of Htr2a-Cre<sup>+</sup> neurons in the CeL/C with PKC $\delta$  and Sst proteins and Htr2a, Tac2 and Crh mRNAs, three to four 50  $\mu$ m (for IHC) or 15  $\mu$ m (for FISH) thick coronal sections per brain and for each marker underwent FISH or immunostaining procedure. Z-stack images were acquired and analysed from anterior to posterior CeA (bregma -1.1 to -1.7 mm) using ImageJ (NIH).

### 5.9.2. Identification of local inputs to CeA<sup>Htr2a</sup> CeA<sup>PKC $\delta$</sup> , CeA<sup>Sst</sup> and PBN-projecting CeA neurons

For quantification of starter cells in the CeA, Z-stack images of every section or every second section from -0.9 to -1.8 mm posterior to bregma were acquired and analysed using ImageJ (NIH). Brains that showed a high number of starter

cells in the CeM and or neighbouring nuclei compared to the CeL/C were excluded from the analysis.

For identification and quantification of local monosynaptic inputs to CeA<sup>Htr2a</sup>, CeA<sup>PKC $\delta$</sup> , CeA<sup>Sst</sup> and PBN-projecting CeA neurons, three to four 50  $\mu$ m (for IHC) or 15  $\mu$ m (for FISH) thick coronal sections per brain and for each marker, underwent FISH or immunostaining procedure. Z-stack images were acquired and analysed from anterior to posterior CeA (bregma  $-1.1$  to  $-1.7$  mm) using ImageJ (NIH).

### 5.9.3. Whole brain monosynaptic inputs to CeA<sup>Htr2a</sup>, CeA<sup>PKC $\delta$</sup> , CeA<sup>Sst</sup>, PBN-projecting CeA and PBN-projecting CeA<sup>Htr2a</sup> neurons

For quantification of starter cells in the CeA, every section or every second section from  $-0.9$  to  $-1.8$  mm posterior to bregma was quantified with ImageJ (NIH). Only brains that showed a high tracing efficiency and the presence of a large number of starter cells mainly restricted to the CeL/C were chosen for the analysis. I also paid attention to only compare animals with similar number of starter cells in the CeL/C in between the different experimental conditions.

For quantifications within all subregions, every section was quantified, but only the input neurons ipsilateral to the injection site were considered. The total number of labelled neurons within subregions was manually scored except for the CeL/C. The approximate number of input cells in the CeL/C for CeA<sup>Htr2a</sup> and CeA<sup>PKC $\delta$</sup>  tracing experiments was estimated by multiplying the total number of starter cells in the CeL/C by the ratio  $\frac{\text{CeL/C inputs}}{\text{CeL/C starters}}$ . This ratio was calculated for each brain by quantifying the number of RABV-eGFP+ only cells and the number of starter cells (TVA-mCherry+ and RABV-eGFP+) in three to twelve 50  $\mu$ m thick coronal sections from anterior to posterior CeA (bregma  $-1.1$  to  $-1.7$  mm).

Boundaries and nomenclature of brain areas are according to the Allen Institute's reference atlas<sup>162</sup>. Boundaries and nomenclature of subregions are based on the Allen Institute's reference atlas<sup>162</sup> with consultation of Paxinos and Franklin's atlas<sup>163</sup>. Our definitions of the VP, SI, aPVT, pPVT, SNL and DR are exclusively according to Paxinos and Franklin's atlas<sup>163</sup>. The cortex (Cx) includes somatosensory, auditory, perirhinal, ectorhinal and temporal association areas. Hippocampus (Hipp.) includes hippocampal and retrohippocampal regions excluding the entorhinal area. The multimodal thalamus (Multimod. T.) includes the medial geniculate nucleus (medial and dorsal part), subparafascicular thalamic nucleus (parvicellular part), supragenulate thalamic nucleus and peripeduncular nucleus. The preoptic hypothalamus (PO H.) includes hypothalamic nuclei that are located between 0.5 mm and  $-0.6$  mm anterior–posterior to the bregma. Tuberal posterior hypothalamus (Tub. p. H.) includes hypothalamic nuclei located in between  $-1.1$  mm and  $-2.1$  mm posterior to the bregma. The posterior hypothalamus (Post. H.) includes hypothalamic nuclei located between  $-2.1$  mm and  $-3.4$  mm posterior to the bregma and excluding the PSTN.

Input subregions that were part of the amygdala complex except for the CeL/C, LA, BLA and BLP were excluded from the analysis, namely the anterior amygdala area, bed nucleus of the accessory olfactory tract, nucleus of the lateral olfactory tract, basomedial amygdala nucleus, intercalated amygdala nucleus, medial amygdala nucleus, cortical amygdala area, posterior amygdala nucleus, piriform-amygdala area and postpiriform transition nucleus. Additionally, a small number of starter neurons were found in the neighbouring nuclei namely GP, CP, SI and the very lateral part of the LH. Although these neurons accounted for a small portion of the total starter neurons, input cells from these areas were excluded of the analysis.

The numbers of input neurons in subregions, were normalized to the total number of input cells counted in each animal. Areas that contained <1% of the total inputs to CeA<sup>Htr2a</sup>, CeA<sup>PKC $\delta$</sup>  and CeA<sup>Sst</sup> neurons all together were excluded.

For comparison of the number of input cells to CeA<sup>Htr2a</sup> and CeA<sup>PKC $\delta$</sup>  that belong to the amygdala complex (CeA, LA, aBLA and pBLA) versus non-amygdala related nuclei (isocortex, olfactory areas, hippocampal formation, pallidum, thalamus, hypothalamus, midbrain and pons) all inputs cells were taken into account for the calculations.

For identification of long range presynaptic partners to CeA<sup>Htr2a</sup>, CeA<sup>PKC $\delta$</sup> , CeA<sup>Sst</sup> neurons, PBN-projecting CeA and PBN-projecting CeA<sup>Htr2a</sup> neurons, input cells that belong to the amygdala complex (CeA, LA, aBLA and pBLA) were excluded of the analysis and only the input cells in the 21 remaining subregions were taken into account for the calculations

#### 5.9.4. Identification of IPBN inputs onto CeA<sup>Htr2a</sup> and CeA<sup>PKC $\delta$</sup> neurons

For quantification of IPBN inputs to CeA<sup>Htr2a</sup> and CeA<sup>PKC $\delta$</sup>  neurons, all 50  $\mu$ m thick coronal sections where RABV-eGFP+ cells were visible in the IPBN (from -5.0 to -5.55 mm posterior to bregma) were immunostained for CGRP protein. Z-stack images were acquired and analysed using ImageJ (NIH).

#### 5.9.5. Identification of axonal projections of CeA<sup>Htr2a</sup> and CeA<sup>PKC $\delta$</sup> neurons

For identification of axonal projections of CeA<sup>Htr2a</sup> and CeA<sup>PKC $\delta$</sup>  neurons, the brains of *Htr2a-Cre* and *Prkcd-Cre* mice that had been stereotaxically injected in the CeA with an AAV-Flex-SynMyc virus were cut into 70  $\mu$ m thick coronal sections and one every third section were immunostained for myc protein. Z-stack images of all immunostained sections were acquired.

### 5.9.6. Digital three-dimensional (3D) CeA and mouse brain reconstructions

For analysis of spatial distribution of CeA<sup>Htr2a</sup> and CeA<sup>PKC $\delta$</sup>  neurons, the CeA of an *Htr2a-Cre;LacZ* mouse was cut into 50  $\mu\text{m}$  thick coronal sections and immunostained for  $\beta$ -Gal (as a marker of Htr2a-Cre<sup>+</sup> neurons) and PKC $\delta$  proteins. Z-stack images of all sections from  $-1.1$  to  $-1.7$  mm posterior to bregma were acquired.

For 3D reconstruction of CeA<sup>Htr2a</sup> neuronal projections, the brain of an *Htr2a-Cre* mice that had been stereotaxically injected in the CeA with an AAV-mCherry virus underwent brain tissue clearing procedure. Z-stack images of all 2 mm thick coronal brain sections were acquired.

For analysis of spatial segregation of CeL/C projection neurons, the CeA of WT mice that had been stereotaxically injected in the BNST and or LH and or PAG and or PBN with CTB conjugates, were cut into 70  $\mu\text{m}$  thick coronal sections. Z-stack images of all sections from  $-1.1$  to  $-1.7$  mm posterior to bregma were acquired.

Processing of Z-stack images and 3D reconstructions were done using Amira software (Visage Imaging). First, fluorescence intensity attenuation in the z direction was corrected using the Correct Z Drop module for each z-stack image. Using the Transform Editor, the spatial positions of each z-stack were then manually transformed using a combination of translations and rotations in order to roughly align them with respect to one another. In order to turn the initial serial images into a correct 3D model, z-stacks were then concatenated (each channel separately) and manually aligned by translating and rotating the upper slices using the Align Slices module. Once one channel was properly aligned, the data set was resampled into a new aligned 3D image and this image was used as a reference to apply the exact same alignment to the other channels.

For analysis of spatial distribution of CeA<sup>Htr2a</sup> and CeA<sup>PKC $\delta$</sup>  neurons, 3D images of  $\beta$ -Gal and PKC $\delta$  immunostained neurons were additionally rotated (using the Transform Editor) in the exact same angle so that the x-axis corresponded to the lateral-medial axis, the y-axis to the dorso-ventral axis and the z-axis to the rostro-caudal axis of the brain. The Spot Detection module in Imaris (Bitplane) was finally used to both detect  $\beta$ -Gal and PKC $\delta$  expressing CeL/C neurons as well as to extract their digital coordinates along the x, y and z axes.

For 3D reconstruction of CeA<sup>Htr2a</sup> neuronal projections, the Segmentation Editor was used to manually segment the neuronal projections and the edge of the brain. 3D rendering of manually segmented brain surface was generated with the Surface View module. A 3D impression of CeA<sup>Htr2a</sup> axonal projections as well as colour coding of the intensity of fluorescence pixels was completed with the Volume Rendering module using as labels the segmented neuronal projections.

For analysis of spatial segregation of CeL/C projection neurons, I additionally needed to compare projection neuron distributions across mice and so to register all tracing brains to one common coordinate system. For this, one tracing brain

was chosen as a reference and all the other ones were registered to the reference brain using the Register Images module. First, the CeL/C of each tracing brain was manually segmented using the Segmentation Editor and based on Paxinos and Franklin's atlas<sup>163</sup> and all segmented CeAs were saved as labels. In the Register Images module I then used as a reference, the CeA label of the chosen tracing brain and as a metric, the option: Label Difference. All transformations were rigid.

I additionally rotated all registered data sets (using the Transform Editor) in the exact same angle so that the x-axis corresponded to the lateral-medial axis, the y-axis to the dorso-ventral axis and the z-axis to the rostro-caudal axis of the brain. Retrogradely labelled cell bodies were reconstructed using the Interactive Thresholding module and as masks, the corresponding segmented CeA labels.

Cell bodies inferior to 12  $\mu\text{m}$  in diameter on the x and y axes were discarded using the Remove Small Spots module. Finally, digital coordinates along the x, y, and z axes of reconstructed cell bodies were extracted using the Measure and Analyse, Individual measures, Label analyses and Basic modules

## 5.10. STATISTICAL ANALYSIS

Frequency distributions, smoothed curves as well as linear and nonlinear least squares (Gaussian) regression fitting were performed using GraphPad Prism (GraphPad). Raw data were smoothed by averaging two neighboring points and fitting the curve to a second order polynomial.

Two-dimensional kernel density estimations were used to estimate the probability density functions of CeA<sup>Htr2a</sup>, CeA<sup>PKC $\delta$</sup> , PAG- and PBN-projecting neurons location along the x and y axes and were created in R (<http://www.r-project.org/>) using the 'kde2d' function provided in the 'MASS' library. Bandwidths in the density estimation were chosen using the "bandwidth.nrd" function. Estimates were graphically displayed as contour plots, with the contour lines connecting points of equal probability density and drawn for probability density values between 10 to 90% of the probability density in step of 20%.

Coefficients of variation were calculated in excel as the ratio of the standard deviation to the mean.

For clustering analysis of input regions, I created a table for each experimental brain containing the exact number of input cells (RABV-eGFP+) counted in each subregion. Pairwise correlations (Pearson coefficient) as well as P values from a two-tailed unpaired t tests were then calculated in Excel (Microsoft). Hierarchically clustered heat maps and dendrograms representing high correlation or anticorrelation between regions were created in R (<http://www.r-project.org/>) using the 'heatmap.2' from the 'gplots' package function.

Significance levels are indicated as follows: \*P < 0.05; \*\*\*P < 0.001.



## LIST OF FIGURES AND TABLE

- Figure 1: Nuclear divisions of the amygdaloid complex.
- Figure 2: Summary of CeA external connectivity.
- Figure 3: Model of LA-BLA-CeA circuits for aversive behaviours.
- Figure 4: Model of CeA's function in appetitive behaviours.
- Figure 5: Cre-dependent rabies virus-based monosynaptic tracing.
- Figure 6: Molecular characterization of CeA<sup>Htr2a</sup> neurons.
- Figure 7: Spatial distribution of CeL/C<sup>Htr2a</sup> and CeL/C<sup>PKC $\delta$</sup>  neurons.
- Figure 8: CeA<sup>Htr2a</sup>, CeA<sup>PKC $\delta$</sup>  and CeA<sup>Sst</sup> neurons as starter cells for rabies-based monosynaptic tracing.
- Figure 9: Local inputs to CeA<sup>Htr2a</sup> neurons.
- Figure 10: Local inputs to CeA<sup>Sst</sup> neurons.
- Figure 11: Local inputs to CeA<sup>PKC $\delta$</sup>  neurons.
- Figure 12: Local inputs to PBN-projecting CeA neurons.
- Figure 13: Model of CeA microcircuits.
- Figure 14: Identification of whole brain inputs to CeA<sup>Htr2a</sup>, CeA<sup>PKC $\delta$</sup>  and CeA<sup>Sst</sup> neurons.
- Figure 15: Long-range presynaptic partners of CeA<sup>Htr2a</sup>, CeA<sup>PKC $\delta$</sup>  and CeA<sup>Sst</sup> neurons.
- Figure 16: Summary of whole brain inputs to CeA<sup>Htr2a</sup>, CeA<sup>PKC $\delta$</sup> , and CeA<sup>Sst</sup> neurons.
- Figure 17: Cell-type-specific IPBN inputs onto CeA<sup>Htr2a</sup> and CeA<sup>PKC $\delta$</sup>  neurons.
- Figure 18: Inter-mouse variability in CeA<sup>Htr2a</sup>, CeA<sup>PKC $\delta$</sup>  and CeA<sup>Sst</sup> tracing experiments.
- Figure 19: Long-range presynaptic partners of PBN-projecting CeA<sup>Htr2a</sup> and PBN-projecting CeA neurons.
- Figure 20: Axonal projections of CeA<sup>Htr2a</sup> neurons.
- Figure 21: Spatial segregation of CeL/C projection neurons.
- Figure 22: Cortical input mapping of CeA projection neurons.
- Figure 23: Schematic model of the organisation of CeA microcircuits.
- Table 1: Stereotaxic coordinates from bregma.



## ABBREVIATIONS

AAV	Adeno-associated virus
aBLA	Basolateral amygdala anterior division
AGRP	Agouti-related protein
aPVT	Paraventricular thalamus, anterior division
Arc	Arcuate nucleus
BLA	Basolateral amygdala
BMA	Basomedial amygdala
BNST	Bed nucleus of the stria terminalis
BSA	Bovine serum albumin
CAV	Canine adenovirus type 2
CeA	Central amygdala
CeC	Central amygdala capsular division
CeL	Central amygdala capsular division
CeL/C	Central amygdala capsular and lateral divisions
CeM	Central amygdala medial division
CGRP	Calcitonin gene-related peptide
CGRPR	Calcitonin gene-related peptide receptor
COA	Cortical amygdala area
CP	Caudoputamen
Crh	Corticotropin-releasing hormone
CTB	Cholera toxin subunit B
CUN	Cuneiform nucleus
CV	Coefficient of variation
Cx	Cortex
DR	Dorsal Raphe
eGFP	Enhanced green fluorescent protein
Enth.	Entorhinal cortex

EnvA	Envelope protein A
FISH	Fluorescent in situ hybridization
FS	FundFSus striatum
GFP	Green fluorescent protein
GP	Globus pallidus
Hipp.	Hippocampus
HSV	Herpes simplex virus
Htr2a	5-Hydroxytryptamine (serotonin) receptor 2a
IA	Intercalated amygdala nucleus
IC	Insula cortex
IHC	Immunohistochemistry
int	Internal capsule
LA	Lateral amygdala
LC	Locus Coeruleus
LH	Lateral hypothalamus
LiCl	Lithium Chloride
IPBN	Lateral parabrachial nucleus
MeA	Medial amygdala
mPBN	Medial parabrachial nucleus
MRN	Midbrain reticular nucleus
mRNA	Messenger ribonucleic acid
Multi. Thal.	Multimodal thalamus
NTS	Nucleus of the solitary tract
Nts	Neurotensin
Opt	Optic tract
PAA	Piriform amygdala area
PAG	Periaqueductal gray
pBLA	Basolateral amygdala posterior division
PBle	external lateral division of the lateral parabrachial nucleus

PBN	Parabrachial nucleus
PBS	Phosphate-buffered saline
PFA	Paraformaldehyde
Pir.	Piriform cortex
PKC $\delta$	Protein kinase C delta
PO H.	Preoptic hypothalamus
POMC	Pro-opiomelanocortin
Post. H.	Posterior hypothalamus
pPVT	Paraventricular thalamus, posterior division
PRN	Pontine reticular nucleus
PSTN	Parasubthalamic nucleus
PVH	Paraventricular hypothalamus
PVT	Paraventricular thalamus
RABV	Rabies virus
RF	Reticular formation
RR	Midbrain reticular nucleus, retrorubral area
RT	Room temperature
SI	Substantia innominata
SN	Substantia nigra
SNL	substantia nigra lateralis
Sst	Somatostatin
Tac2	Tachykinin 2
TR	Postpiriform transition area
Tub. p. H.	Tuberal posterior hypothalamus
vIPAG	Ventrolateral periaqueductal gray
vmPFC	Ventromedial-prefrontal cortex
VP	Ventral pallidum
VPMpc	Ventral posteromedial nucleus of the thalamus, parvicellular part
VTA	Ventral tegmental area
$\beta$ -Gal	Beta-galactosidase



## REFERENCES

1. Herry, C. & Johansen, J. P. Encoding of fear learning and memory in distributed neuronal circuits. *Nat. Neurosci.* **17**, 1644–1654 (2014).
2. Janak, P. H. & Tye, K. M. From circuits to behaviour in the amygdala. *Nature* **517**, 284–292 (2015).
3. Brown, S. & Schafer, E. A. An Investigation into the Functions of the Occipital and Temporal Lobes of the Monkey's Brain. *Philos. Trans. R. Soc. London B Biol. Sci.* **179**, 303–327 (1888).
4. Anton, B. S. Proceedings of the American Psychological Association for the legislative year 2012: minutes of the annual meeting of the Council of Representatives, February 24–26, 2012, Washington, DC, and August 2 and 5, 2012, Orlando, Florida, and minutes of the February, June, August, October, and December 2012 meetings of the Board of Directors. *Am. Psychol.* **68**, 337–358 (2013).
5. Blanchard, D. C. & Blanchard, R. J. Innate and conditioned reactions to threat in rats with amygdaloid lesions. *J. Comp. Physiol. Psychol.* **81**, 281–290 (1972).
6. LeDoux, J., Cicchetti, P., Xagoraris, A. & Romanski, L. The lateral amygdaloid nucleus: sensory interface of the amygdala in fear conditioning. *J. Neurosci.* **10(4)**, 1062–1069 (1990).
7. Murray, E. A. The amygdala, reward and emotion. *Trends Cogn. Sci.* **11**, 489–497 (2007).
8. Balleine, B. W. & Killcross, S. Parallel incentive processing: an integrated view of amygdala function. *Trends Neurosci.* **29**, 272–279 (2006).
9. Van Hoesen, G. W. in *Handbook of Chemical Neuroanatomy* 77–90 (1981).
10. Swanson, L. W. & Petrovich, G. D. What is the amygdala? *Trends Neurosci.* **21**, 323–331 (1998).
11. McDonald, A. J. Cortical pathways to the mammalian amygdala. *Progress in Neurobiology* **55**, 257–332 (1998).
12. García-López, M. *et al.* Histogenetic compartments of the mouse centromedial and extended amygdala based on gene expression patterns during development. *J. Comp. Neurol.* **506**, 46–74 (2008).
13. Cassell, M. D., Gray, T. S. & Kiss, J. Z. Neuronal architecture in the rat central nucleus of the amygdala: A cytological, hodological, and immunocytochemical study. *J. Comp. Neurol.* **246**, 478–499 (1986).
14. Martina, M., Royer, S. & Paré, D. Physiological properties of central medial and central lateral amygdala neurons. *J. Neurophysiol.* **82**, 1843–54 (1999).

15. Paré, D. & Smith, Y. Distribution of GABA immunoreactivity in the amygdaloid complex of the cat. *Neuroscience* **57**, 1061–1076 (1993).
16. Gray, T. S., Cassell, M. D. & Kiss, J. Z. Distribution of pro-opiomelanocortin-derived peptides and enkephalins in the rat central nucleus of the amygdala. *Brain Res.* **306**, 354–358 (1984).
17. Weber, E. & Barchas, J. D. Immunohistochemical distribution of dynorphin B in rat brain: relation to dynorphin A and alpha-neoendorphin systems. *Proc. Natl. Acad. Sci. U. S. A.* **80**, 1125–1129 (1983).
18. Roberts, G. W., Woodhams, P. L., Polak, J. M. & Crow, T. J. Distribution of neuropeptides in the limbic system of the rat: The hippocampus. *Neuroscience* **11**, 35–77 (1984).
19. Duarte, C. R., Schütz, B. & Zimmer, A. Incongruent pattern of neurokinin B expression in rat and mouse brains. *Cell Tissue Res.* **323**, 43–51 (2006).
20. McDonald, A. J. Coexistence of somatostatin with neuropeptide Y, but not with cholecystikinin or vasoactive intestinal peptide, in neurons of the rat amygdala. *Brain Res.* **500**, 37–45 (1989).
21. Ciriello, J., Rosas-Arellano, M. P., Solano-Flores, L. P. & De Oliveira, C. V. R. Identification of neurons containing orexin-B (hypocretin-2) immunoreactivity in limbic structures. *Brain Res.* **967**, 123–131 (2003).
22. Skofitsch, G. & Jacobowitz, D. M. Calcitonin gene-related peptide: Detailed immunohistochemical distribution in the central nervous system. *Peptides* **6**, 721–745 (1985).
23. Veening, J. G., Swanson, L. W. & Sawchenko, P. E. The organization of projections from the central nucleus of the amygdala to brainstem sites involved in central autonomic regulation: A combined retrograde transport-immunohistochemical study. *Brain Res.* **303**, 337–357 (1984).
24. Martone, M. E., Edelman, V. M., Ellisman, M. H. & Nef, P. Cellular and subcellular distribution of the calcium-binding protein NCS-1 in the central nervous system of the rat. *Cell Tissue Res.* **295**, 395–407 (1999).
25. Kim, J., Zhang, X., Muralidhar, S., LeBlanc, S. A. & Tonegawa, S. Basolateral to Central Amygdala Neural Circuits for Appetitive Behaviors. *Neuron* **93**, 1464–1479 (2017).
26. Chieng, B. C. H., Christie, M. J. & Osborne, P. B. Characterization of neurons in the rat central nucleus of the amygdala: Cellular physiology, morphology, and opioid sensitivity. *J. Comp. Neurol.* **497**, 910–927 (2006).
27. Honkaniemi, J. *et al.* Colocalization of peptide and glucocorticoid receptor immunoreactivities in rat central amygdaloid nucleus. *Neuroendocrinology* **55**, 451–459 (1992).
28. Yoon, Y. R. & Baik, J. H. Melanocortin 4 Receptor and Dopamine D2

Receptor Expression in Brain Areas Involved in Food Intake. *Endocrinol. Metab. (Seoul, Korea)* **30**, 576–83 (2015).

29. Veinante, P. & Freund-Mercier, M. J. Distribution of oxytocin- and vasopressin-binding sites in the rat extended amygdala: A histoautoradiographic study. *J. Comp. Neurol.* **383**, 305–325 (1997).
30. Hohmann, J. G. *et al.* Distribution and regulation of galanin receptor 1 messenger RNA in the forebrain of wild type and galanin-transgenic mice. *Neuroscience* **117**, 105–117 (2003).
31. De Souza, E. B. *et al.* Corticotropin-releasing factor receptors are widely distributed within the rat central nervous system: an autoradiographic study. *J. Neurosci.* **5**, 3189–3203 (1985).
32. Haubensak, W. *et al.* Genetic dissection of an amygdala microcircuit that gates conditioned fear. *Nature* **468**, 270–276 (2010).
33. Shimada, S. *et al.* Coexistence of peptides (corticotropin releasing factor/neurotensin and substance P/somatostatin) in the bed nucleus of the stria terminalis and central amygdaloid nucleus of the rat. *Neuroscience* **30**, 377–383 (1989).
34. Day, H. E. W., Curran, E. J., Watson, S. J. & Akil, H. Distinct Neurochemical Populations in the Rat Central Nucleus of the Amygdala and Bed Nucleus of the Stria Terminalis : Evidence for Their Selective Activation by Interleukin-1B. *J. Comp. Neurol.* **413**, 113–128 (1999).
35. Seki, T., Namba, T., Mochizuki, H. & Onodera, M. Clustering, migration, and neurite formation of neural precursor cells in the adult rat hippocampus. *J Comp Neurol* **502**, 275–290 (2007).
36. Li, H. *et al.* Experience-dependent modification of a central amygdala fear circuit. *Nat. Neurosci.* **16**, 332–339 (2013).
37. Han, S., Soleiman, M., Soden, M., Zweifel, L. & Palmiter, R. D. Elucidating an Affective Pain Circuit that Creates a Threat Memory. *Cell* **162**, 363–374 (2015).
38. Isosaka, T. *et al.* Htr2a-Expressing Cells in the Central Amygdala Control the Hierarchy between Innate and Learned Fear. *Cell* **163**, 1153–1164 (2015).
39. Carleton, A., Accolla, R. & Simon, S. A. Coding in the mammalian gustatory system. *Trends in Neurosciences* **33**, 326–334 (2010).
40. Yamamoto, T. & Ueji, K. Brain Mechanisms of Flavor Learning. *Front. Syst. Neurosci.* **5**, (2011).
41. Rosen, A. M., Victor, J. D. & Di Lorenzo, P. M. Temporal coding of taste in the parabrachial nucleus of the pons of the rat. *J. Neurophysiol.* **105**, 1889–96 (2011).
42. Tokita, K. & Boughter, J. D. Sweet-bitter and umami-bitter taste interactions in single parabrachial neurons in C57BL/6J mice. *J.*

- Neurophysiol.* **108**, 2179–2190 (2012).
43. Hermanson, O. & Blomqvist, A. Subnuclear localization of FOS-like immunoreactivity in the parabrachial nucleus after orofacial nociceptive stimulation of the awake rat. *J. Comp. Neurol.* **387**, 114–123 (1997).
  44. Richard, S., Engblom, D., Paues, J., Mackerlova, L. & Blomqvist, A. Activation of the parabrachio-amygdaloid pathway by immune challenge or spinal nociceptive input: A quantitative study in the rat using Fos immunohistochemistry and retrograde tract tracing. *J. Comp. Neurol.* **481**, 210–219 (2005).
  45. Geerling, J. C. & Loewy, A. D. Sodium deprivation and salt intake activate separate neuronal subpopulations in the nucleus of the solitary tract and the parabrachial complex. *J. Comp. Neurol.* **504**, 379–403 (2007).
  46. Geerling, J. C. *et al.* FoxP2 expression defines dorsolateral pontine neurons activated by sodium deprivation. *Brain Res.* **1375**, 19–27 (2011).
  47. Becskei, C., Grabler, V., Edwards, G. L., Riediger, T. & Lutz, T. A. Lesion of the lateral parabrachial nucleus attenuates the anorectic effect of peripheral amylin and CCK. *Brain Res.* **1162**, 76–84 (2007).
  48. Wu, Q., Clark, M. S. & Palmiter, R. D. Deciphering a neuronal circuit that mediates appetite. *Nature* **483**, 594–597 (2012).
  49. Chamberlin, N. L. & Saper, C. B. Topographic organization of cardiovascular responses to electrical and glutamate microstimulation of the parabrachial nucleus in the rat. *J. Comp. Neurol.* **326**, 245–262 (1992).
  50. Nakamura, K. & Morrison, S. F. A thermosensory pathway that controls body temperature. *Nat. Neurosci.* **11**, 62–71 (2008).
  51. Reilly, S. The parabrachial nucleus and conditioned taste aversion. *Brain Research Bulletin* **48**, 239–254 (1999).
  52. Alhadeff, A. L., Hayes, M. R. & Grill, H. J. Leptin receptor signaling in the lateral parabrachial nucleus contributes to the control of food intake. *AJP Regul. Integr. Comp. Physiol.* **307**, R1338–R1344 (2014).
  53. Alhadeff, A. L., Baird, J. P., Swick, J. C., Hayes, M. R. & Grill, H. J. Glucagon-like peptide-1 receptor signaling in the lateral parabrachial nucleus contributes to the control of food intake and motivation to feed. *Neuropsychopharmacology* **39**, 2233–2243 (2014).
  54. Baird, J. P., Travers, J. B. & Travers, S. P. Parametric analysis of gastric distension responses in the parabrachial nucleus. *Am J Physiol Regul Integr Comp Physiol* **281**, R1568–80 (2001).
  55. Sabbatini, M. *et al.* The pattern of c-Fos immunoreactivity in the hindbrain of the rat following stomach distension. *Exp. Brain Res.* **157**,

(2004).

56. D'Hanis, W., Linke, R. & Yilmazer-Hanke, D. M. Topography of thalamic and parabrachial Calcitonin Gene-Related Peptide (CGRP) immunoreactive neurons projecting to subnuclei of the amygdala and extended amygdala. *J. Comp. Neurol.* **505**, 268–291 (2007).
57. Carter, M. E., Soden, M. E., Zweifel, L. S. & Palmiter, R. D. Genetic identification of a neural circuit that suppresses appetite. *Nature* **503**, 111–114 (2013).
58. Schwaber, J. S., Sternini, C., Brecha, N. C., Rogers, W. T. & Card, J. P. Neurons containing calcitonin gene-related peptide in the parabrachial nucleus project to the central nucleus of the amygdala. *J. Comp. Neurol.* **270**, 416–426 (1988).
59. Saper, C. & Loewy, A. Efferent connections of the parabrachial nucleus in the rat. *Brain Res.* **197**, 291–317 (1980).
60. McDonald, A. J., Shammah-Lagnado, S. J., Shi, C. & Davis, M. Cortical afferents to the extended amygdala. in *Annals of the New York Academy of Sciences* **877**, 309–338 (1999).
61. Nakashima, M. *et al.* An anterograde and retrograde tract-tracing study on the projections from the thalamic gustatory area in the rat: Distribution of neurons projecting to the insular cortex and amygdaloid complex. *Neurosci. Res.* **36**, 297–309 (2000).
62. Turner, B. H. & Herkenham, M. Thalamoamygdaloid projections in the rat: A test of the amygdala's role in sensory processing. *J. Comp. Neurol.* **313**, 295–325 (1991).
63. Shi, C. J. & Cassell, M. D. Cortical, thalamic, and amygdaloid connections of the anterior and posterior insular cortices. *J. Comp. Neurol.* **399**, 440–468 (1998).
64. Schiff, H. C. *et al.* An insula-central amygdala circuit for behavioral inhibition. *bioRxiv* 156216 (2017). doi:10.1101/156216
65. Knapska, E., Radwanska, K., Werka, T. & Kaczmarek, L. Functional Internal Complexity of Amygdala: Focus on Gene Activity Mapping After Behavioral Training and Drugs of Abuse. *Physiol. Rev.* **87**, 1113–1173 (2007).
66. Yamaguchi, M. Functional Sub-Circuits of the Olfactory System Viewed from the Olfactory Bulb and the Olfactory Tubercle. *Front. Neuroanat.* **11**, 1–6 (2017).
67. LeDoux, J. E., Sakaguchi, A. & Reis, D. J. Subcortical efferent projections of the medial geniculate nucleus mediate emotional responses conditioned to acoustic stimuli. *J. Neurosci.* **4**, 683–698 (1984).
68. Kishi, T., Tsumori, T., Yokota, S. & Yasui, Y. Topographical projection from the hippocampal formation to the amygdala: A combined

- anterograde and retrograde tracing study in the rat. *J. Comp. Neurol.* **496**, 349–368 (2006).
69. Canteras, N. S. & Swanson, L. W. Projections of the ventral subiculum to the amygdala, septum, and hypothalamus: A PHAL anterograde tract-tracing study in the rat. *J. Comp. Neurol.* **324**, 180–194 (1992).
  70. McDonald, A. J. & Mascagni, F. Projections of the lateral entorhinal cortex to the amygdala: A Phaseolus vulgaris leucoagglutinin study in the rat. *Neuroscience* **77**, 445–459 (1997).
  71. Xu, C. *et al.* Distinct Hippocampal Pathways Mediate Dissociable Roles of Context in Memory Retrieval. *Cell* **167**, 961–972.e16 (2016).
  72. Heckers, S. & Mesulam, M. M. Two types of cholinergic projections to the rat amygdala. *Neuroscience* **60**, 383–397 (1994).
  73. Usunoff, K. G., Itzev, D. E., Rolfs, A., Schmitt, O. & Wree, A. Brain stem afferent connections of the amygdala in the rat with special references to a projection from the parabigeminal nucleus: A fluorescent retrograde tracing study. *Anat. Embryol. (Berl)*. **211**, 475–496 (2006).
  74. Hasue, R. H. & Shammah-Lagnado, S. J. Origin of the dopaminergic innervation of the central extended amygdala and accumbens shell: A combined retrograde tracing and immunohistochemical study in the rat. *J. Comp. Neurol.* **454**, 15–33 (2002).
  75. Wilson, M. A. & Molliver, M. E. The organization of serotonergic projections to cerebral cortex in primates: Retrograde transport studies. *Neuroscience* **44**, 555–570 (1991).
  76. Asan, E. Introduction. *Adv. Anat. Embryol. Cell Biol.* **142**, 1–3 (1998).
  77. Han, J. S., Holland, P. C. & Gallagher, M. Disconnection of the amygdala central nucleus and substantia innominata/nucleus basalis disrupts increments in conditioned stimulus processing in rats. *Behav. Neurosci.* **113**, 143–151 (1999).
  78. Smith, E. S., Fabian, P., Rosenthal, A., Kaddour-Djebbar, A. & Lee, H. J. The roles of central amygdala D1 and D2 receptors on attentional performance in a five-choice task. *Behav. Neurosci.* **129**, 564–575 (2015).
  79. Kask, A. & Schiöth, H. B. Tonic inhibition of food intake during inactive phase is reversed by the injection of the melanocortin receptor antagonist into the paraventricular nucleus of the hypothalamus and central amygdala of the rat. *Brain Res.* **887**, 460–464 (2000).
  80. Beckman, T. R., Shi, Q., Levine, A. S. & Billington, C. J. Amygdalar opioids modulate hypothalamic melanocortin-induced anorexia. *Physiol. Behav.* **96**, 568–573 (2009).
  81. Fekete, É., Vigh, J., Bagi, É. E. & Lénárd, L. Gastrin-releasing peptide microinjected into the amygdala inhibits feeding. *Brain Res.* **955**, 55–63

(2002).

82. Fekete, É. M., Bagi, É. E., Tóth, K. & Lénárd, L. Neuromedin C microinjected into the amygdala inhibits feeding. *Brain Res. Bull.* **71**, 386–392 (2007).
83. Kovács, A. *et al.* Microinjection of RFRP-1 in the central nucleus of amygdala decreases food intake in the rat. *Brain Res. Bull.* **88**, 589–595 (2012).
84. Paredes, J., Winters, R. W., Schneiderman, N. & McCabe, P. M. Afferents to the central nucleus of the amygdala and functional subdivisions of the periaqueductal gray: Neuroanatomical substrates for affective behavior. *Brain Res.* **887**, 157–173 (2000).
85. Reardon, F. & Mitrofanis, J. Organisation of the amygdalo-thalamic pathways in rats. *Anat. Embryol. (Berl)*. **201**, 75–84 (2000).
86. Moga, M. M. *et al.* Organization of cortical, basal forebrain, and hypothalamic afferents to the parabrachial nucleus in the rat. *J. Comp. Neurol.* **295**, 624–661 (1990).
87. Huang, T., Yan, J. & Kang, Y. Role of the central amygdaloid nucleus in shaping the discharge of gustatory neurons in the rat parabrachial nucleus. *Brain Res. Bull.* **61**, 443–452 (2003).
88. Lundy, R. F. & Norgren, R. Activity in the hypothalamus, amygdala, and cortex generates bilateral and convergent modulation of pontine gustatory neurons. *J. Neurophysiol.* **91**, 1143–1157 (2004).
89. Petrovich, G. D., Canteras, N. S. & Swanson, L. W. Combinatorial amygdalar inputs to hippocampal domains and hypothalamic behavior systems. *Brain Research Reviews* **38**, 247–289 (2001).
90. LeDoux, J. E., Iwata, J., Cicchetti, P. & Reis, D. J. Different projections of the central amygdaloid nucleus mediate autonomic and behavioral correlates of conditioned fear. *J. Neurosci.* **8**, 2517–2529 (1988).
91. Rizvi, T. A., Ennis, M., Behbehani, M. M. & Shipley, M. T. Connections between the central nucleus of the amygdala and the midbrain periaqueductal gray: Topography and reciprocity. *J. Comp. Neurol.* **303**, 121–131 (1991).
92. Tovote, P. *et al.* Midbrain circuits for defensive behaviour. *Nature* **534**, 206–212 (2016).
93. Mota-Ortiz, S. R., Sukikara, M. H., Felicio, L. F. & Canteras, N. S. Afferent connections to the rostral part of the periaqueductal gray: A critical region influencing the motivation drive to hunt and forage. *Neural Plast.* **2009**, (2009).
94. Han, W. *et al.* Integrated Control of Predatory Hunting by the Central Nucleus of the Amygdala. *Cell* **168**, 311–324.e18 (2017).
95. Hopkins, D. A. & Holstege, G. Amygdaloid projections to the

- mesencephalon, pons and medulla oblongata in the cat. *Exp. Brain Res.* **32**, 529–547 (1978).
96. van der Kooy, D., Koda, L. Y., McGinty, J. F., Gerfen, C. R. & Bloom, F. E. The organization of projections from the cortex, amygdala, and hypothalamus to the nucleus of the solitary tract in rat. *J. Comp. Neurol.* **224**, 1–24 (1984).
  97. Loewy, A. D. Chapter 12 Forebrain nuclei involved in autonomic control. *Prog. Brain Res.* **87**, 253–268 (1991).
  98. Viviani, D. *et al.* Oxytocin selectively gates fear responses through distinct outputs from the central amygdala. *Science (80-. )*. **333**, 104–107 (2011).
  99. Wallace, D. M., Magnuson, D. J. & Gray, T. S. Organization of amygdaloid projections to brainstem dopaminergic, noradrenergic, and adrenergic cell groups in the rat. *Brain Res. Bull.* **28**, 447–454 (1992).
  100. Zahm, D. S. *et al.* Inputs to the midbrain dopaminergic complex in the rat, with emphasis on extended amygdala-recipient sectors. *J. Comp. Neurol.* **519**, 3159–3188 (2011).
  101. Hermann, D. M., Luppi, P. H., Peyron, C., Hinckel, P. & Jouvet, M. Afferent projections to the rat nuclei raphe magnus, raphe pallidus and reticularis gigantocellularis pars  $\alpha$  demonstrated by iontophoretic application of cholera toxin (subunit b). *J. Chem. Neuroanat.* **13**, 1–21 (1997).
  102. Petrovich, G. D. & Swanson, L. W. Projections from the lateral part of the central amygdalar nucleus to the postulated fear conditioning circuit. *Brain Res.* **763**, 247–254 (1997).
  103. Bourgeois, L., Gauriau, C. & Bernard, J. F. Projections from the nociceptive area of the central nucleus of the amygdala to the forebrain: A PHA-L study in the rat. *Eur. J. Neurosci.* **14**, 229–255 (2001).
  104. Uwano, T., Nishijo, H., Ono, T. & Tamura, R. Neuronal responsiveness to various sensory stimuli, and associative learning in the rat amygdala. *Neuroscience* **68**, 339–361 (1995).
  105. Pitkänen, A., Savander, V. & LeDoux, J. E. Organization of intra-amygdaloid circuitries in the rat: An emerging framework for understanding functions of the amygdala. *Trends in Neurosciences* **20**, 517–523 (1997).
  106. Royer, S., Martina, M. & Paré, D. An inhibitory interface gates impulse traffic between the input and output stations of the amygdala. *J. Neurosci.* **19**, 10575–10583 (1999).
  107. Royer, S., Martina, M. & Paré, D. Polarized synaptic interactions between intercalated neurons of the amygdala. *J. Neurophysiol.* **83**, 3509–18 (2000).

108. Dong, H. W., Petrovich, G. D. & Swanson, L. W. Topography of projections from amygdala to bed nuclei of the stria terminalis. *Brain Research Reviews* **38**, 192–246 (2001).
109. Duvarci, S. & Pare, D. Amygdala microcircuits controlling learned fear. *Neuron* **82**, 966–980 (2014).
110. Romanski, L. M., Clugnet, M. C., Bordi, F. & LeDoux, J. E. Somatosensory and Auditory Convergence in the Lateral Nucleus of the Amygdala. *Behav. Neurosci.* **107**, 444–450 (1993).
111. Uwano, T., Nishijo, H., Ono, T. & Tamura, R. Neuronal responsiveness to various sensory stimuli, and associative learning in the rat amygdala. *Neuroscience* **68**, 339–361 (1995).
112. Paré, D., Smith, Y. & Paré, J. F. Intra-amygdaloid projections of the basolateral and basomedial nuclei in the cat: Phaseolus vulgaris-leucoagglutinin anterograde tracing at the light and electron microscopic level. *Neuroscience* **69**, 567–583 (1995).
113. Duvarci, S., Popa, D. & Paré, D. Central amygdala activity during fear conditioning. *J. Neurosci.* **31**, 289–94 (2011).
114. Jolkkonen, E. & Pitkänen, A. Intrinsic connections of the rat amygdaloid complex: Projections originating in the central nucleus. *J. Comp. Neurol.* **395**, 53–72 (1998).
115. Ciochi, S. *et al.* Encoding of conditioned fear in central amygdala inhibitory circuits. *Nature* **468**, 277–282 (2010).
116. Blair, H. T. Synaptic Plasticity in the Lateral Amygdala: A Cellular Hypothesis of Fear Conditioning. *Learn. Mem.* **8**, 229–242 (2001).
117. Sigurdsson, T., Doyère, V., Cain, C. K. & LeDoux, J. E. Long-term potentiation in the amygdala: A cellular mechanism of fear learning and memory. *Neuropharmacology* **52**, 215–227 (2007).
118. LeDoux, J. E. Emotion Circuits in the Brain. *Focus (Madison)*. **7**, 274–274 (2009).
119. Nader, K. Damage to the Lateral and Central, but Not Other, Amygdaloid Nuclei Prevents the Acquisition of Auditory Fear Conditioning. *Learn. Mem.* **8**, 156–163 (2001).
120. Quirk, G. J., Repa, J. C. & LeDoux, J. E. Fear conditioning enhances short-latency auditory responses of lateral amygdala neurons: Parallel recordings in the freely behaving rat. *Neuron* **15**, 1029–1039 (1995).
121. Rogan, M. T., Staubli, U. V. & LeDoux, J. E. Fear conditioning induces associative long-term potentiation in the amygdala. *Nature* **390**, 604–607 (1997).
122. McKernan, M. G. & Shinnick-Gallagher, P. Fear conditioning induces a lasting potentiation of synaptic currents in vitro. *Nature* **390**, 607–611 (1997).

123. Herry, C. *et al.* Switching on and off fear by distinct neuronal circuits. *Nature* **454**, 600–606 (2008).
124. Namburi, P. *et al.* A circuit mechanism for differentiating positive and negative associations. *Nature* **520**, 675–678 (2015).
125. Penzo, M. A. *et al.* The paraventricular thalamus controls a central amygdala fear circuit. *Nature* **519**, 455–459 (2015).
126. Do-Monte, F. H., Quinones-Laracuente, K. & Quirk, G. J. A temporal shift in the circuits mediating retrieval of fear memory. *Nature* **519**, 460–463 (2015).
127. Smith, Y. & Paré, D. Intra-amygdaloid projections of the lateral nucleus in the cat: PHA-L anterograde labeling combined with postembedding GABA and glutamate immunocytochemistry. *J. Comp. Neurol.* **342**, 232–248 (1994).
128. Goosens, K. A. Contextual and Auditory Fear Conditioning are Mediated by the Lateral, Basal, and Central Amygdaloid Nuclei in Rats. *Learn. Mem.* **8**, 148–155 (2001).
129. Anglada-Figueroa, D. Lesions of the Basal Amygdala Block Expression of Conditioned Fear But Not Extinction. *J. Neurosci.* **25**, 9680–9685 (2005).
130. Jimenez, S. A. & Maren, S. Nuclear disconnection within the amygdala reveals a direct pathway to fear. *Learn. Mem.* **16**, 766–768 (2009).
131. Beyeler, A. *et al.* Divergent Routing of Positive and Negative Information from the Amygdala during Memory Retrieval. *Neuron* **90**, 348–361 (2016).
132. Petreanu, L., Huber, D., Sobczyk, A. & Svoboda, K. Channelrhodopsin-2-assisted circuit mapping of long-range callosal projections. *Nat. Neurosci.* **10**, 663–668 (2007).
133. Knobloch, H. S. *et al.* Evoked axonal oxytocin release in the central amygdala attenuates fear response. *Neuron* **73**, 553–566 (2012).
134. Fadok, J. P. *et al.* A competitive inhibitory circuit for selection of active and passive fear responses. *Nature* **542**, 96–99 (2017).
135. Yu, K., Garcia da Silva, P., Albeanu, D. F. & Li, B. Central Amygdala Somatostatin Neurons Gate Passive and Active Defensive Behaviors. *J. Neurosci.* **36**, 6488–6496 (2016).
136. Cassell, M. D., Gray, T. S. & Kiss, J. Z. Neuronal architecture in the rat central nucleus of the amygdala: A cytological, hodological, and immunocytochemical study. *J. Comp. Neurol.* **246**, 478–499 (1986).
137. Penzo, M. A., Robert, V. & Li, B. Fear Conditioning Potentiates Synaptic Transmission onto Long-Range Projection Neurons in the Lateral Subdivision of Central Amygdala. *J. Neurosci.* **34**, 2432–2437 (2014).
138. Tye, K. M. *et al.* Amygdala circuitry mediating reversible and bidirectional control of anxiety. *Nature* **471**, 358–362 (2011).

139. Carola, V., D'Olimpio, F., Brunamonti, E., Mangia, F. & Renzi, P. Evaluation of the elevated plus-maze and open-field tests for the assessment of anxiety-related behaviour in inbred mice. *Behav. Brain Res.* **134**, 49–57 (2002).
140. Botta, P. *et al.* Regulating anxiety with extrasynaptic inhibition. *Nat. Neurosci.* **18**, 1493–1500 (2015).
141. Cai, H., Haubensak, W., Anthony, T. E. & Anderson, D. J. Central amygdala PKC- $\delta$ + neurons mediate the influence of multiple anorexigenic signals. *Nat. Neurosci.* **17**, 1240–1248 (2014).
142. Gallagher, M. *et al.* The amygdala central nucleus and appetitive Pavlovian conditioning: Lesions impair one class of conditioned behavior. *J. Comp. Physiol.* **10**, 1906–1911 (1990).
143. Hiroi, N. & White, N. M. The lateral nucleus of the amygdala mediates expression of the amphetamine-produced conditioned place preference. *J. Neurosci.* **11**, 2107–2116 (1991).
144. Hatfield, T., Han, J. S., Conley, M., Gallagher, M. & Holland, P. Neurotoxic lesions of basolateral, but not central, amygdala interfere with Pavlovian second-order conditioning and reinforcer devaluation effects. *J. Neurosci.* **16**, 5256–5265 (1996).
145. Parkinson, J. A., Robbins, T. W. & Everitt, B. J. Dissociable roles of the central and basolateral amygdala in appetitive emotional learning. *Eur. J. Neurosci.* **12**, 405–413 (2000).
146. Holland, P. C., Hatfield, T. & Gallagher, M. Rats with basolateral amygdala lesions show normal increases in conditioned stimulus processing but reduced conditioned potentiation of eating. *Behav. Neurosci.* **115**, 945–950 (2001).
147. Murray, E. A. The amygdala, reward and emotion. *Trends Cogn. Sci.* **11**, 489–497 (2007).
148. Corbit, L. H. Double Dissociation of Basolateral and Central Amygdala Lesions on the General and Outcome-Specific Forms of Pavlovian-Instrumental Transfer. *J. Neurosci.* **25**, 962–970 (2005).
149. Robinson, M. J. F., Warlow, S. M. & Berridge, K. C. Optogenetic Excitation of Central Amygdala Amplifies and Narrows Incentive Motivation to Pursue One Reward Above Another. *J. Neurosci.* **34**, 16567–16580 (2014).
150. Warlow, S. M., Robinson, M. J. F. & Berridge, K. C. Optogenetic central amygdala stimulation intensifies and narrows motivation for cocaine. *J. Neurosci.* 3141–16 (2017). doi:10.1523/JNEUROSCI.3141-16.2017
151. Seo, D. *et al.* A GABAergic Projection from the Centromedial Nuclei of the Amygdala to Ventromedial Prefrontal Cortex Modulates Reward Behavior. *J. Neurosci.* **36**, 10831–10842 (2016).

152. Xiu, J. *et al.* Visualizing an emotional valence map in the limbic forebrain by TAI-FISH. *Nat. Neurosci.* **17**, 1552–1559 (2014).
153. Kim, J., Pignatelli, M., Xu, S., Itohara, S. & Tonegawa, S. Antagonistic negative and positive neurons of the basolateral amygdala. *Nat. Neurosci.* **19**, 1636–1646 (2016).
154. Wickersham, I. R. *et al.* Monosynaptic Restriction of Transsynaptic Tracing from Single, Genetically Targeted Neurons. *Neuron* **53**, 639–647 (2007).
155. Ghanem, A. & Conzelmann, K. K. G gene-deficient single-round rabies viruses for neuronal circuit analysis. *Virus Res.* **216**, 41–54 (2016).
156. Callaway, E. M. & Luo, L. Monosynaptic Circuit Tracing with Glycoprotein-Deleted Rabies Viruses. *J. Neurosci.* **35**, 8979–8985 (2015).
157. Wertz, A. *et al.* Single-cell-initiated monosynaptic tracing reveals layer-specific cortical network modules. *Science (80-. ).* **349**, 70–74 (2015).
158. Arenkiel, B. R. *et al.* Activity-induced remodeling of olfactory bulb microcircuits revealed by monosynaptic tracing. *PLoS One* **6**, e29423 (2011).
159. Wall, N. R., Wickersham, I. R., Cetin, A., De La Parra, M. & Callaway, E. M. Monosynaptic circuit tracing in vivo through Cre-dependent targeting and complementation of modified rabies virus. *Proc. Natl. Acad. Sci. U. S. A.* **107**, 21848–21853 (2010).
160. Watabe-Uchida, M., Zhu, L., Ogawa, S. K., Vamanrao, A. & Uchida, N. Whole-Brain Mapping of Direct Inputs to Midbrain Dopamine Neurons. *Neuron* **74**, 858–873 (2012).
161. Schwarz, L. A. *et al.* Viral-genetic tracing of the input-output organization of a central noradrenergic circuit. *Nature* **524**, 88–92 (2015).
162. Lein, E. S. *et al.* Genome-wide atlas of gene expression in the adult mouse brain. *Nature* **445**, 168–176 (2007).
163. Demil, B. & Bensédrine, J. *Processes of Legitimization and Pressure Toward Regulation. International Studies of Management & Organization* **35**, (2005).
164. Veinante, P., Yalcin, I. & Barrot, M. The amygdala between sensation and affect: a role in pain. *J. Mol. Psychiatry* **1**, 9 (2013).
165. Morton, G. J., Meek, T. H. & Schwartz, M. W. Neurobiology of food intake in health and disease. *Nat. Rev. Neurosci.* **15**, 367–378 (2014).
166. Liang, C. L., Sinton, C. M. & German, D. C. Midbrain dopaminergic neurons in the mouse: Co-localization with calbindin-D(28K) and calretinin. *Neuroscience* **75**, 523–533 (1996).
167. Okaty, B. W. *et al.* Multi-Scale Molecular Deconstruction of the Serotonin Neuron System. *Neuron* **88**, 774–791 (2015).

168. SAH, P., FABER, E. S. L., LOPEZ DE ARMENTIA, M. & POWER, J. The Amygdaloid Complex: Anatomy and Physiology. *Physiol. Rev.* **83**, 803–834 (2003).
169. Sternson, S. M. & Eiselt, A.-K. Three Pillars for the Neural Control of Appetite. *Annu. Rev. Physiol.* **79**, 401–423 (2017).
170. Balleine, B. Instrumental Performance Following a Shift in Primary Motivation Depends on Incentive Learning. *J. Exp. Psychol. Anim. Behav. Process.* **18**, 236–250 (1992).
171. Balleine, B. W. Neural bases of food-seeking: Affect, arousal and reward in corticostriatolimbic circuits. *Physiol. Behav.* **86**, 717–730 (2005).
172. Rossi, M. A. & Stuber, G. D. Overlapping Brain Circuits for Homeostatic and Hedonic Feeding. *Cell Metab.* **27**, 42–56 (2017).
173. Rossi, M. A., Sukharnikova, T., Hayrapetyan, V. Y., Yang, L. & Yin, H. H. Operant Self-Stimulation of Dopamine Neurons in the Substantia Nigra. *PLoS One* **8**, (2013).
174. Berridge, K. C. The debate over dopamine's role in reward: The case for incentive salience. *Psychopharmacology* **191**, 391–431 (2007).
175. Berridge, K. C. 'Liking' and 'wanting' food rewards: Brain substrates and roles in eating disorders. *Physiol. Behav.* **97**, 537–550 (2009).
176. Hajnal, A. & Lénárd, L. Feeding-related dopamine in the amygdala of freely moving rats. *Neuroreport* **8**, 2817–2820 (1997).
177. Fallon, S., Shearman, E., Sershen, H. & Lajtha, A. Food reward-induced neurotransmitter changes in cognitive brain regions. *Neurochem. Res.* **32**, 1772–1782 (2007).
178. Jennings, J. H. *et al.* Distinct extended amygdala circuits for divergent motivational states. *Nature* **496**, 224–228 (2013).
179. Magableh, A. & Lundy, R. Somatostatin and corticotrophin releasing hormone cell types are a major source of descending input from the forebrain to the parabrachial nucleus in mice. *Chem. Senses* **39**, 673–682 (2014).
180. Wood, J. *et al.* Structure and function of the amygdaloid NPY system: NPY Y2 receptors regulate excitatory and inhibitory synaptic transmission in the centromedial amygdala. *Brain Struct. Funct.* **221**, 3373–3391 (2016).
181. Hunt, S., Sun, Y., Kucukdereli, H., Klein, R. & Sah, P. Intrinsic Circuits in the Lateral Central Amygdala. *Eneuro* **4**, ENEURO.0367-16.2017 (2017).
182. Kempainen, S. & Pitkänen, A. Distribution of parvalbumin, calretinin, and calbindin-D(28k) immunoreactivity in the rat amygdaloid complex and colocalization with  $\gamma$ -aminobutyric acid. *J. Comp. Neurol.* **426**, 441–467 (2000).
183. Schultz, W., Dayan, P. & Montague, P. R. A neural substrate of

- prediction and reward. *Science (80-. )*. **275**, 1593–1599 (1997).
184. Schultz, W. Updating dopamine reward signals. *Current Opinion in Neurobiology* **23**, 229–238 (2013).
  185. Livneh, Y. *et al.* Homeostatic circuits selectively gate food cue responses in insular cortex. *Nature* **546**, 611–616 (2017).
  186. Balleine, B. W. & Dickinson, a. The effect of lesions of the insular cortex on instrumental conditioning: evidence for a role in incentive memory. *J. Neurosci.* **20**, 8954–8964 (2000).
  187. Gogolla, N. The insular cortex. *Curr. Biol.* **27**, R580–R586 (2017).
  188. Braesicke, K. *et al.* Autonomic arousal in an appetitive context in primates: A behavioural and neural analysis. *Eur. J. Neurosci.* **21**, 1733–1740 (2005).
  189. Miyamichi, K. *et al.* Cortical representations of olfactory input by trans-synaptic tracing. *Nature* **472**, 191–199 (2011).
  190. Albisetti, G. W. *et al.* Identification of two classes of somatosensory neurons that display resistance to retrograde infection by rabies virus. *J. Neurosci.* **37**, 1277–17 (2017).
  191. Grewe, B. F. *et al.* Neural ensemble dynamics underlying a long-term associative memory. *Nature* **543**, 670–675 (2017).
  192. Voigt, J. P. & Fink, H. Serotonin controlling feeding and satiety. *Behavioural Brain Research* **277**, 14–31 (2015).
  193. Gasque, G., Conway, S., Huang, J., Rao, Y. & Vosshall, L. B. Small molecule drug screening in *Drosophila* identifies the 5HT2A receptor as a feeding modulation target. *Sci. Rep.* **3**, 1–8 (2013).
  194. Takeoka, A., Vollenweider, I., Courtine, G. & Arber, S. Muscle spindle feedback directs locomotor recovery and circuit reorganization after spinal cord injury. *Cell* **159**, 1626–1639 (2014).
  195. Niedworok, C. J. *et al.* Charting Monosynaptic Connectivity Maps by Two-Color Light-Sheet Fluorescence Microscopy. *Cell Rep.* **2**, 1375–1386 (2012).
  196. Chung, K. *et al.* Structural and molecular interrogation of intact biological systems. *Nature* **497**, 332–337 (2013).

PUBLICATION FROM THE WORK PRESENTED IN THIS DISSERTATION

**Central amygdala circuits modulate food consumption through a positive-valence mechanism.**

Douglass AM\*, Kucukdereli H\*, **Ponserre M\***, Markovic M, Gründemann J, Strobel C, Alcalá Morales PL, Conzelmann KK, Lüthi A, Klein R.

*Nature Neuroscience*. 2017 Oct; 20(10):1384-1394.

\* Equal contribution



# CURRICULUM VITAE

**MARION PONSERRE**

mponserre@neuro.mpg.de

## EDUCATION

**Max Planck Institute of Neurobiology - Ludwig-Maximilians-Universität München (LMU)**

DR. RER. NAT

Martinsried, Germany

2012 – Present

**School of Engineering, Polytech Marseilles**

MSC IN BIOTECHNOLOGIES

Marseilles, France

2008 – 2011

**Lycée Marie Curie**

BSC IN BIOTECHNOLOGIES WITH HONOURS: 1<sup>ST</sup> OF 100 STUDENTS

Marseilles, France

2006 – 2008

## RESEARCH EXPERIENCE

**Max Planck Institute of Neurobiology, Dr Rüdiger Klein**

PH.D CANDIDATE

Investigation of central amygdala circuits regulating appetitive and aversive behaviours.

Martinsried, Germany

2012 – Present

**Architecture and Function of Biological Macromolecules (AFMB),  
Dr Alain Roussel.**

RESEARCH ENGINEER

Assess the phagocytic activity of a membrane glycoprotein which had been described as a pattern recognition receptor for bacteria.

Marseilles, France

2011 – 2012

(4 months)

**Novartis Pharmaceuticals, Dr Gino Van Heeke**

MASTER THESIS

Development of an *in vitro* cell model of transcytosis.

Horsham, UK

2011

(6 months)

**Developmental Biology Institute of Marseilles Luminy (IBDML),  
Dr André Le Bivic**

RESEARCH TECHNICIAN

Study the role of two paralogue PDZ domain-containing proteins in the migration of epithelial cells.

Marseilles, France

2010

(4 months)

**Architecture and Function of Biological Macromolecules (AFMB),  
Dr Bruno Canard**

BACHELOR THESIS

Identification of inhibitors of the Dengue virus polymerase in a cellular assay.

Marseilles, France

2007 – 2008

(2 months)

## CONFERENCES

**State of the Brain: Genetic Dissection of Brain Circuits and Behavior in Health and Disease** Keystone, CO, USA  
2018

ORAL PRESENTATION

**Federation of European Neuroscience Societies, Annual meeting** Copenhagen, Denmark  
2016

POSTER PRESENTATION

**Champalimaud 5<sup>th</sup> Neuroscience Symposium** Lisbon, Portugal  
2015

POSTER PRESENTATION

**Amygdala Function in Emotion, Cognition and Disease, Gordon Research Conference** Easton, MA, USA  
2015

ATTENDANCE

**Federation of European Neuroscience Societies, Annual meeting** Milan, Italy  
2014

ATTENDANCE

## PUBLICATIONS

Douglass AM\*, Kucukdereli H\*, **Ponserre M\***, Markovic M, Gründemann J, Strobel C, Alcala Morales PL, Conzelmann KK, Lüthi A, Klein R. Central amygdala circuits modulate food consumption through a positive-valence mechanism. *Nat Neurosci.* 2017; 20(10):1384-1394. \* Equal contribution

Schaupp A, Sabet O, Dudanova I, **Ponserre M**, Bastiaens P, Klein R. The composition of EphB2 clusters determines the strength in the cellular repulsion response. *J Cell Biol.* 2014; 204(3):409-22.

Assémat E, Crost E, **Ponserre M**, Wijnholds J, Le Bivic A, Massey-Harroche D. The multi-PDZ domain protein-1 (MUPP-1) expression regulates cellular levels of the PALS-1/PATJ polarity complex. *Exp Cell Res.* 2013; 319(17):2514-25.

## SKILLS

**Languages** French (native), English (fluent), German

**Technical Skills** Mouse genetics and rodent stereotaxic surgery; viral circuit tracing; histology: immunohistochemistry and *in situ* hybridization; confocal microscopy; in vivo optogenetics; fundamental cloning techniques; cell biology: primary and tissue cultures, cell transfection, gene silencing by RNA interference; biochemistry: Western-Blot, ELISA, protein production in mammalian cells; flow cytometry.

**Data Analysis** ImageJ (NIH), Amira (Visage Imaging), R (<http://www.r-project.org/>).

## SUPERVISION

**Supervision of a student lab helper Tommaso Caudullo** Martinsried  
June 2015 – May 2017

## OTHER

**Elected representative of the Ph.D. students of the MPI of Neurobiology** Martinsried  
2015

